

Selection of Wind Direction Segment Size in Wind Farm Layout Optimization

by

Siyun Ge

A thesis submitted in partial fulfillment of the requirements for the degree of

Master of Science

in

ENGINEERING MANAGEMENT

Department of Mechanical Engineering

University of Alberta

© Siyun Ge, 2021

Abstract

Wind energy is a popular electricity resource across the world in the last few decades and is becoming increasingly important. In wind farm constructions, wake effect is an inevitable problem to be addressed. The wake generated by the upstream wind turbines may decrease the wind speed and reduce the power output of the downstream wind turbines, which will influence the power generation capacity of the wind farm. Therefore, mitigating the wake effect is important in wind energy studies.

Wind farm layout optimization is one of the most effective ways to mitigate the wake effect, aiming to minimize the energy loss due to wake effect by optimizing the positions of wind turbines. Wake effect is sensitive to wind directions, which are typically divided into equally spaced segments in wind resource modeling. Use of an inappropriate wind direction segment size in wind farm layout optimization may lead to unreliable optimization results or high computing time during the optimization process. However, few studies investigated the selection of wind direction segment sizes in wind farm layout optimization. In reported studies, the selection of wind direction segment sizes is mainly based on the consistency of the optimization results without considering the computing time. The accuracy of the estimated wind farm power output was not verified properly, and wind farms with different sizes were not investigated when making recommendations.

This thesis proposes a comprehensive approach for selecting proper wind direction segment sizes in wind farm layout optimization studies. Wind farm power output and its estimation accuracy, together with computing time, are considered in the optimization process. The proposed approach involves five steps: modeling the wind farm power

output and defining the objective function, pre-processing the data of the target wind farm, selecting an appropriate wind resource sample size for wind farm layout optimization, evaluating the estimated power output of the target wind farm, and optimizing the wind farm layout using genetic algorithm (GA). The proposed approach is demonstrated by case studies.

The results show that the wind direction segment size has a clear impact on wind farm layout optimization. Smaller wind direction segment sizes generally result in better layouts with higher wind farm power output. The computing time for the optimization process increases with the decrease of wind direction segment size. For wind farms of different sizes and number of wind turbines, we are able to recommend suitable wind direction segment sizes. By applying the proposed approach to the target wind farm, the power output and cost performance are improved compared with randomly designed layouts. The results also show that 1° is the most reliable, 1° to 15° are acceptable, and 3° is the optimal wind direction segment size.

With the proposed approach, different wind farm power output models can be incorporated to select proper wind direction segment sizes in wind farm layout optimization. The results will benefit wind farm operators, wind farm developers and researchers in selecting recommended wind direction segment sizes in wind farm power output calculation and layout optimization.

Preface

The material presented in this thesis is based on the original work by Siyun Ge under the supervision of Dr. Ming J. Zuo and Dr. Zhigang Tian. The focus of this thesis is to investigate selecting proper wind direction segment sizes in wind farm layout optimization. A comprehensive approach to select proper wind direction segment sizes in wind farm layout optimization is proposed. The proposed approach is demonstrated by case studies and proper wind direction segment sizes are presented based on the optimization results.

The data in Chapter 4 is observed in a wind farm. The target wind farm in Chapter 4 is hypothetical to protect the confidentiality of the real wind farm. Besides, for the concerns of data transparency, the number of wind turbines and power output values shown in text, figures and tables in Chapter 4 are scaled by fixed ratios.

The Matlab code for calculating the average power output of the wind farm and optimizing the layout of the wind farm in Chapter 4 and Chapter 5 is wrote by myself.

Acknowledgement

I would like to express my deep gratitude to my supervisor Dr. Ming J. Zuo for his patient guidance and encouragement on my research work. I have gained academic training and learnt skills to solve research problems reasonably and effectively. I would also like to thank Dr. Zhigang Tian for his valuable suggestions and great assistance on my thesis writing. My sincere thank also goes to my examining committee members.

I am grateful for the assistance given by members of Reliability Research Lab (RRL) during my MSc study. I would also like to extend my thanks to my friends for their concern about my life in Canada.

Finally, I would like to express my great appreciation to my family for their understanding, support and encouragement.

Contents

Chapter 1 Introduction	1
1.1 Background.....	1
1.2 Wind turbines	2
1.3 Onshore Wind Farms.....	3
1.4 Wake effect.....	5
1.5 Motivations.....	6
1.6 Research objectives	7
Chapter 2 Literature Review and Fundamentals	10
2.1 General framework of wind farm layout optimization	11
2.2 Wind characteristics	12
2.3 Wake effect model.....	16
2.4 Wind turbine power curve	20
2.5 Objective functions.....	21
2.6 Optimization process.....	23
Chapter 3 Models and Methodologies	25
3.1 Wind resource model.....	25
3.2 Position model	26
3.3 Wake effect model.....	29
3.3.1 Aerodynamics of wind turbines.....	29
3.3.2 Single wake effect	33
3.3.3 Wake conditions	36
3.3.4 Multiple wake effects	39
3.3.5 Wind speed estimation process by wake effect model	41
3.4 Power output model.....	44
3.4.1 Wind turbine power curve	44
3.4.2 Wind farm power output model.....	46
3.5 Objective functions.....	46
3.5.1 Objective 1: maximizing the APO of the wind farm.....	46
3.5.2 Objective 2: minimizing the CoP of the wind farm.....	47

3.6	Genetic Algorithm	49
3.7	Proposed approach for wind direction segment size selection	52
3.8	Summary.....	57
Chapter 4 Data Description and Wind Farm Power Output Assessment.....		58
4.1	Data description.....	59
4.2	Coefficient calibration	59
4.3	Wind characteristics result.....	63
4.4	Wind farm power output assessment.....	68
4.4.1	Wind resource sample size selection	68
4.4.2	Evaluation of wind direction segment sizes for wind farm power output calculation.....	71
4.5	Summary.....	73
Chapter 5 Wind Farm Layout Optimization Results Discussion.....		75
5.1	Evaluation framework	76
5.2	Wind farm layout optimization with a fixed number of wind turbines	77
5.2.1	Case 1	77
5.2.2	Case 2	80
5.2.3	Case 3	84
5.2.4	Summary.....	93
5.3	Wind farm layout optimization with various number of wind turbines	94
5.3.1	Case 4	94
5.3.2	Summary.....	98
Chapter 6 Summary and Future Work		99
6.1	Summary.....	99
6.2	Future work	101
Bibliography.....		103

List of Tables

Table 2.1 Frequency distribution of wind resource of a wind farm	13
Table 3.1 Terrain classification and the corresponding decay constant [69]	35
Table 3.2 GA parameters.....	52
Table 4.1 Wind turbine properties.....	60
Table 4.2 Wind characteristics of the target wind farm with 15° as the wind direction segment size.....	67
Table 5.1 Description of 4 case studies	75
Table 5.2 Optimized result with different wind direction segment sizes for Case 3.....	87
Table 5.3 Comparison of APO improvement of different optimized wind farms.....	89
Table 5.4 Comparison of Layout-1, Layout-2, Layout-3 and optimized wind farm	96

List of Figures

Figure 1.1 Configuration of a wind turbine	2
Figure 1.2 An onshore wind farm	3
Figure 1.3 How the wind farm works	4
Figure 1.4 Wind turbine wake effect [16].....	5
Figure 2.1 Wind rose of a wind farm	14
Figure 2.2 Jensen’s model [48].....	17
Figure 2.3 Larsen’s model [48].....	17
Figure 2.4 Frandsen’s model [48].....	18
Figure 2.5 Gaussian based model	19
Figure 3.1 Wind direction and wind turbine.....	27
Figure 3.2 Illustration of the position model	28
Figure 3.3 Idealized wind turbine and air flow	30
Figure 3.4 Relationship of power coefficient C_p and α	32
Figure 3.5 Top view of Jensen’s model	34
Figure 3.6 Front views of wake conditions.....	36
Figure 3.7 Two views of partial wake effect	38
Figure 3.8 Multiple wake effects in a wind farm.....	40
Figure 3.9 Flow chart of wind speed estimation process by wake effect model	42
Figure 3.10 A typical wind turbine power curve	45
Figure 3.11 Cost for a single wind turbine by Mosetti’s model	49
Figure 3.12 Flowchart of the GA [71]	50
Figure 3.13 An example of the breeding process in the GA.....	52
Figure 3.14 Flow chart of the proposed approach for wind direction segment size selection in wind farm layout optimization	53
Figure 4.1 RMSE of the estimated and observed power output with different rated wind speeds.....	61
Figure 4.2 Original and calibrated power curves.....	62
Figure 4.3 Thrust coefficient of the wind turbine.....	63
Figure 4.4 An example of the baseline wind turbine and surrounding wind turbines	64
Figure 4.5 Wind rose of the target wind farm.....	65
Figure 4.6 Proportion of wind direction with 15° as the wind direction segment size.....	66
Figure 4.7 Comparison of RE and CPU time with different wind resource sample sizes	71
Figure 4.8 Comparison of RE and CPU time for different wind direction segment sizes calculated by 3500 wind resource data	72
Figure 5.1 Optimized wind farm layouts with different wind direction segment sizes for Case 1	78
Figure 5.2 <i>Pre</i> of optimized wind farms in Case 1	79

Figure 5.3 CPU time of wind farm layout optimization with different wind direction segment sizes in Case 1.....	80
Figure 5.4 Optimized wind farm layouts with different wind direction segment sizes for Case 2.....	82
Figure 5.5 <i>Pre</i> of optimized wind farms with different wind direction segment sizes in Case 2.....	83
Figure 5.6 CPU time of wind farm layout optimization with different wind direction segment sizes in Case 2.....	84
Figure 5.7 Optimized wind farm layout with different wind direction segment sizes for Case 3.....	86
Figure 5.8 Randomly designed wind farms	88
Figure 5.9 Comparison of APO of different optimized wind farms in Case 3	90
Figure 5.10 Fitness curve of the optimized wind farm layout with 1° as the wind direction segment size	91
Figure 5.11 Relative error of wind farm power output of different optimized wind farms calculated by the simulated and observed wind resource	92
Figure 5.12 Optimized wind farm with the minimal CoP	95
Figure 5.13 Fitness curve of the optimized wind farm with the minimal CoP.....	95
Figure 5.14 CoP and APO of the optimized wind farms with various number of turbines	97
Figure 5.15 Wind farm efficiency of optimized wind farms with various number of turbines.....	97

List of Symbols

A_0	wind turbine rotor swept area
A_{ij}	overlapped area of wake and rotor swept area
A_{shadow}	overlapped area for partial wake condition
a	axial induction factor
a_k	scale parameter of Weibull distribution at k^{th} segment
b_k	shape parameter of Weibull distribution at k^{th} segment
$Cost$	cost of the wind farm
$Cost_s$	non-dimensionalized cost per year of a single wind turbine
C_p	power coefficient
C_t	thrust coefficient
D	wind turbine rotor diameter
Def_{ij}	wind speed deficit at T_i affected by T_j
\overline{Def}_i	wind speed deficit at T_i by multiple wake effect
d_{min}	minimum distance between two wind turbines
F	dynamic force of wind
$f_{estimate}$	estimated wind turbine power output
f_{best}	best fitness value by GA
$f(v_l, \beta_k)$	PDF of wind speed v_l occurring at wind direction β_k
k	number of wind direction segments
L_{ij}	transversal distance between T_i and T_j
l	number of wind speed segments
M	wind resource sample size
\dot{m}	mass flow rate
n	number of wind turbine
P	idealized wind turbine power output

$P_{estimate}$	estimated APO of the target wind farm
P_{farm}	observed APO of the target wind farm
P_{ideal}	wind farm power output without wake effect
$P_{optimize}$	optimized APO of the wind farm
P_r	rated power output
P_{re}	re-evaluated APO of the optimized wind farm
P_{ri}	APO improvement of the optimized wind farm
$P_{T_i}(v_i)$	power output of T_i
\bar{P}_{T_i}	APO of T_i
P_{tot}	APO of a wind farm
P_{un}	APO of the unoptimized wind farm
P_w	kinetic energy per unit time of the free wind stream
$P_w(v_i)$	non-linear part of power curve
p	dynamic pressure
p_k	proportion of wind direction β_k for k^{th} segment
p_s	semi-perimeter of a triangle
RE_r	relative error of P_{re} and $P_{optimize}$
r_0	wind turbine rotor radius
r_{ij}	wake radius at T_i affected by T_j
S	amount of the observed power output data
T	thrust at the actuator disk
T_i	wind turbine i
T_j	wind turbine j
U	free stream wind speed for the idealized wind turbine
v	wind speed behind the rotor of wind turbine
v_{cut-in}	cut-in wind speed

$v_{cut-out}$	cut-out wind speed
v_{rated}	rated wind speed
v_0	free wind speed of the wind farm
v_l	wind direction at l^{th} segment
\mathbf{X}	matrix stores x-coordinates of wind turbines
X_{lb}	lower boundary of the wind farm on x -axis
X_{ub}	upper boundary of the wind farm on x -axis
x_i	x coordinate of T_i
x_{ij}	axial distance between T_j and T_i
\mathbf{Y}	matrix stores y-coordinates of wind turbines
Y_{lb}	lower boundary of the wind farm on y -axis
Y_{ub}	upper boundary of the wind farm on y -axis
y_i	y coordinate of T_i
z	wind turbine height
z_0	surface roughness length
α	dimensionless scalar
β_k	wind direction at k^{th} segment
θ_k	transformed wind direction at k^{th} segment
μ	wind farm efficiency
$\mu_{improve}$	wind farm efficiency improvement by the optimized layout
$\mu_{optimize}$	wind farm efficiency with the optimized layout
μ_{un}	wind farm efficiency with an unoptimized layout
φ	observed power output
ρ	air density

List of Acronyms

AEP	annual energy production
APO	average power output
CFD	computational fluid dynamic
CoE	cost of energy
CoP	cost of power output
GA	Genetic Algorithm
JEDI	Jobs and Economic Development Impact
LCoE	levelized cost of energy
PDF	probability density function
RE	relative error
RMSE	root mean square error
UTM	Universal Transverse Mercator

Chapter 1

Introduction

1.1 Background

Energy is of vital importance to modern society. The energy demand is evolving with the development of technology and society. On one hand, the growth of the population and newly built factories increases the energy demand. On the other hand, traditional energies have the drawbacks of being non-renewable and not clean. The latter drawback will lead to environmental pollution. To cope with these drawbacks, renewable and clean energies have been developed, such as solar energy, hydro energy, and wind energy.

Wind energy is a popular electricity resource across the world in the last few decades. Compared with traditional fossil fuels, wind energy is clean and sustainable. Using wind energy helps to reduce the emission of greenhouse gas and puts a brake on global warming, a great challenge we meet today. The development of wind energy is a global trend given its lower adverse impact on the environment. In 2015, 19% of renewable energy was captured from wind [1], which was about 7% of the sum of global power generation [2]. Global Wind Energy Council [3] reported that global wind energy is 651 GW in 2019, which increased by 10% compared with 2018. Wind energy is producing an increasing amount of power year by year.

In many countries, wind energy plays an important role in producing electricity. In China, wind energy has become the second-largest renewable energy [4]. In 2018, the total wind power output in the U.S. accounted for 6.5% of the electricity to the consumers [5]. Germany has a further onshore wind farm construction expectation and it is estimated that the onshore wind farm will contribute 40% of electricity demand [6].

Canada has developed wind energy projects decades ago. The Canada Wind Energy Association (CanWEA) reported that wind power generation was about 13,413 MW in 2019, which accounts for 6% of the total electricity in Canada [7]. CanWEA also outlines

the wind energy projects will supply 20% of the country's energy demand by 2025. It will cut down the proportion of energy generated from fossil fuels and carbon compounds, which lowers the impact on the environment. Besides, the development of wind energy will also create more corresponding jobs and promote the economy. Therefore, research on wind power generation is essential.

1.2 Wind turbines

A wind turbine is mainly composed of four parts: the tower, hub, blades, and nacelle. Figure 1.1 shows the configurations of the wind turbine. The tower supports the weight of the hub, nacelle, and blades. The hub connects the blades with the shaft of the wind turbine. Normally a wind turbine has two or three blades. The blades rotate at the horizontal axis. The design of turbine blades will directly affect the wind energy production capacity of the wind turbine. The nacelle is a vital part of a wind turbine. It has components like the main shaft, gearbox, generator, voltage transformer, hydraulic unit, cooler system, and rotor lock system. Besides, the wind sensor or called anemometer is usually installed on the nacelle. The anemometer monitors the wind speed and direction. The sensor will send the signal to the control system if the wind speed is too high and shut down the turbine for self-protection.

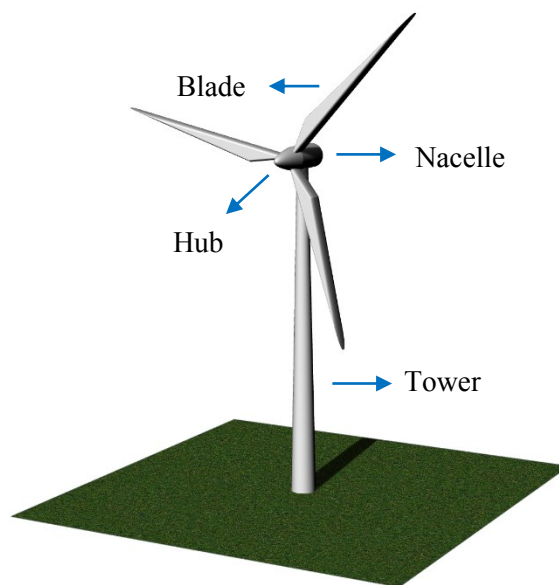


Figure 1.1 Configuration of a wind turbine

1.3 Onshore Wind Farms

Wind farms can be classified to onshore and offshore, which are built on the land and in the ocean, respectively. This thesis will focus on onshore wind farms. The history of the construction of onshore wind farms can be traced back to the 1980s [8]. The onshore wind farm projects started to develop in the U.S. and Europe. Years ago, the wind farm project design strategy is still a hot topic in wind energy study. In the past decade, onshore wind farms took a dominant position in wind farm construction projects [9]. In 2015, the world's onshore wind farm contributed 420 GW power output, whereas offshore wind farms generated 12 GW power output [2]. Figure 1.2 is an onshore wind farm in Canada.



Figure 1.2 An onshore wind farm

Although the potential of constructing offshore wind farms seems higher than onshore wind farms due to the available land resource is reducing quickly and operating risks on the land [10], onshore wind farms still have lots of advantages that offshore wind farms cannot match. Compared with the offshore wind farm, onshore wind farms cost less on construction and maintenance. The construction cost of the offshore wind farm involves fundamental structures (e.g., the submarine cables) and special transportation and installation methods [11]. Installing wind turbines in the ocean is more difficult than on the land. Meanwhile, the maintenance cost of offshore wind farms is also much higher than that of onshore wind farms. The complexity of the ocean environment increases the difficulty of maintenance work. In general, the cost of offshore wind farms is about 2 or 3

times higher than onshore wind farms [12]. Besides, onshore wind farms have a lower adverse impact on the environment. The offshore wind farm may pollute the ocean during construction and maintenance. The offshore wind farm will also affect the marine ecosystem. We still do not have a clear version of the influence of offshore wind farms on wildlife in the ocean.

The onshore wind farm is usually built in regions with rich wind energy resources. It can be built in either a flat area or complex terrain like mountains. A constructed wind farm involves not only wind turbines but also transformer and substation. Figure 1.3 is a simplified process on how wind farm produces electricity by devices. First, the wind blows through the blades of wind turbines will result in the pressure difference between up and down blades to drive blades rotating. The rotating generator will convert the kinetic energy to electrical energy. Second, the transformer (denoted by (2) in Figure 1.3) will increase the low voltage from the wind turbine generator to high voltage. In Figure 1.3 (3), the electricity is collected by the transmission lines for long-distance transmission and the electricity will be delivered to consumers by local electricity distribution companies.

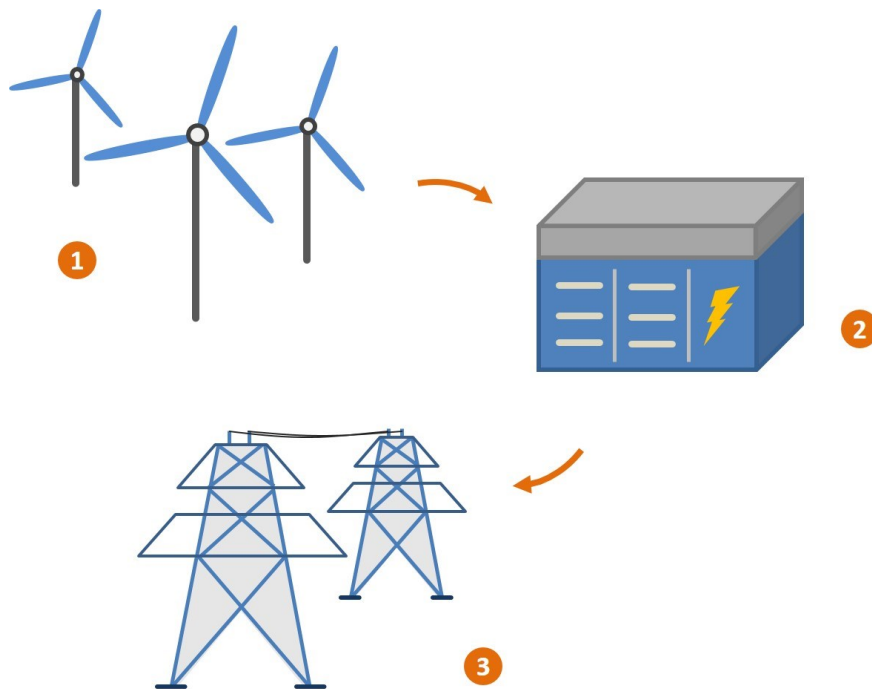


Figure 1.3 How the wind farm works

1.4 Wake effect

Wind turbines installed on a wind farm are connected with cables that transport the electricity to the main power grid. The sum of the power output of individual wind turbines is the total power output of the wind farm. However, not all the wind turbines can produce energy at its full capacity. Wind turbines at upstream will generate wake that affects turbines downstream. The wake will reduce wind speed and increase turbulence [13]. The deficit wind speed will decrease the power output of wind turbines downstream. The increased turbulence will aggravate the mechanical loading of wind turbines at downstream, which will raise wind turbine failure probability. The wake effect is an inevitable problem in wind farms. Therefore, mitigating the wake effect is important in wind energy studies.

A simple representation of the wake effect is shown in Figure 1.4. The area that the wind crosses the blades of a wind turbine is called the near wake region. The wind will mix in the far wake region where turbulence becomes the dominating factor [14]. There is no obvious boundary between the near wake and far wake region. Usually, 2 to 3 rotor diameter behind the wind turbine is seen as near wake region [14][15].

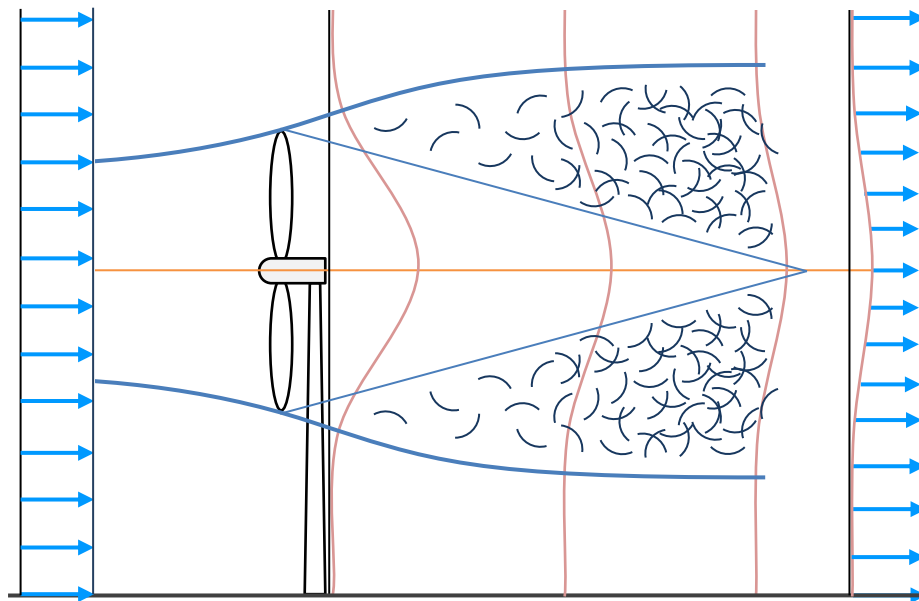


Figure 1.4 Wind turbine wake effect [16]

Several ways can reduce the wake effect, such as wind turbine yaw control, wind farm site selection, wind turbine type selection and wind farm layout optimization [17][18]. Among these methods, wind farm layout optimization is one of the most effective ways to decrease the wake effect. The energy lost by wake effect can be minimized by proper arrangement of positions of wind turbines, which is wind farm layout optimization. Wind farm layout optimization is a comprehensive research topic. A good layout of the wind farm will improve the power output of the wind farm and reduce the load on wind turbines.

1.5 Motivations

Modeling the wind of the wind farm is the starting point to solve wind farm layout optimization problem. Normally, the wind resource involves wind speed and direction. Wind turbine wake effect is sensitive to wind direction. A study shows 10° change in wind direction may decrease 43% of power output [19]. Therefore, using an appropriate wind resource model in wind farm layout optimization will improve the estimation accuracy of wind farm power output and the optimized wind farm layout will be more convincing. Wind farm layout optimization studies use the sector-wise Weibull distribution [20] and joint distribution [21] to characterize the wind resource. Wind speed and direction are separated to sectors and analyzed by statistical distributions. Normally, wind farm layout optimization studies use 30° [22], 15° [23], 10° [20], 5° [24] and 1° [25] as the wind direction segment size to characterize the wind resource. The most commonly used wind direction segment sizes are 30° [22] and 15° [23]. The selection of segment size for wind directions will affect the estimated result of wind farm power output [19]. However, few studies investigated the selection of wind direction segment sizes in wind farm layout optimization. An inappropriate wind direction segment size used in wind farm layout optimization may lead to unreliable optimization results or high computing time during the optimization process.

Feng and Shen [21] evaluated the optimized wind farm layout by using 30° , 10° , 5° , 3° , and 1° as wind direction segment sizes. Wind speed and direction are characterized by joint distributions in their study. They recommended using 1° as the wind direction segment size in layout optimization to obtain a consistent result. Due to the wind speed

and direction are generated randomly, the estimated wind farm power output exists uncertainty. The accuracy of the estimated wind farm power output was not verified properly in their study. The computing time of wind farm layout optimization with different wind direction segment sizes was not considered in their work. In addition, wind farms with different sizes were not investigated when making recommendations.

The selection of wind direction segment sizes will affect the result in wind farm layout optimization. A universal and comprehensive guideline for selecting proper wind direction segment sizes in wind farm layout optimization studies is required. Therefore, in this thesis, an approach for wind direction segment size selection in wind farm layout optimization will be proposed. Wind farm power output and its estimation accuracy, together with computing time, will be considered in the optimization process. In addition, case studies are important in wind farm layout optimization. The proposed approach will be demonstrated by case studies and the result will be beneficial to wind farm operators, researchers and developers. For wind farm operators, strategies on power output calculation with high estimation accuracy will be provided. For researchers, the presented wind direction segment sizes can be selected based on their requirements on estimation accuracy, computing time and improvement on wind farm power output. For wind farm developers, this thesis will provide a complete process for optimizing the wind farm, which can guide wind farm developers to design wind farms in the future.

1.6 Research objectives

This thesis has two main objectives: 1) proposing a comprehensive approach for selecting proper wind direction segment sizes in wind farm layout optimization studies. 2) demonstrating the proposed approach by case studies and presenting different wind direction segment size selection strategies based on the optimization results.

The proposed approach involves five steps: modeling the wind farm power output and defining the objective function, pre-processing the data of the target wind farm, selecting an appropriate wind resource sample size for wind farm layout optimization, evaluating the estimated power output of the target wind farm, and optimizing the wind farm layout

using genetic algorithm (GA). The proposed approach will be illustrated by case studies. The case studies involve a real onshore wind farm with one-year observed data. Based on the results, future wind farm layout optimization studies that use the same wind farm power output model with this thesis can directly apply the suggested wind direction segment size to optimize the wind farm layout. With the proposed approach, different wind farm power output models can be incorporated to select proper wind direction segment sizes in wind farm layout optimization.

In order to obtain a convincing optimized wind farm layout, the accuracy of the estimated wind farm power output is crucial to this problem. Before the optimization process, the estimated wind farm power output will be evaluated by comparing with the observed wind farm power output. An appropriate wind resource sample size with high power output estimation accuracy will be selected for wind farm layout optimization, which is not studied in other wind farm layout optimization problems. Ten different wind direction segment sizes will be tested in wind farm power output calculation and evaluated by the mean relative change, range of relative change and CPU time. By comparing the evaluated results, the most accurate way to estimate the wind farm power output will be presented.

In case studies, wind farm layouts will be optimized, which will mitigate the wake effect to a great extent and promote the power generation capacity of the wind farm. This thesis mainly solves two problems: one aiming to improve the average power output of the wind farm, and the other aiming to minimize the cost of the unit power output of the wind farm.

For the first problem, this thesis aims to maximize the average power output (APO) of the wind farm by optimizing the wind farm layout with a fixed number of wind turbines. The maximum wind farm power output generation is achieved by selecting the best positions of wind turbines. Three case studies will be investigated. Wind farm layouts will be optimized with 10 different wind direction segment sizes. Wind farm power output and its estimation accuracy, together with computing time, are considered in the optimization process. Based on the evaluated results, different wind direction segment size selection strategies will be presented.

For the second problem, this thesis aims to minimize the cost of the unit power output of the wind farm by optimizing the wind farm layout with various number of wind turbines. The cost of unit power output is denoted by CoP in this thesis. The difference between the first and second optimization cases is that the turbine number is already fixed or not. In most of the real cases, both the numbers and positions of wind turbines should be considered when designing a wind farm [18]. Installing more wind turbines will generate higher power output, but the corresponding cost will also increase. Although a specific number of wind turbines may generate high wind farm power output, the profit from the wind farm with such a number of turbines might be low. Therefore, CoP is used as the objective function of the wind farm layout optimization problem when the number of wind turbines is undecided. Due to the time limitation of the master's program, only one wind direction segment size will be used as an example to minimize the CoP.

This thesis is organized as follows. Chapter 2 presents a literature review of wind farm layout optimization. The review provides the fundamental knowledge and published studies in each step of solving this problem. Chapter 3 introduces models used to calculate the wind farm power output, objective functions, algorithms and the proposed approach for selecting proper wind direction segment sizes in wind farm layout optimization. Chapter 4 describes the target wind farm data and assesses the wind farm power output. Chapter 5 presents the optimization results and evaluations of the optimized wind farms. Finally, Chapter 6 concludes this thesis and gives meaningful future works.

Chapter 2

Literature Review and Fundamentals

As mentioned in Section 1.3, wind farm layout optimization is one of the most effective ways to mitigate the wake effect. Wind farm layout optimization was first studied by Mosetti *et al.* [26] in 1994. They optimized a wind farm layout with 10×10 grids by using the Genetic Algorithm (GA) to minimize the cost of energy (CoE) which they first proposed. Mosetti's study gave us a general framework on how to solve this layout optimization problem. The framework involves characterizing the wind speed and direction, modeling the wake effect of the wind farm, defining the average power output function of the wind farm and optimizing the wind farm layout to improve the average wind farm power output. However, Mosetti's study simplified the wind speed levels to three velocities (i.e., 8 m/s, 12 m/s, and 17 m/s) which is not realistic. Their study also used the GA without enough iterations and applied single wake effect. Grady *et al.* [27] improved the configurations of GA used in Mosetti's study. They increased gene numbers and the number of iterations to ensure that the obtained optimal result is global. Years ago, wind farm layout optimization became a comprehensive research topic. Studies on this problem is not limited on improving the work by Mosetti *et al.* Complex factors and multiple objects are gradually considered in the optimization problem, such as noise level [28], the participation of landowners [29], and a trade-off between the average and variance power output [30]. In this chapter, we will first explain the fundamentals of wind farm layout optimization in Section 2.1. Afterwards, critical reviews will be conducted in Section 2.2-2.6. Section 2.2 reviews wind characteristic. Section 2.3 reviews the wake effect model used in this problem. Section 2.4 introduces the wind turbine power curve. Section 2.5 explains two commonly used objective functions in this problem. Section 2.6 presents optimization process.

2.1 General framework of wind farm layout optimization

Although wind farm layout optimization is a comprehensive research topic, most of studies follow a general framework to solve this problem [31][25]. The problem is formulated by following modules.

- 1) Characterizing wind resources. Normally, the wind resource involves wind speed and direction. Wind speed and direction of the wind farm will be determined and used in the wake effect model later.
- 2) Modeling the wind turbine wake effect. As mentioned in Section 1.4, the wake effect generated by upstream wind turbines will reduce downstream wind speed. The area of the wake effect is changing with wind direction. The wake effect model will mathematically describe the wind speed reduction phenomenon, and thus enable the calculation of wind speeds at each wind turbine in the wind farm based on the wind speed and direction given by the wind resource model.
- 3) Estimating the power output of the wind farm. The wind turbine power output is highly correlated with wind speed at the wind turbine. People use the wind turbine power curve to estimate the wind turbine power output at various wind speeds [32]. The estimated wind farm power output is the sum of individual wind turbine power outputs.
- 4) Defining the objective function of wind farm layout optimization. The objective functions might be different based on the specific research interests in wind farm layout optimization. Normally, wind farm layout optimization aims to maximize the wind farm power output. Other typical objective functions include minimizing the CoE of the wind farm [29], minimizing noise level [28] and power variance [30].
- 5) Optimizing the wind farm layout. In this last module, the wind farm layout optimization problem is solved using algorithms such as gradient-based methods or evolutionary methods, and thus we obtain the optimal wind farm layout that maximize the wind farm power output or minimize the CoE of the wind farm.

Critical review for each module will be presented in Section 2.2 to 2.6.

2.2 Wind characteristics

Wind data analysis is the starting point for wind farm layout optimization. An appropriate wind resource model is crucial for the predication of the wind farm power output accurately. The wind resource is characterized with wind speed and direction in a time period.

Wind speed analysis methods can be classified to non-statistical and statistical methods. The non-statistical method involves direct use of data [33] and method of bins [25]. Feng and Shen [21] investigated the numerical calculation of wind modeling with different wind speed bin sizes. They showed that choosing a small enough bin size is critical to obtain reliable and consistent optimization results. The statistical method considers the wind speed as a random variable [34]. The probability distribution of wind speed describes the likelihood of the occurrence of a random wind speed. Weibull distribution provides a good representation on wind speed. Justus *et al.* [35] used Weibull distribution to fit wind speed data at approximately 135 sites across the United States. Corotis *et al.* [36] compared the fitting performance of Weibull distribution and Chi-squared distribution on observed wind speed and power histogram using goodness-of-fit test. The result showed that Weibull distribution has a slight improvement on fitting performance compared with Chi-squared distribution. Weibull distribution was also compared with square-root-normal distribution on fitting 30 months observed wind speed at Concord by Justus *et al.* [37]. They found that Weibull distribution has a smaller root mean square error. Garcia *et al.* [38] compared the suitability of Weibull distribution and Lognormal distribution on describing the wind speed frequency curve by R^2 coefficient. It was found that both distributions fit well, whereas Weibull distribution gives a higher R^2 coefficient. In summary, Weibull distribution presents many advantages such as high flexibility and simplicity of parameters estimation, which is widely used in wind speed analysis studies [39].

Many studies solve the wind farm layout optimization problem considering simplified wind resources: wind with constant speed and fixed direction, or wind with constant speed and variable directions [27][40][41]. The optimized wind farm layouts are not convincing. A more realistic case is to consider wind with variable speeds and directions.

A common way to show the relationship of wind speed and direction is to draw a wind rose. Table 2.1 is an example of the frequency distribution of wind speeds occurring at different wind directions. The wind resource data is obtained from a real wind farm. Figure 2.1 shows the wind rose of the wind farm. Compared with Table 2.1, the wind rose give a succinct view on the distribution of wind speed and direction. In Figure 2.1, the wind direction from 0° to 360° is divided into 12 equal sectors and wind speed is divided into 6 ranges marked with different colors. Circles in Figure 2.1 accounts for 4.2%, 8.5%, 12.7% and 16.9% respectively. The portion marked by a single color in a wind direction sector means the wind speed occurring in that wind direction bin. The sum of colored portions in the wind rose is 100%.

Table 2.1 Frequency distribution of wind resource of a wind farm

Directions	0-4 m/s	4-6 m/s	6-8 m/s	8-10 m/s	10-12 m/s	12-25 m/s	Total
North	0.67 %	1.34 %	0.67 %	0.94 %	0.27 %	0.4 %	4.29 %
NNE	1.88 %	1.75 %	0.13 %	0	0.13 %	0	3.89 %
NE	2.15 %	1.21 %	0.13 %	0	0	0.13 %	3.62 %
ENE	2.02 %	0.94 %	0	0	0	0	2.96 %
East	2.96 %	1.48 %	0.54 %	0.27 %	0.13 %	0	5.38 %
ESE	1.34 %	2.15 %	1.21 %	0.54 %	0	0.13 %	5.37 %
SE	2.02 %	2.02 %	0.54 %	1.61 %	0.27 %	0	6.46 %
SSE	2.82 %	1.61 %	1.21 %	2.28 %	1.61 %	0.81 %	10.34 %
South	3.23 %	0.94 %	0.27 %	0.4 %	0	0	4.84 %
SSW	1.61 %	0.4 %	0.27 %	0	0	0	2.28 %
SW	1.21 %	1.08 %	1.08 %	0.27 %	0.13 %	0	3.77 %
WSW	1.75 %	0.54 %	0.81 %	0.27 %	0	0	3.37 %
West	1.34 %	0.81 %	0.94 %	1.61 %	0.54 %	0.27 %	5.51 %
WNW	3.9 %	0.81 %	2.15 %	2.02 %	0.67 %	0.27 %	9.82 %
NW	4.84 %	4.44 %	2.28 %	2.15 %	1.88 %	1.34 %	16.93 %
NNW	2.96 %	3.63 %	2.42 %	0.67 %	0.94 %	0.54 %	11.16 %
Total	36.7 %	25.15 %	14.65 %	13.03 %	6.57 %	3.89 %	100 %

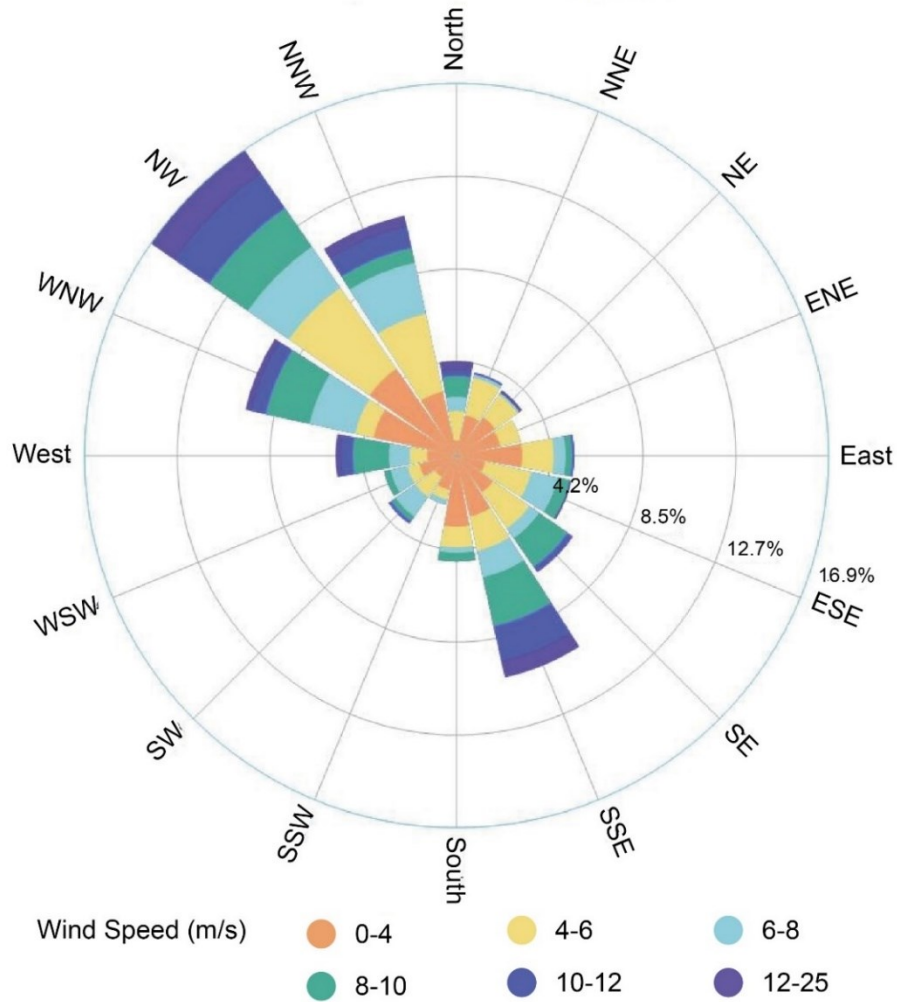


Figure 2.1 Wind rose of a wind farm

In order to show the uncertainty of wind resource, most wind farm layout optimization studies characterize wind speed and direction by sector-wise Weibull distribution [25][23]. The wind direction is separated to bins or called sectors with equal size [25]. The wind speed in each bin of wind direction is characterized by Weibull distribution [23].

Some studies considers the variation of wind speed and direction comprehensively in a single model [42][21]. Carta *et al.* [42] used a joint probability density function of wind speed and direction to analyze the wind energy. Feng and Shen [21] applied joint distribution in wind farm layout optimization. They first obtained the parameters by the fitted Weibull distribution. Then using the parameters to construct three joint

distributions: piecewise, linear and spline joint distribution of the wind speed and direction. The result showed spline joint distribution best fits the data obtained from a wind farm they investigated.

Porté-Agel *et al.* [19] found wind turbine wake effect is very sensitive to wind direction. The worst case in their study shows 10° change in wind direction can decrease 43% of power output. The selection of segment size for wind direction will affect the estimated result of wind farm power output and optimized result of wind farm layout [21]. The wind direction is divided into segments by sector-wise Weibull distribution [24] and joint distribution [21] in wind farm layout optimization studies. Wind farm layout optimization studies use 30° [22], 15° [23], 10° [20], 5° [24] and 1° [25] as wind direction segment sizes to characterize the wind resource. Among these wind direction segment sizes, 30° [22] and 15° [23] are the most widely used wind direction segment sizes. However, few studies investigated the selection of wind direction segment sizes in wind farm layout optimization.

Feng and Shen [21] investigated the choice of segment sizes for wind speed and wind direction in wind farm power output calculation and layout optimization. They found the segment size for wind speed has a slight effect on the optimized result, while the selection of wind direction segment is crucial to wind farm layout optimization. The wind resource is characterized by joint distributions and 30° , 10° , 5° , 3° and 1° are the investigated wind direction segment sizes in their study. They concluded that 10° is a better choice for wind farm power output calculation, which has high estimation accuracy and without increase CPU time dramatically. Besides, they re-evaluated the power output of the optimized layouts by using different wind resource samples and found 1° gives a more consistent power output improvement. However, the uncertainty of wind farm power output estimation was not considered in their study. Due to the wind resource is randomly generated, the estimated power output is different in each simulation. They only calculated the power output of the original wind farm one time and the analyze is not convincing enough. The stability analysis for the estimated wind farm power output should be considered. The computing time of wind farm layout optimization with different wind direction segment sizes was not considered in their work. In addition, wind

farms with different sizes were not investigated when making recommendations. The wind direction segment size should be selected by evaluating different aspects in the optimization process.

2.3 Wake effect model

Modeling the wind turbine wake effect is essential to calculate the wind speeds at wind turbines. As mentioned in Section 1.4, the wind turbine wake is separated to near wake region and far wake region. Researches on the near wake region often focus on the performance and physical process of power extraction, whereas researches on the far wake region aim to the mutual influence when wind turbines are placed in clusters, like wind farms [43]. In wind farm layout optimization problem, normally the safe distance between two wind turbines is farther than the near wake distance. Therefore, only far wake region is considered in wind farm layout optimization.

The wind speed deficit by wake effect can be expressed by analytic models and computational models [44]. The analytical models follow the law of conservation of momentum. They ignored the initial wake effect expanding region and the change of turbulence intensity behind the wind turbine [14]. Jensen's model [45], Larsen's model [46], and Frandsen' model [47] are famous analytical models. These three models are shown in Figure 2.2, Figure 2.3, Figure 2.4, respectively [48], which will be explained later. The computational models based on computational fluid dynamic (CFD) aims at solving fluid flow equations to obtain wake velocity field [14], which has a high computational complexity.

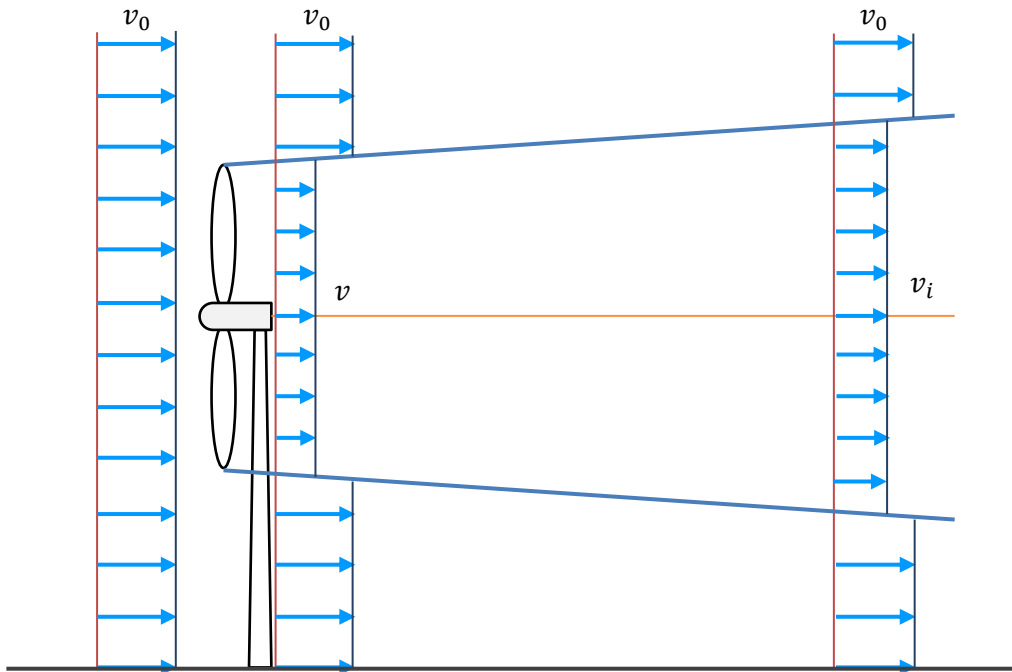


Figure 2.2 Jensen's model [48]

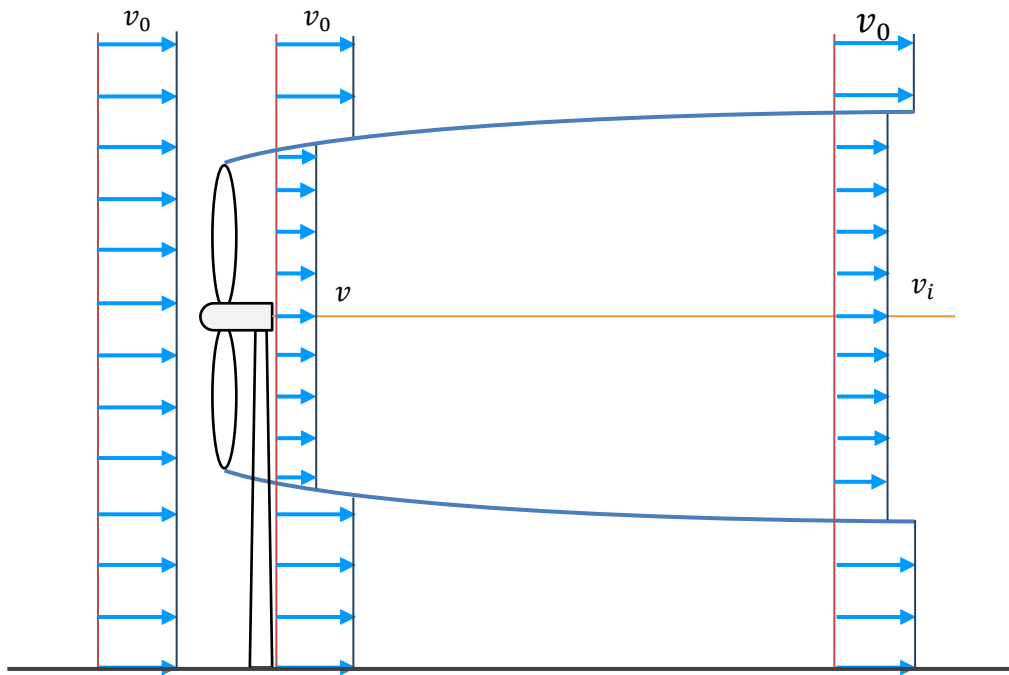


Figure 2.3 Larsen's model [48]

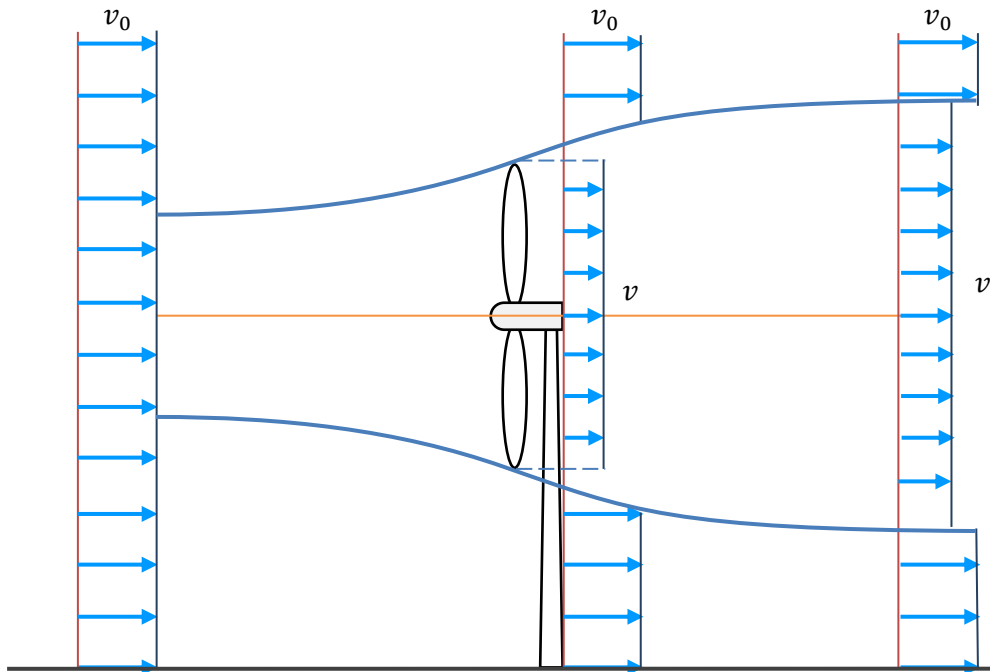


Figure 2.4 Frandsen's model [48]

Jensen's model is the most widely used wake effect model in wind farm layout optimization [27][25][40]. It is one of the most classical wake effect models, which is proposed by N. O. Jensen in 1983 [45] and modified later by Katic *et al.* [49]. Figure 2.2 shows Jensen's model. The wake behind the wind turbine spreads like a cone. Jensen's model is concerned with a single wind turbine. The multiple wake effect models applied to wind farm layout optimization can be derived from Jensen's model [30][25]. The wind speed deficit at the downstream wind turbine is the root sum square of single wind speed deficit by Jensen's model.

Larsen's model is based on the Prandtl turbulent boundary layer equations [14]. The axis-symmetric form of Reynolds-averaged Navier-Stokes equations is considered in Larsen's model using the first and second order approximations [13]. As shown in Figure 2.3, the flow behind the wind turbine is assumed symmetric on axis but does not spread linearly. The wake expands and diminishes gradually with the increase of distance behind the wind turbine.

Frandsen's model considers the initial flow around and through the wind turbine [27]. It follows the conservation of momentum law, similar to Jensen's model. Figure 2.4 shows the wake expansion of Frandsen's model. The wake area equals to the cylinder cross-section area and the wind speed is the same on the horizontal axis [48].

Gaussian-based model is another widely used wake effect model in recent years [44][41]. Figure 2.5 shows the Gaussian-based model. Bastankhah and Porté-Agel [44] investigated wind turbine wake effect by proposing a new model with the wind speed deficit in the wake region followed a Gaussian distribution. Their study showed the wind speed deficit by Gaussian distribution is acceptable with the computational fluid dynamic simulations. Later, the Gaussian-based model was applied in wind farm layout optimization by Parada *et al.* [41]. They implemented the Gaussian-based model to a wind farm with three conditions: constant wind speed and direction, constant wind speed and variable wind direction, and variable wind speed and direction as shown in Grady's work [27] and compared the results. They found that the Gaussian-based model showed robust performance in optimization result. However, for complex wind farm conditions, the Gaussian-based model cannot lead to greater efficiency on optimization.

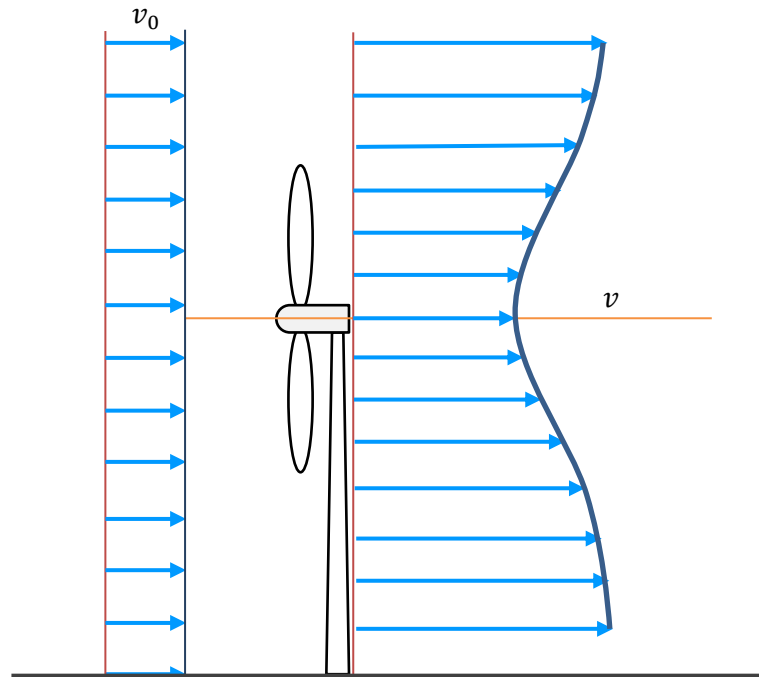


Figure 2.5 Gaussian based model

Except for the wake effect models mentioned above, another type of wake effect model considers the complex terrain. Sun and Yang [50] proposed a three-dimensional wake effect model based on the flow flux conservation law. The three-dimensional wake model can describe the spatial distribution of wind speed effectively and provide theoretical contribution to the single wake effect study. The three-dimensional wake effect model was extended by Sun *et al.* [51] from single wind turbine wake to multiple wind turbines wake. By comparing the analytical results with the observed wind speed, their model showed good accuracy at far wake positions on horizontal axis. For the vertical direction, the proposed wake model had better predictions on high positions than near-ground positions. Brogna *et al.* [52] proposed a wake model applied to complex terrain by developing the Gaussian-based model from two dimensions to three dimensions. The centerline of the Gaussian shaped model will change based on the streamline behind the wind turbine. Their method of developing the Gaussian-based model can also be applied to other wake effect models and optimizes the wind farm with complex terrain.

2.4 Wind turbine power curve

In order to evaluate the amount of power a wind farm generates, the power output of each wind turbine in the wind farm needs to be estimated. According to the kinetic energy formula, the power output of a wind turbine is dependent on the wind speed at the wind turbine [33]. Wind turbine power curve is used to illustrate the relationship of the wind speed and power output. Normally, the power curve is divided into two categories: deterministic and probabilistic. The deterministic power curve builds a fixed relationship between the wind speed and the corresponding power output [32]. The probabilistic power curve shows the status of power generation under given wind speeds in a time period.

Deterministic power curves can be further classified into parametric and non-parametric [53]. The parametric power curves are continuous and fitted by the raw wind speed and power output data, such as polynomial power curve, cubic power curve, approximate cubic power curve and exponential power curve [54]. Usually, these curves are fitted by least squares method by minimizing the sum squares of the residuals

between estimated power output and the observed power output. Typical non-parametric models include bins methods [55] and artificial neural network models [56].

The probabilistic power curve estimates wind speeds considering the uncertainty of power output. Jin and Tian [57] proposed a dynamic power curve. They assumed that wind turbine will generate random power output at the given wind speed. The power output at the given wind speed is characterized by mean and a constant standard deviation of the power output at this wind speed. Yan *et al.* [32] used Gaussian density function with a stochastic standard deviation to represent the difference between the observed and fitted power output at different wind speeds. The random power output is generated by Monte Carlo simulation. Compared with the deterministic model, the probabilistic model is more difficult to fit and requires a higher CPU time.

In wind farm layout optimization, the power curve was applied on wind energy estimation [58] and wind turbine selection [18]. The deterministic power curve is clear and concise to show the dependency of wind speed and power output. The probabilistic power curve is more complex than the deterministic one, which will increase the computational complexity significantly. Wind farm layout optimization usually requires a large number of evaluations of layouts to get the final optimal layout. Using probabilistic power curve will likely make the wind farm layout optimization computationally impossible. Therefore, the deterministic power curve is more frequently used in wind farm layout optimization than its counterpart.

2.5 Objective functions

Two objective functions are widely used in wind farm layout optimization: maximizing the average power output (APO) of the wind farm [25] and minimizing the cost of energy (CoE) [40].

The first objective aims to maximize the APO of the wind farm by optimizing the wind farm layout. Wind farm projects use the annual energy production (AEP) to estimate the overall electrical energy that the wind farm can produce in a year [18]. AEP is the product of hours of a year and the average power output of the wind farm. The result is measured in kilowatt-hour or megawatt-hour. Maximizing AEP is identical to

maximizing the APO of the wind farm. However, maximizing the APO of a wind farm is not an appropriate objective function when the number of wind turbines is undecided. Installing more wind turbines on the wind farm can generate higher power output in total. But, the cost will also increase. Therefore, the second objective is more suitable in wind farm layout optimization when the number of wind turbines is variable.

The second objective is to minimize the CoE of the wind farm. The CoE was first proposed by Mosetti *et al.* [26], in which the cost only depends on the quantity of turbines in the wind farm. Later, researchers [59][29] proposed to consider more factors concerned with wind farm cost in the CoE. Chen [59] considered Jobs and Economic Development Impact (JEDI) and used the wind farm cost data in Texas, USA. The CoE became more practical as JEDI involves the cost on wind farmland lease, labor and job market. Chen and MacDonald [29] considered maintenance, replacement overhaul and landowner remittance cost in the CoE. The levelized cost of energy (LCoE) is also used in wind farm financial evaluation [60]. The LCoE estimates the mean cost of energy throughout the lifetime of a wind farm [61]. The LCoE considers cost incurred in the initial cost, operation and maintenance cost and variable cost such as fuel cost and tax cost in each year. The discount rate is an important coefficient in the LCoE function, which is the interest rate of how much the future cash flow is at present. Izquierdo-Pérez *et al.* [60] applied LCoE function in wind farm layout optimization problem. The LCoE is more useful for the financial evaluation of a real wind farm. The difficulty for implementing the LCoE model is the need of the real cost data and other corresponding coefficients such as the discount rate, which may be hard to collect.

Some studies consider more factors in addition to wind resources in the objective function of wind farm layout optimization. Chen *et al.* [28] considered the noise level and the lease soft cost of the wind farm in the CoE function. Their work used the real house locations and aimed to minimize the CoE of the wind farm with the participation of landowners. They also incorporated the relationship of the noise level and corresponded probabilistic compensation of the landowners. Chen and MacDonald [29] minimized the LCoE of the wind farm together with the landowner participation rate. Chowdhury *et al.* [18] provided an optimal decision-making strategies on both wind turbine position

selection and type selection. Their optimal solutions aimed to minimize the CoE of the wind farm.

There are some other studies focus on the trade-off between multiple objectives in wind farm layout optimization. Wang *et al.* [30] proposed a strategy to optimize the wind farm layout by trading off the average and variance of the wind farm power output. They used the weighted optimization and confidence interval optimization on the objective function respectively. The two optimizations are compared in terms of the performance on trading off the wind farm power output and the power variance. Mittal *et al.* [62] proposed a strategy on another multi-object problem: maximizing AEP and minimizing noise. Their work provided alternative solutions of a trade-off between energy and noise to the decision maker.

The solutions of wind farm layout optimization will change based on different factors and objectives. Considering more factors and objectives will be closer to the real situations, but it also requires more corresponding data and sometimes it might be difficult. The comprehensive studies are useful guidelines for wind farm design.

2.6 Optimization process

In the optimization process, we first select a design method for the wind farm layout, and then optimize the layout by an optimization algorithm.

The design methods can be mainly classified to the grid method [27][41][63] and the unrestricted coordinate method [18][31][64]. The grid method separates the wind farm to many square grids with equal sizes. The wind turbine can only be placed at the center of the grid. The unrestricted coordinate method, or coordinate method, places the wind farm into the Cartesian coordinate system. Wind turbines can be freely placed at any position in the wind farm. The positions where wind turbines can be placed are restricted by the grid method. Therefore, the coordinate method is superior to the grid method on the optimization accuracy and best fitness result. However, the optimization efficiency should also be studied to evaluate these two methods comprehensively. Wang *et al.* [40] compared the grid method with three grid densities (i.e., 10×10 , 20×20 and 50×50) and unrestricted coordinate method on a square wind farm. They found that the optimized

result by the grid method with high grid density was closer to the optimized result by the coordinate method. However, the CPU time also increased significantly. The grid method and coordinate method on wind farm with irregular shape was compared later in [23]. The result showed the wind farm power output of the optimized layout by the high-density grid method was close to the result by the coordinate method.

The optimization algorithms can be divided into gradient-based and gradient-free algorithms [52]. The gradient-based algorithm needs the derivative information. The drawback of the gradient-based algorithm is that the optimization tends to fail if the objective function is too complicated. In addition, it needs a good initial guess; otherwise, it will be hard to converge or be trapped in a local minimizer. Wind farm layout optimization has high complexity on variable numbers and iterative evaluations of wind speeds. Therefore, applying gradient-based algorithms to this problem is not preferred. Various gradient-free algorithms have been applied to the wind farm layout optimization problem, such as Genetic Algorithm [26][27], Random Search Algorithm [25], Simulated Annealing [65] and Particle Swarm Algorithm [66][67]. Brogna *et al.* [52] compared eight commonly used optimization algorithms in their study on a wind farm with a complex terrain. Among them, six are gradient-free and two are gradient-based. Although all algorithms in their study improved the wind farm layout, the gradient-free algorithms performed better than gradient-based algorithms in general. The result showed gradient-based algorithms required higher computation time on one computing iteration compared with gradient-free algorithms. The optimization results by gradient-based algorithms were also worse than gradient-free algorithms. In addition, they found the Random Search Algorithm got the best optimization result for their target wind farm.

In summary, wind farm layout optimization is a complex problem. The problem is formulated by sections in this chapter. Models and methods used to solve wind farm layout optimization are reviewed in each section. In the next chapter, detailed models and methodologies used in this thesis will be introduced, including the proposed approach for wind direction segment size selection in wind farm layout optimization.

Chapter 3

Models and Methodologies

In this chapter, the detailed models to calculate the wind farm power output will be introduced. The objective functions and optimization algorithm will be explained. Besides, the approach for wind direction segment size selection in wind farm layout optimization will be proposed. Section 3.1 introduces the wind resource model. Section 3.2 presents the position model, which is not explained clearly in most of wind farm layout optimization studies. Section 3.3 explains the wake effect model used in this study. Section 3.4 presents the power output model. Section 3.5 defines two objective functions of wind farm layout optimization. Section 3.6 explains the algorithm used in optimization process. Section 3.7 proposes the approach for selecting proper wind direction segment sizes in wind farm layout optimization. The last section is the summary.

3.1 Wind resource model

An appropriate wind resource model has high accuracy on wind farm power output estimation [25]. The wind resource involves wind speed and wind direction. Many studies simplify the wind resource to wind with constant speed and fixed direction, or wind with constant speed and variable directions [26][27]. The wind resource is modeled idealized in the simplified cases, which will lead to a great error on the estimated result of wind farm power output. In a real wind farm, wind speed and direction are changing continuously. Therefore, an appropriate wind resource model should be capable to show the variation of wind speed and direction in the wind farm.

In this thesis, the sector-wise Weibull distribution [24] will be used to characterize the wind resource. Wind direction from 0° to 360° is separated to k segments with equal segment size. The wind direction distribution is represented by the proportion of wind direction for each segment. The proportion of wind direction β_k for k -th segment is represented by p_k . The wind speed occurring in each wind direction segment is approximated by the Weibull distribution. Weibull distribution is widely used in wind

speed analysis [39] and wind farm layout optimization [23]. The probability density function (PDF) of wind speed v_l occurring at wind direction β_k is denoted by $f(v_l, \beta_k)$, where l is the step size of wind speed. The expression of $f(v_l, \beta_k)$ is

$$f(v_l, \beta_k) = \frac{b_k}{a_k} \left(\frac{v_l}{a_k}\right)^{b_k-1} e^{-\left(\frac{v_l}{a_k}\right)^{b_k}} \quad (3.1)$$

where a_k and b_k are the scale and shape parameter of Weibull distribution at k -th wind direction segment. The simulated wind speed will be the free wind speed of the wind farm, which is not affected by the wake of wind turbines. Two assumptions are made for wind conditions: 1) The wind direction is the same at any position of the wind farm. 2) Wind speed occurs in the same wind direction segment follows the same Weibull distribution at any position of the wind farm. Monte Carlo simulation will be used to randomly generate the wind speed data following the correlated Weibull distribution.

3.2 Position model

Many studies of wind farm layout optimization did not show a clear version on how they build the wind farm coordinate system at different wind directions [23][30]. In this section, a position model will be presented to indicate the relationship of the wind direction and positions of wind turbines.

The wind direction is supposed to be parallel with the nacelles of all wind turbines in the wind farm. In this study, the wind turbine yaw control system will not be considered. The wake effect direction only depends on wind direction. In order to absorb the maximal energy from wind, the blades of the wind turbine should keep orthogonal with the wind direction, which is illustrated in Figure 3.1.



Figure 3.1 Wind direction and wind turbine

The wind farm is put into a coordinate system. The positions of wind turbines are represented by coordinates. θ_k is used to represent the wind direction in the position model. Suppose that θ_k is 0 degree on negative x-axis. When θ_k equals to 0, the wind farm coordinate system is represented by $[\mathbf{X}, \mathbf{Y}]^T$, where \mathbf{X} and \mathbf{Y} are two matrices store x-coordinates and y-coordinates of wind turbines respectively. When θ_k is not 0, $[\mathbf{X}, \mathbf{Y}]^T$ will be transferred to $[\mathbf{X}_k, \mathbf{Y}_k]^T$ to keep the nacelle of the wind turbine always be aligned with θ_k . Figure 3.2 is the illustration of the position model.

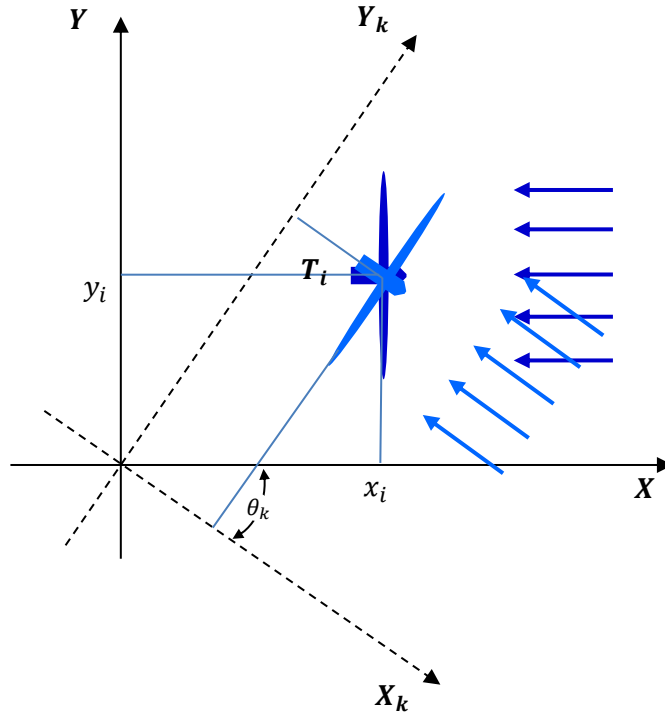


Figure 3.2 Illustration of the position model

The wind farm coordinate system rotates clockwise with the increase of θ_k . The position model for the wind farm is shown below [31]:

$$\begin{bmatrix} X_k \\ Y_k \end{bmatrix} = \begin{bmatrix} \cos\theta_k & -\sin\theta_k \\ \sin\theta_k & \cos\theta_k \end{bmatrix} \begin{bmatrix} X \\ Y \end{bmatrix} \quad (3.2)$$

The measurement of wind direction in the position model is different from that used for wind sensors. In the real wind farm, normally the 0-degree wind observed by the wind sensor is from North to South, which is denoted by negative y-axis in the coordinate system. However, 0-degree wind in the position model is on negative x-axis. Therefore, the observed wind direction should be transformed to the calculated direction in the position model. Equation (3.3) is the transformation of the observed wind direction β_k and the calculated wind direction θ_k in the position model. Both of them are measured in radian.

$$\theta_k = \begin{cases} \beta_k + \frac{3\pi}{2}, & \beta_k < \frac{\pi}{2} \\ \beta_k - \frac{\pi}{2}, & \beta_k \geq \frac{\pi}{2} \end{cases} \quad (3.3)$$

3.3 Wake effect model

The wake effect model is the key model to calculate the wind farm power output. It estimates the wind speed at each wind turbine in the wind farm. In this section, the wake effect model will be explained from simple to complex and the process for wind speed estimation by wake effect model will be proposed.

Section 3.3.1 introduces the aerodynamics of wind turbines, which is the foundation of the wind turbine wake effect. Section 3.3.2 introduces Jensen's model, which is the single wake effect model in this thesis. Section 3.3.3 explains the wake conditions. Section 3.3.4 presents the multiple wake effect model. Section 3.3.5 proposes the wind speed estimation process by the wake effect model.

3.3.1 Aerodynamics of wind turbines

The aerodynamics is important to wind turbines as it explains how wind turbines capture energy. The power output generated by the wind turbine depends on the interaction of rotor and wind [33]. The aerodynamic forces by the wind determines the wind turbine performance such as power output and loads. The analysis of wind turbine aerodynamics is not limited to any particular type of wind turbine [33].

An idealized wind turbine is assumed based on the one-dimensional momentum theory [33], which is shown in Figure 3.3. The characteristics of the idealized wind turbine involves: steady air flow, no friction during the whole process, and uniform thrust over the blades [33]. In this section, the idealized model will be used to analyze the maximum energy that the wind turbine can extract from the kinetic energy. In addition, important coefficients for wind turbines will also be introduced.

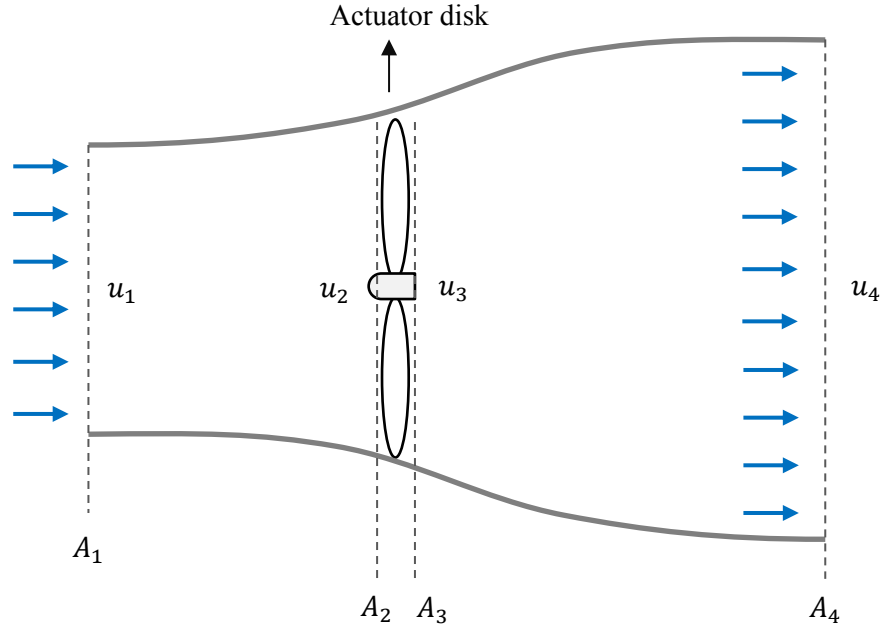


Figure 3.3 Idealized wind turbine and air flow

The mass of air flow passing per unit time is the mass flow rate, which is represented by \dot{m} . According to the conservation of momentum law, the mass flow rate for a constant flow in Figure 3.3 can be written as:

$$\dot{m} = \rho A_1 u_1 = \rho A_2 u_2 = \rho A_4 u_4 \quad (3.4)$$

where A_1 , A_2 and A_4 are the vertical wind cross-section area, u_1 , u_2 and u_4 are wind speeds of the idealized wind turbine at indicated locations and ρ is the air density. The wind cross-section area at each side of actuator disk is the same, which means A_2 equals to A_3 . The wind across the rotor disk remains the same speed, which means u_2 equals to u_3 .

The thrust of wind is the force that the wind acts on the actuator disk. Set Δu as the difference of u_1 and u_4 . According to the momentum theory in fluid dynamics, the thrust T is calculated as:

$$T = \dot{m} \cdot \Delta u = \rho A_2 u_2 (u_1 - u_4) \quad (3.5)$$

The thrust multiplies the wind speed at the actuator disk is the power output of the wind turbine. The formula of power output P is expressed as:

$$P = T \cdot u_2 = \rho A_2 u_2^2 (u_1 - u_4) \quad (3.6)$$

The power output of the idealized wind turbine can also be represented by the energy absorbed in a unit time, which is written as:

$$P = \frac{\frac{1}{2} m u_1^2 - \frac{1}{2} m u_4^2}{\Delta t} = \frac{1}{2} \dot{m} (u_1^2 - u_4^2) = \frac{1}{2} \rho A_2 u_2 (u_1^2 - u_4^2) \quad (3.7)$$

By equating Equation (3.6) and Equation (3.7), the following relationship of u_1 , u_2 and u_4 can be obtained:

$$u_2 = \frac{u_1 + u_4}{2} \quad (3.8)$$

The axial induction factor a is the fractional decrease between u_1 and u_2 , which is given by [33]:

$$a = \frac{u_1 - u_2}{u_1} \quad (3.9)$$

By substituting Equation (3.8) into Equation (3.9), the expressions of u_2 and u_4 are shown in Equations (3.10) and (3.11). Equations (3.10) and (3.11) can also be obtained by applying Bernoulli function to the idealized wind turbine model. The detailed process can be found in [33].

$$u_2 = u_1 (1 - a) \quad (3.10)$$

$$u_4 = u_1 (1 - 2a) \quad (3.11)$$

By substituting Equations (3.10) and (3.11) into Equation (3.6), the expression of P can be obtained:

$$P = \frac{1}{2} \rho A_2 u_1^4 4a(1 - a)^2 = \frac{1}{2} \rho A_0 U^4 4a(1 - a)^2 \quad (3.12)$$

where the power output is represented by ρ , A_0 , U and a . A_0 is the wind turbine rotor swept area, which is the same as A_2 . U is the free stream wind speed, which is the same as u_1 .

The power in the wind P_w is the kinetic energy per unit time of the free wind stream, which is given by:

$$P_w = \frac{1}{2} \rho A_0 U^3 \quad (3.13)$$

Generally, the performance of wind turbine rotor is characterized by the power coefficient C_p [33]. The power coefficient shows the power transfer efficiency of the wind turbine. It represents the fraction of the power in the wind that is extracted by the wind turbine [33]. The power coefficient C_p is expressed as:

$$C_p = \frac{P}{P_w} = \frac{\frac{1}{2}\rho A_0 U^4 a(1-a)^2}{\frac{1}{2}\rho A_0 U^3} = 4a(1-a)^2 \quad (3.14)$$

According to Betz law, the maximal mechanical energy that the wind turbine can transform from the kinetic energy is 59.3% of the kinetic energy. The theory can be proved by Figure 3.4, which shows the relationship of a and C_p . When a is $1/3$, C_p gets the maximum value 0.593. The power coefficient is unique to different types of wind turbines. The value of C_p depends on the design of blades and tip angle [54]. No wind turbine can generate electrical energy more than 59.3% of the kinetic energy. We can only get close to the maximum C_p as much as possible by proper wind turbine design.

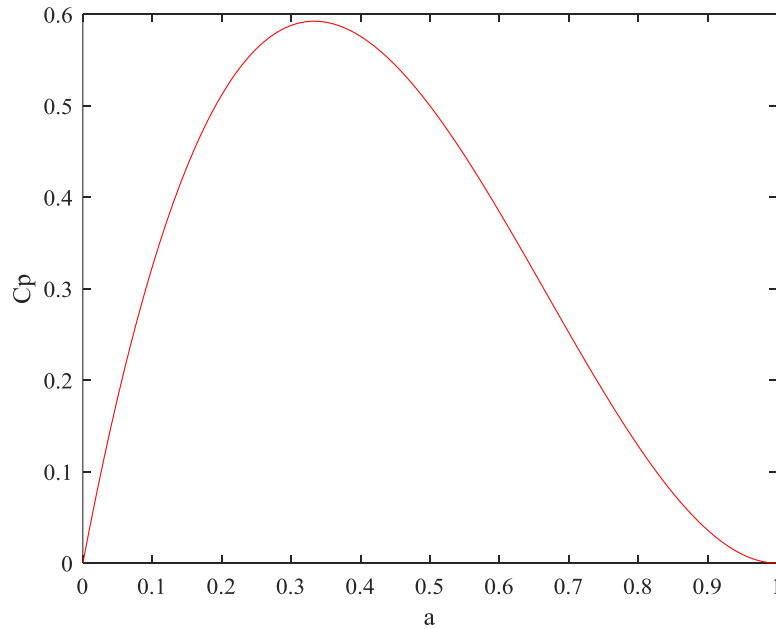


Figure 3.4 Relationship of power coefficient C_p and a

The thrust T on the actuator disk can be obtained by substituting Equations (3.10) and (3.11) into Equation (3.5):

$$T = \frac{1}{2}\rho A_2 u_1^2 4a = \frac{1}{2}\rho A_0 U^2 4a(1-a) \quad (3.15)$$

where A_2 is replaced by A_0 and u_1 is replaced by U .

The dynamic force of the wind F equals to the dynamic pressure p multiplies the rotor swept area A , which is written as:

$$F = pA = \frac{1}{2}\rho U^2 A_0 \quad (3.16)$$

The thrust coefficient C_t is another important coefficient for a wind turbine. The thrust coefficient C_t is the proportion of the thrust force on the wind turbine T and dynamic force of the wind F . The expression of C_t is shown in Equation (3.17). The maximum C_t is 1 when a is 0.5.

$$C_t = \frac{T}{F} = \frac{\frac{1}{2}\rho A_0 U^2 4a(1-a)}{\frac{1}{2}\rho U^2 A_0} = 4a(1-a) \quad (3.17)$$

Next section we will introduce Jensen's model, which is derived from wind turbine aerodynamics.

3.3.2 Single wake effect

Jensen's model is the most widely used single wake effect model. It is proposed by Jensen [45] in 1983. The single wake effect means a downstream wind turbine is only in the wake effect area generated by one upstream wind turbine. Jensen's model assumes that the wake expands linearly like a cone behind the rotor. Besides, it ignores the near wake region. The top view of Jensen's model is shown in Figure 3.5, in which j is the upstream wind turbine and i is the downstream wind turbine.

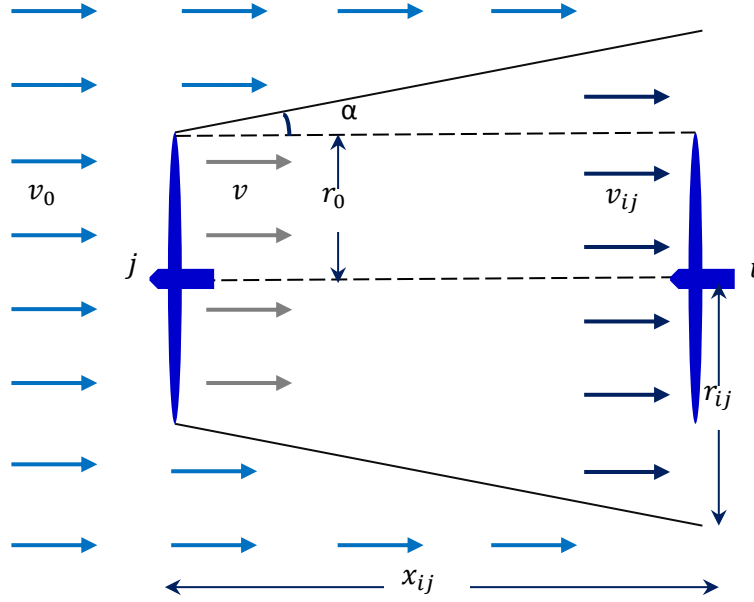


Figure 3.5 Top view of Jensen's model

Wind turbine i and j are denoted by T_i and T_j respectively. In Figure 3.5, x_{ij} is the axial distance between T_j and T_i , r_0 is the rotor radius of T_j and T_i , r_{ij} is the wake radius at the position of T_i , v_0 is the free wind speed, v is the wind speed behind the rotor of T_j and v_{ij} is the wind speed at T_i . The expression for the law of conservation of momentum for T_i and T_j is given below:

$$\pi r_0^2 v + \pi (r_{ij}^2 - r_0^2) v_0 = \pi r_{ij}^2 v_{ij} \quad (3.18)$$

The wake radius r_{ij} is written as:

$$r_{ij} = r_0 + \alpha x_{ij} \quad (3.19)$$

where α is the dimensionless scalar or called decay constant [14]. It shows the wake effect spreading condition with the growth of distance. The decay constant α is dependent on the wind turbine height z and wind turbine location surface roughness length z_0 . The expression of α is given as [68]:

$$\alpha = \frac{0.5}{\ln\left(\frac{z}{z_0}\right)} \quad (3.20)$$

A surface is rougher if it has more protrusions. Kollwitz [69] summarized the terrain classification and corresponding decay constant α , which is shown in Table 3.1. Normally people use 0.075 and 0.04 as the value of α for onshore and offshore wind farms respectively [14]. It may have a slight difference based on the specific terrain of the wind farm area. In this study, the target wind farm is a flat onshore wind farm, so 0.075 will be used as the decay constant.

Table 3.1 Terrain classification and the corresponding decay constant [69]

Terrain classification	Decay constant value
Offshore	0.040
Mixed water and land	0.052
Open farmland	0.075
Trees and farmland	0.092
Forests and villages	0.100
Large towns and cities	0.108
Large build up cities	0.117

As explained in Section 3.3.1, v can be represented by a and v_0 , which is given by:

$$v = (1 - 2a)v_0 \quad (3.21)$$

By substituting Equations (3.17), (3.19) and (3.21) into Equation (3.18), the expression of the wind speed at T_i is obtained. Equation (3.22) is the estimated wind speed v_{ij} by Jensen's model.

$$v_{ij} = v_0 - v_0 \left(1 - \sqrt{1 - C_T}\right) \left(\frac{r_0}{r_0 + \alpha x_{ij}}\right)^2 \quad (3.22)$$

In Jensen's model, the downstream wind speed is dependent on the free wind speed, thrust coefficient, rotor radius, decay constant and the axial distance between the

upstream and downstream wind turbines. Jensen's model is a single wake effect model. The downstream wind turbine is only affected by the wake of an upstream wind turbine. Moreover, the downstream wind turbine is fully in the wake region of the upstream wind turbine. However, in a real wind farm, the downstream wind turbine may not always be completely in a wake area. The positions of wind turbines and the change of wind direction will affect the wake conditions at wind turbines in the wind farm. Therefore, different wake conditions should be considered in Jensen's model.

3.3.3 Wake conditions

The wake condition reflects the overlapped area of the wake area and wind turbine rotor swept area. In Jensen's model, the rotor swept area of a downstream wind turbine is completely in the wake region of an upstream wind turbine, which is under an idealized wake condition. The wake conditions can be divided into three categories: complete wake, partial wake and no wake. Assuming T_j and T_i are upstream and downstream wind turbines respectively, Figure 3.6 shows the front views of three wake conditions that T_j may generate on T_i .

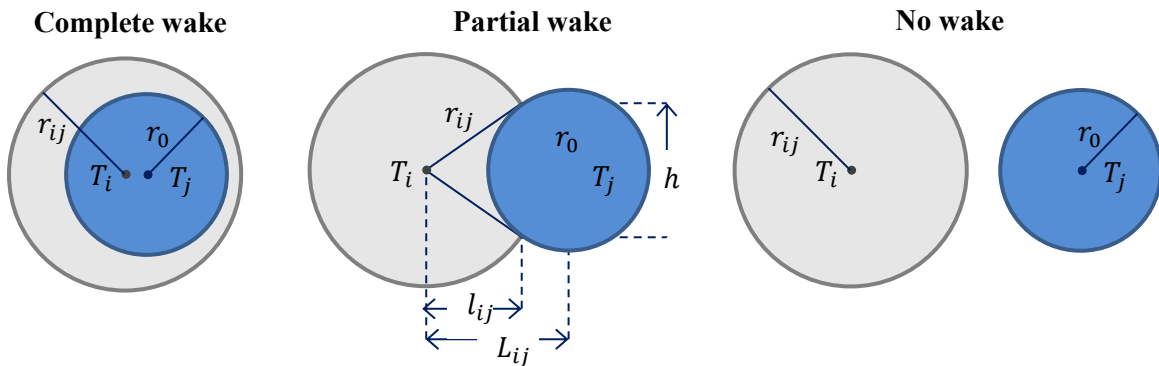


Figure 3.6 Front views of wake conditions

In Figure 3.6, the grey area is the vertical-section of wake area generated by T_j at the position of T_i and the blue area is the rotor swept area of T_i . The explanation of three wake conditions are as follows:

- Complete wake: T_i is fully covered by the wake generated by T_j ;
- Partial wake: only partial wake generated by T_j overlaps the rotor swept area of T_i ;
- No wake: T_i is not in the wake region of T_j .

Jensen's model considers the wake conditions is written as [68]:

$$v_{ij} = v_0 - v_0(1 - \sqrt{1 - C_T}) \left(\frac{r_0}{r_0 + \alpha x_{ij}} \right)^2 \left(\frac{A_{ij}}{A_0} \right) \quad (3.23)$$

where A_0 is the rotor swept area and A_{ij} is the overlapped area of the wake and rotor swept area. The wind speed deficit ratio is represented by the proportion of A_{ij} and A_0 .

The expression for three wake conditions are different. For the complete wake and no wake conditions, A_{ij} equals to A_0 and 0 respectively. For the partial wake condition, the overlapped area is denoted by A_{shadow} . Set L_{ij} as the transversal distance between T_i and T_j , the expression of A_{ij} for three wake conditions is written as:

$$A_{ij} = \begin{cases} \pi r_0^2, & L_{ij} \leq r_{ij} - r_0 \\ A_{shadow}, & r_{ij} - r_0 < L_{ij} < r_0 + r_{ij} \\ 0, & L_{ij} \geq r_0 + r_{ij} \end{cases} \quad (3.24)$$

Figure 3.7 (a) and (b) are the top view and front view of partial wake effect. T_i is in the partial wake of T_j when the wind direction is θ . The red area in Figure 3.7 (b) is the overlapped area A_{shadow} . The expression of the overlapped area A_{shadow} is:

$$A_{shadow} = r_{ij}^2 \arccos \frac{l_{ij}}{r_{ij}} + r_0^2 \arccos \frac{L_{ij} - l_{ij}}{r_0} - \frac{1}{2} L_{ij} h_{ij} \quad (3.25)$$

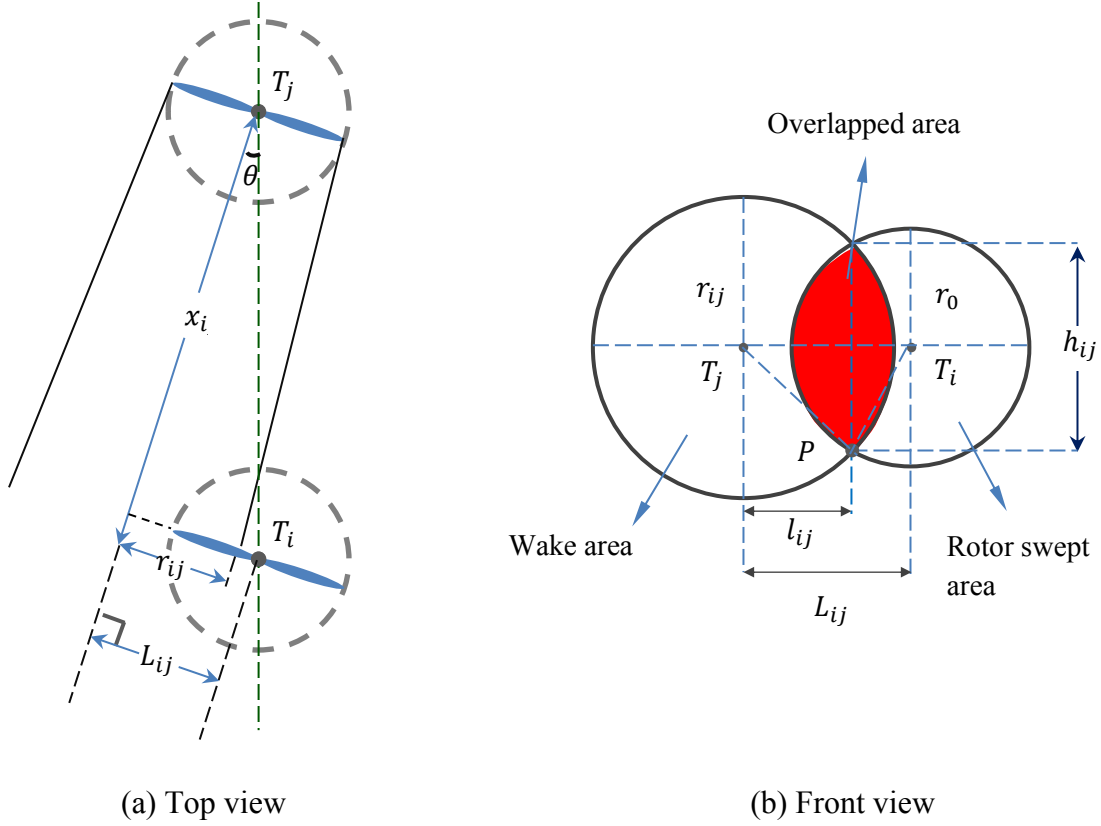


Figure 3.7 Two views of partial wake effect

According to Heron's formula for calculating the area of a triangle, the following equations can be obtained:

$$p_s = \frac{r_{ij} + r_0 + L_{ij}}{2} \quad (3.26)$$

$$S_{\Delta T_i P T_j} = \sqrt{p_s(p_s - r_{ij})(p_s - r_0)(p_s - L_{ij})} \quad (3.27)$$

$$h_{ij} = \frac{4S_{\Delta T_i P T_j}}{L_{ij}} \quad (3.28)$$

$$l_{ij} = \sqrt{r_{ij}^2 - \frac{h_{ij}^2}{4}} \quad (3.29)$$

where p_s is the semi-perimeter of $\Delta T_i P T_j$ and $S_{\Delta T_i P T_j}$ is the area of $\Delta T_i P T_j$. By substituting Equations (3.26), (3.27), (3.28) and (3.29) to Equation (3.25), the expression of partial wake area A_{shadow} can be obtained:

$$A_{shadow} = r_{ij}^2 \arccos \frac{L_{ij}^2 + r_{ij}^2 - r_0^2}{2L_{ij}r_{ij}} + r_0^2 \arccos \frac{L_{ij}^2 + r_0^2 - r_{ij}^2}{2L_{ij}r_0} - \frac{1}{2} \sqrt{(r_{ij} + r_0 + L_{ij})(-r_{ij} + r_0 + L_{ij})(r_{ij} - r_0 + L_{ij})(r_{ij} + r_0 - L_{ij})} \quad (3.30)$$

In summary, the wake effect is divided into three conditions: complete wake, partial wake and no wake. Three wake conditions have different wake effect overlapped areas, which will affect the wind speed at the downstream wind turbine. The single wake effect model is improved by considering wake conditions, which is more suitable to show the wake that one wind turbine may affect on another. However, in a real wind farm, a wind turbine might be in the wake effect area by several other wind turbines simultaneously. In the next section, multiple wake effect on the wind turbine will be considered.

3.3.4 Multiple wake effects

Jensen's model is used to estimate the downstream wind speed affected by only one wake region. However, wake effect in real farms is much more complex. One wind turbine might be affected by several wake of other wind turbines, which is called multiple wake effects. Figure 3.8 is an example of multiple wake effects in a wind farm. The status of eight wind turbines in the sample wind farm is shown below:

- T_1, T_2, T_3 and T_4 are facing free wind stream v_0 , which are wake-free;
- T_5 is in the single wake region of T_2 ;
- T_6 is in the wake regions of T_1 and T_2 ;
- T_7 is in the wake regions of T_3 and T_4 ;
- T_i is affected by the wake of T_1, T_2, T_3 and T_5 .

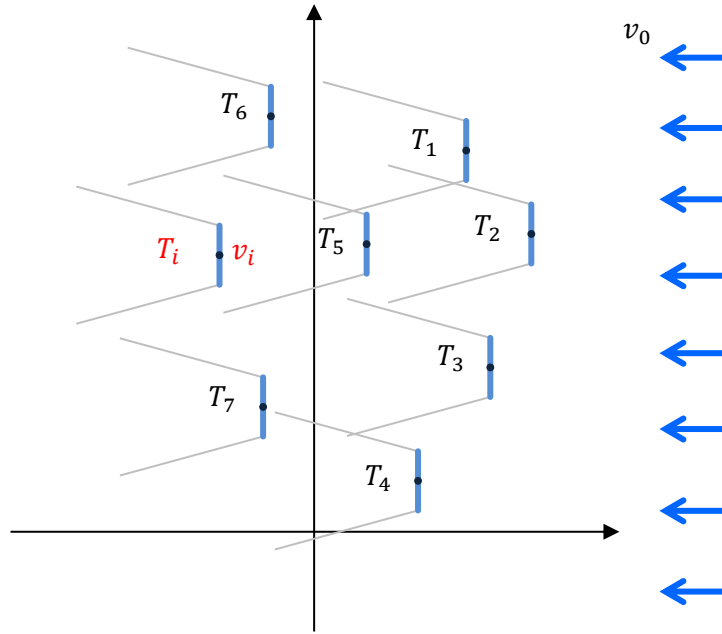


Figure 3.8 Multiple wake effects in a wind farm

The wind speed deficit at T_i affected by the single wake of T_j is denoted by Def_{ij} , which is written as:

$$Def_{ij} = v_0 - v_{ij} \quad j \in [1, n], i \neq j \quad (3.31)$$

where v_0 is the free wind speed, v_{ij} is the wind speed at T_i affected by T_j and n is the total number of wind turbines in the wind farm.

The multiple wake effects is the combination of several single wake effects [14]. The wind speed deficit at T_i by multiple wake effects is the root sum square of single wind speed deficit, which is given by \overline{Def}_i in Equation (3.32).

$$\overline{Def}_i = \sqrt{\sum_{j=1}^n Def_{ij}^2} \quad j \in [1, n], i \neq j \quad (3.32)$$

The wind speed v_i at T_i affected by multiple wake equals to the free wind speed v_0 minus \overline{Def}_i . Based on Jensen's model with considering the wake conditions, the multiple wake effect model is given below [25]:

$$v_i = v_0 - \overline{Def}_i = v_0 - v_0(1 - \sqrt{1 - C_{T(v_0)}}) \left(\frac{r_0^2}{A_0}\right) \sqrt{\sum_{j=1}^n \left(\frac{A_{ij}}{(r_0 + \alpha|x_{ij}|)^2}\right)^2} \quad (3.33)$$

where $C_{T(v_0)}$ is the trust coefficient at wind speed v_0 , and v_i is the wind speed at T_i affected by multiple wake.

The multiple wake effect model is suitable on simulating wind speeds at wind turbines in the wind farm. The multiple wake effect model will be applied to estimate wind speeds in the wind farm. In the next section, the detailed process of estimating wind speeds at wind turbines in a wind farm by wake effect model will be explained.

3.3.5 Wind speed estimation process by wake effect model

The wind speed estimation is a critical process in wind farm layout optimization. The free wind speed, positions of wind turbines and wind direction will affect the estimated wind speed at each wind turbine.

Figure 3.9 is the flow chart of wind speed estimation process for T_i by wake effect model. Suppose n is the total number of wind turbines in the target wind farm, T_i is the target wind turbine for estimating the wind speed and T_j represents another wind turbine in the wind farm with $j = [1, 2, 3, \dots, n]$. The wind speed and direction of the wind farm are v_l and β_k respectively, which are generated by the wind resource model. The free wind speed v_0 in wake effect model equals to v_l . The layout of the wind farm is represented by $[\mathbf{X}_k, \mathbf{Y}_k]^T$. The coordinates of T_i and T_j are (x_i, y_i) and (x_j, y_j) respectively. The coordinate distance of T_i and T_j on x-axis is denoted by x_{ij} and the absolute distance of T_i and T_j on y-axis is denoted by L_{ij} , which are given by:

$$x_{ij} = x_i - x_j \quad (3.34)$$

$$L_{ij} = |y_i - y_j| \quad (3.35)$$

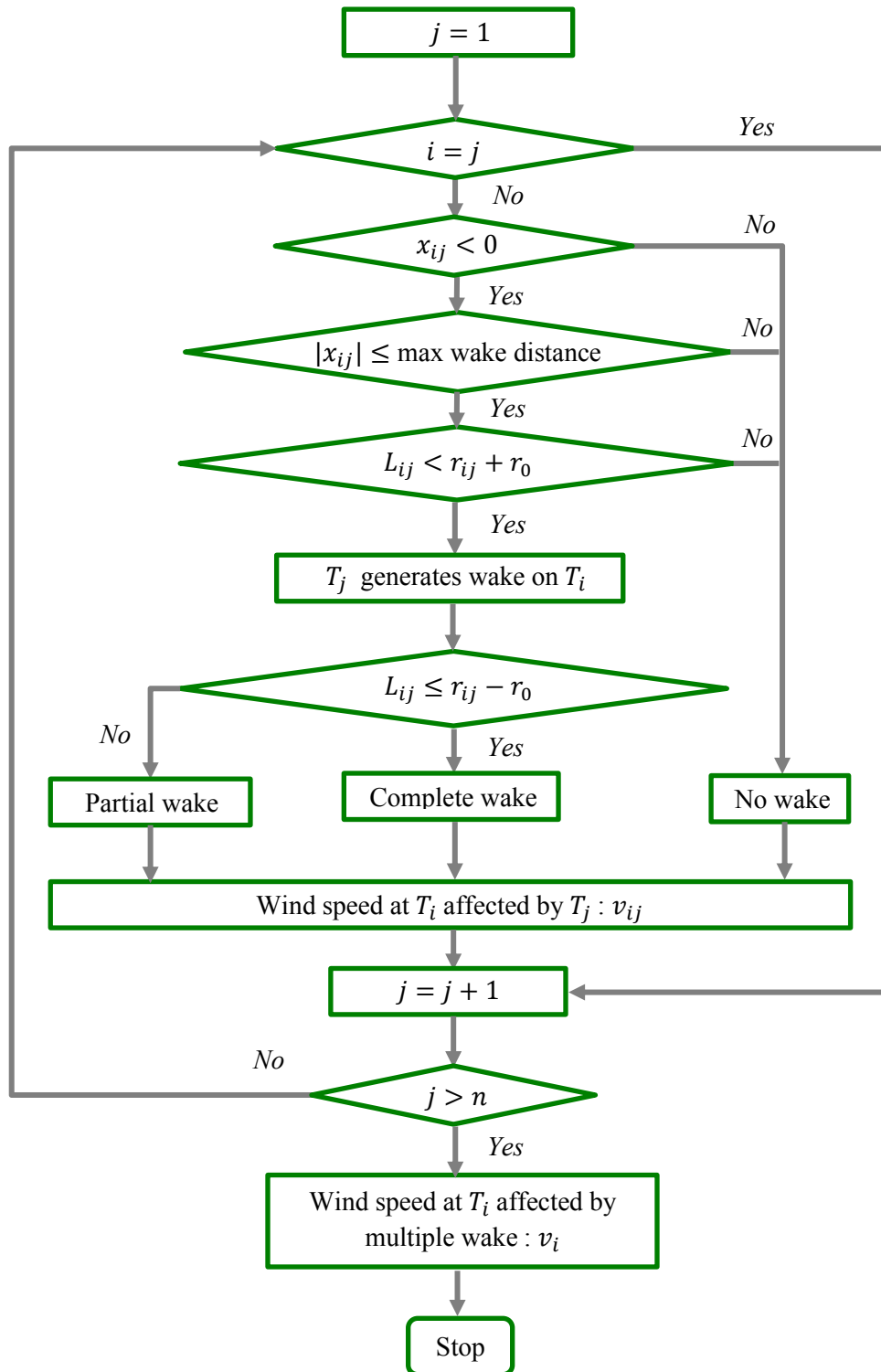


Figure 3.9 Flow chart of wind speed estimation process by wake effect model

Following steps are the detailed explanation for the process in Figure 3.9:

Step 1: Set $j = 1$.

Step 2: If $i = j$, go to Step 8. If not, go to the next step.

Step 3: If x_{ij} is not negative, T_j is not the upstream wind turbine to T_i and will not generate wake effect on T_i . Go to Step 7. If x_{ij} is negative, go to the next step.

Step 4: If the absolute value of x_{ij} exceeds the maximum wake effect length, T_i will not be affected by the wake of T_j . Studies show that the wake has the minimal effect on wind speed deficit after 10 times rotor diameter ($10D$) [15]. The air flow is mixing in the far wake region and it is found that the wind speed is almost recover when the distance is no less than $20D$ [70]. Therefore, in this study, the maximum wake effect spreading distance is assumed to be $20D$. Go to the next step if the absolute value of x_{ij} is smaller than $20D$; otherwise, T_i is not affected by the wake of T_j and go to Step 7.

Step 5: If $L_{ij} < r_{ij} + r_0$, T_i is in the wake region of T_j . It can be confirmed that T_j generates wake effect on T_i . Go to the next step for further judgment. If $L_{ij} \geq r_{ij} + r_0$, there is no wake that T_j generates on T_i . Go to Step 7.

Step 6: If $L_{ij} \leq r_{ij} - r_0$, T_i is completely in the wake region of T_j ; otherwise, T_i is in the partial wake of T_j . Make a judgement and go to the next step.

Step 7: Based on the wake condition that T_j generates on T_i , using Equation (3.23) to calculate v_{ij} at T_i affected by T_j .

Step 8: Set $j = j + 1$.

Step 9: If j is greater than the number of wind turbines, go to the next step; otherwise go to step 2.

Step 10: Calculate the wind speed v_i at T_i by the multiple wake effect model.

With a given wind speed and direction, wind speeds at all wind turbines in the wind farm can be calculated following the wind speed estimation flow chart. The estimated wind speed will be used to calculate the wind farm power output in the next section.

3.4 Power output model

Wind farm power output estimation is an important procedure when designing a wind farm. In order to forecast the wind farm power generation capacity, we need to estimate the individual wind turbine power output, which is modeled by wind turbine power curve. In this section, the wind turbine power curve will be introduced first and then wind farm power output model will be explained.

3.4.1 Wind turbine power curve

Wind turbine power curve indicates the electrical power output that a turbine can generate at various wind speeds. Different types of wind turbines have different power curves based on wind turbine properties. Figure 3.10 is a typical wind turbine power curve. Suppose v_{cut-in} is the cut-in wind speed, v_{rated} is the rated wind speed, $v_{cut-out}$ is the cut-out wind speed and P_r is the rated power output. The power curve is divided into four regions. In the first region, wind speed is from 0 to v_{cut-in} . The wind turbine will not generate available power output. In the second region, wind speed is from v_{cut-in} to v_{rated} . The wind turbine power output grows with the increase of wind speed and reaches P_r at v_{rated} . In the third region, wind speed is from v_{rated} to $v_{cut-out}$. The wind turbine generates constant power output P_r . In the last region, wind speed is beyond $v_{cut-out}$. The wind speed is too high and the wind turbine will shut down in case of breakdown overloaded.

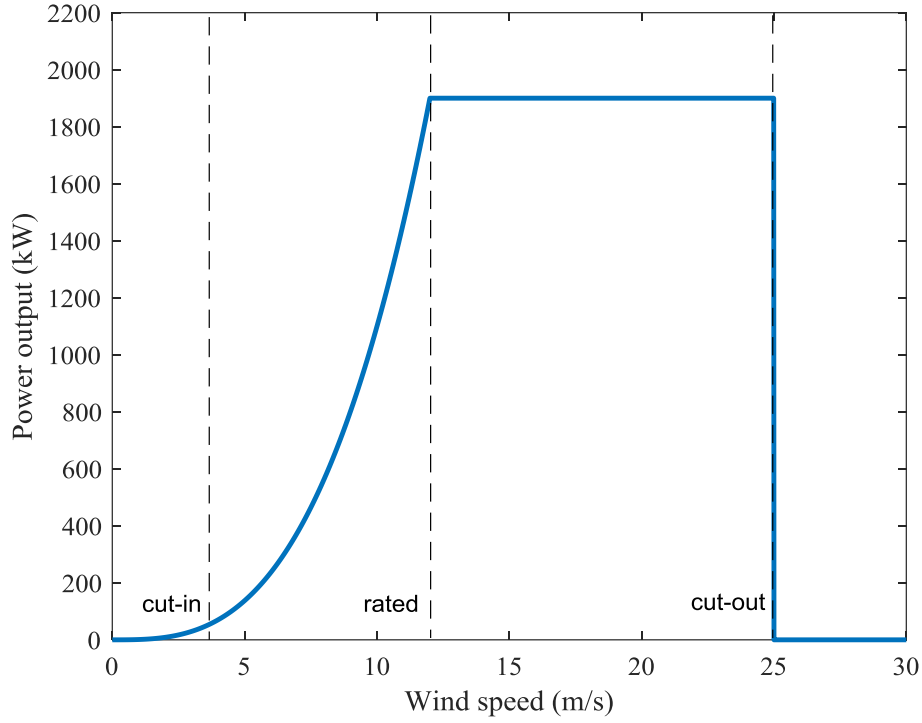


Figure 3.10 A typical wind turbine power curve

The non-linear part of the power curve is denoted by $P_w(v_i)$, which is from the cut-in wind speed to rated wind speed. In this thesis, $P_w(v_i)$ is represented by the cubic power curve [54], which is also the most widely used deterministic power curve model. The function of cubic power curve is:

$$P_w(v_i) = \frac{1}{2} \rho A_0 v_i^3 C_p \quad (3.36)$$

where ρ is the air density, A_0 is the rotor swept area, v_i is the wind speed at the wind turbine and C_p is the power coefficient. The cubic power curve follows the Betz law explained in Section 3.1.1. Suppose $P_{T_i}(v_i)$ is the power output of T_i , the power curve of T_i is given in Equation (3.37). $P_{T_i}(v_i)$ will be used to estimate the power output of wind turbines in the wind farm.

$$P_{T_i}(v_i) = \begin{cases} 0, & 0 \leq v_i < v_{cut-in} \\ \frac{1}{2} \rho A_0 v_i^3 C_p, & v_{cut-in} \leq v_i < v_r \\ P_r, & v_r \leq v_i < v_{cut-out} \\ 0, & v_i \geq v_{cut-out} \end{cases} \quad (3.37)$$

3.4.2 Wind farm power output model

The wind farm power output model is used to calculate the APO of a wind farm. The APO of a wind farm in a given time period is the sum of the APO of individual wind turbines. As mentioned in Section 3.3.5, v_i at T_i is dependent on the free wind speed v_0 , wind direction β_k and wind farm layout $[\mathbf{X}_k, \mathbf{Y}_k]^T$, which can be denoted by $v_i(v_0, \beta_k, [\mathbf{X}_k, \mathbf{Y}_k]^T)$. Suppose the wind resource sample size is M and the APO of T_i is represented by \bar{P}_{T_i} . The expression of \bar{P}_{T_i} is given as:

$$\bar{P}_{T_i} = \frac{1}{M} \sum_{m=1}^M P_{T_i}(v_i(v_0, \beta_k, [\mathbf{X}_k, \mathbf{Y}_k]^T)) \quad (3.38)$$

The APO of a wind farm with n wind turbines is represented by P_{tot} , which is written as:

$$P_{tot} = \sum_{i=1}^n \bar{P}_{T_i} \quad (3.39)$$

The annual energy production (AEP) is a commonly used measurement for the overall electrical energy a wind farm can produce in one year [18]. It is the product of hours in one year and APO of the wind farm, which is measured in kilowatt-hour or megawatt-hour. Maximizing AEP is identical to maximizing the APO of the wind farm. Therefore, this study will directly maximize the APO, which is also the first objective of wind farm layout optimization in this thesis.

3.5 Objective functions

In this section, two objective functions for wind farm layout optimization of this thesis will be explained. The difference of two objective functions is one is for wind farm layout optimization with a fixed number of wind turbines and the other is for that with various number of wind turbines. The wind farm in this thesis will be optimized based on the two objective functions respectively.

3.5.1 Objective 1: maximizing the APO of the wind farm

The first objective is maximizing the APO of the wind farm by optimizing the wind farm layout with a fixed number of wind turbines. Based on the wind farm power output model in Chapter 3, the first objective function is written as:

$$\text{Maximize: } P_{tot} = \sum_{i=1}^n \bar{P}_{T_i} \quad (3.40)$$

where n is the total number of wind turbines in the wind farm, \bar{P}_{T_i} and P_{tot} are the APO of T_i and APO of the wind farm in one year respectively.

The variables of the first objective function are positions of wind turbines, which compose the layout of the wind farm. The wind farm in this thesis is considered to be a regular shape, which is supposed to be a rectangle. The first objective function is subject to the following constraints:

$$\text{Subject to:} \quad X_{lb} \leq x_i \leq X_{ub}$$

$$Y_{lb} \leq y_i \leq Y_{ub}$$

$$\sqrt{(x_i - x_j)^2 + (y_i - y_j)^2} \geq d_{min} \quad \text{for } i, j = 1, 2, \dots, n \text{ and } i \neq j \quad (3.41)$$

The three constraints guarantee that all wind turbines are placed in the wind farm area and keep safe distance between each other. The first and second constraints are the boundary constraints, where X_{lb} and X_{ub} are the lower and upper boundary of the wind farm on x -axis, respectively, Y_{lb} and Y_{ub} are the lower and upper boundary of the wind farm on y -axis, respectively, and (x_i, y_i) is the coordinate of T_i . The third constraint is the proximity constraint, where d_{min} is the minimum distance between any two wind turbines. In a real wind farm, wind turbines must keep a safe distance in case of accidents. Usually people use 5 times rotor diameter ($5D$) as the safe distance between two wind turbines [41]. Therefore, d_{min} equals to $5D$ in Equation (3.41). With the given constraints, this thesis aims to select the best positions of wind turbines to maximize the APO of the wind farm.

3.5.2 Objective 2: minimizing the CoP of the wind farm

The second objective is minimizing the CoP of the wind farm. Compared with the first objective, the number of wind turbines is varying in the second objective. As mentioned in Section 2.5, although installing more wind turbines can improve the wind farm power output, the cost of the wind farm will also increase. Therefore, maximizing the APO is improper to be the objective function if the number of wind turbines is undecided.

Minimizing the CoP of the wind farm should be the objective function if both the number and positions of wind turbines are variables.

The CoP is the average cost per unit power output of a wind farm. It aims to maximize the APO and minimize the cost of the wind farm. Many studies use the cost of energy (CoE) to measure the average cost of electricity generation of the wind farm annually [26][27]. Minimizing the CoE is identical to minimizing the CoP. Thus, this thesis will directly minimize the CoP of the wind farm, which is written as:

$$\text{Minimize: } CoP = \frac{Cost}{P_{tot}} \quad (3.42)$$

where P_{tot} is the APO of the wind farm and $Cost$ denotes the cost of the wind farm. The cost function in Mosetti's model will be used to represent $Cost$, which is widely used in wind farm layout optimization [26][40]. The expression of $Cost$ is:

$$Cost = n \times Cost_s = n \left(\frac{2}{3} + \frac{1}{3} e^{-0.00174n^2} \right) \quad (3.43)$$

where n is the total number of wind turbines and $Cost_s$ is the non-dimensionalized cost per year of a single wind turbine. In Mosetti's model, the cost is only correlated with the number of wind turbines. Figure 3.11 shows the relationship of $Cost_s$ and the number of wind turbines. $Cost_s$ decreases with the increased number of wind turbines. As shown in Figure 3.11, $Cost_s$ can be saved if the number of wind turbines is large enough, approximately greater than 50.

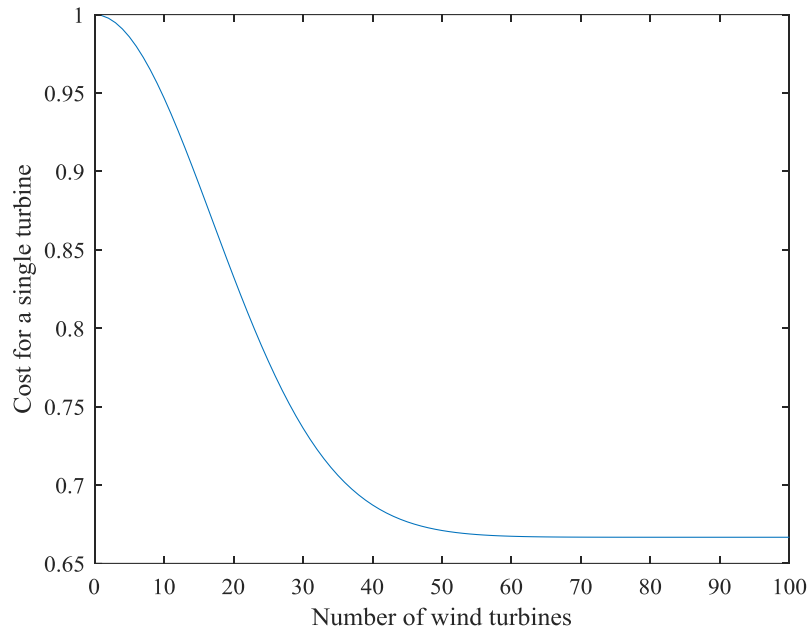


Figure 3.11 Cost for a single wind turbine by Mosetti’s model

The second objective is subject to the boundary constraints and proximity constraint shown in Equation (3.41). The second objective aims to optimize the number and positions of wind turbines by minimizing the CoP of the wind farm.

3.6 Genetic Algorithm

Genetic Algorithm (GA) is an evolutionary algorithm using the population-based search technique to solve optimization problems. Compared with gradient-based algorithms, GA is global and robust to search optimal solutions for complex problems. Wind farm layout optimization is a non-linear problem, which has high complexity on iterative evaluations of layouts. Thus, applying GA on this problem is better than using gradient-based algorithms, which might be stuck at the local minimum.

In this thesis, GA in MATLAB will be applied to solve wind farm layout optimization. For the first objective, GA will be used to find the optimum layout of the wind farm among all feasible solutions. For the second objective, GA will be used to find the best number and the optimum positions of wind turbines in the wind farm. Figure 3.12 is the process to implement GA [71].

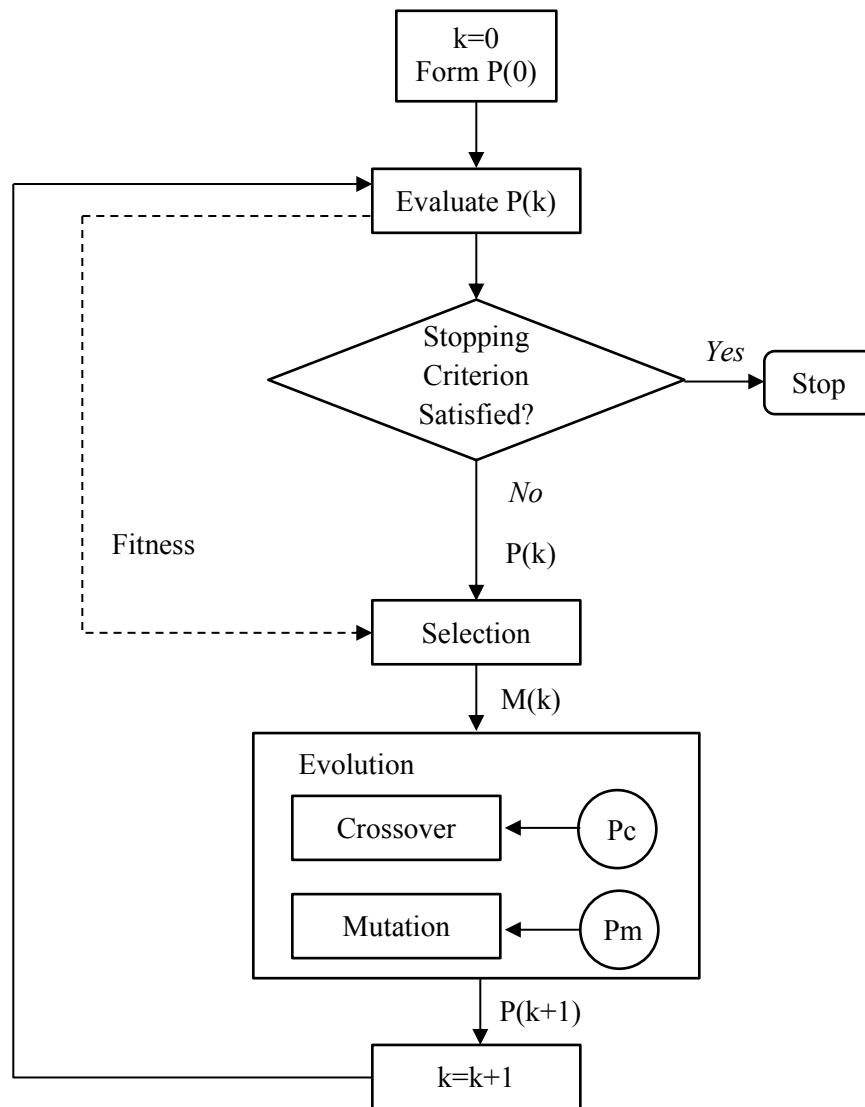


Figure 3.12 Flowchart of the GA [71]

Assuming k is the generations of GA, the general steps of solving wind farm layout optimization by GA are given as follows.

Step 1: Set $k=0$. GA starts with an initial population $P(0)$ involving a group of points called individuals. In a binary coded genetic algorithm, individuals are strings composed by 1 and 0 [27]. A binary string is also called a chromosome in GA terminology. In wind farm layout optimization, each individual is one kind of layout of the wind farm. The initial points in $P(0)$ are created randomly.

Step 2: Evaluate $P(k)$. The objective function at each point will be evaluated. The result is the fitness value of each point.

Step 3: If the stopping criterion is met, stop GA and generate the output. If not, go to the next step. In this thesis, two stopping criteria are set for the wind farm layout optimization: when GA reaches the maximum generation or the best fitness value in the last 50 generations keeps the same. GA will stop once one of the stopping criteria is satisfied.

Step 4: The individuals in $P(k)$ will be selected to the mating pool $M(k)$ based on their fitness values. The individuals that have fitter values are more possible to be selected and one individual might be selected more than once. The roulette-wheel method or tournament scheme method will be used to randomly select individuals to the mating pool [71]. The individuals in the mating pool are called parents.

Step 5: Evolve $M(k)$ to form $P(k+1)$. Parents in the mating pool will reproduce offsprings of the current population. The population size will keep the same during the breeding operation. The breeding process uses cross-over and mutation to generate offsprings to the new population $P(k+1)$. The cross-over point in the binary string is choosing randomly. The cross-over probability will determine whether a pair of parents will exchange the bits of chromosomes. The mutation process randomly switches a bit in a string to the opposite value. The mutation probability will be used to determine whether the mutation is performed on a binary string. An example of the breeding process of the GA is illustrated in Figure 3.13. After cross-over and mutation process are operated on all chromosomes in the mating pool, the new population $P(k+1)$ can be obtained.

Step 6: Set $k=k+1$, and then go to Step 2. The GA process will stop till it meets the stopping criterion.

The parameters of the GA in this study are shown in Table 3.2.

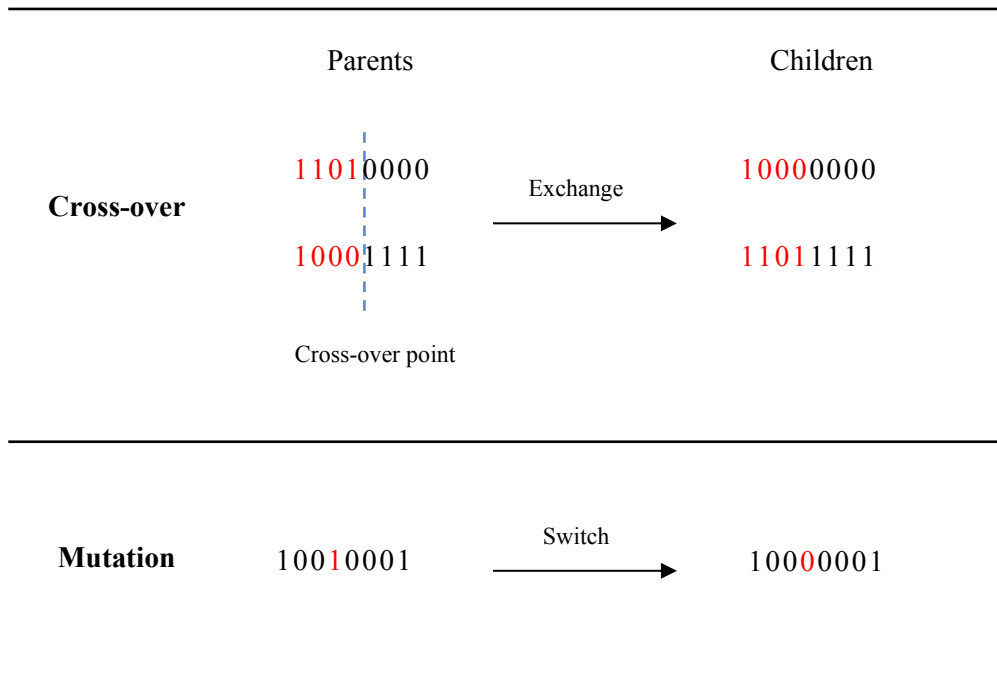


Figure 3.13 An example of the breeding process in the GA

Table 3.2 GA parameters

Population size	Generation	Cross-over rate	Mutation rate
50	5,000	0.8	0.01

3.7 Proposed approach for wind direction segment size selection

In this section, the proposed approach for selecting proper wind direction segment sizes in wind farm layout optimization will be introduced. The proposed approach can be applied to any wind farm power output model in wind farm layout optimization to select proper wind direction segment sizes. Figure 3.14 is the flow chart of the proposed approach, which involves five steps. Proper wind direction segment sizes will be selected based on the result of last two steps.

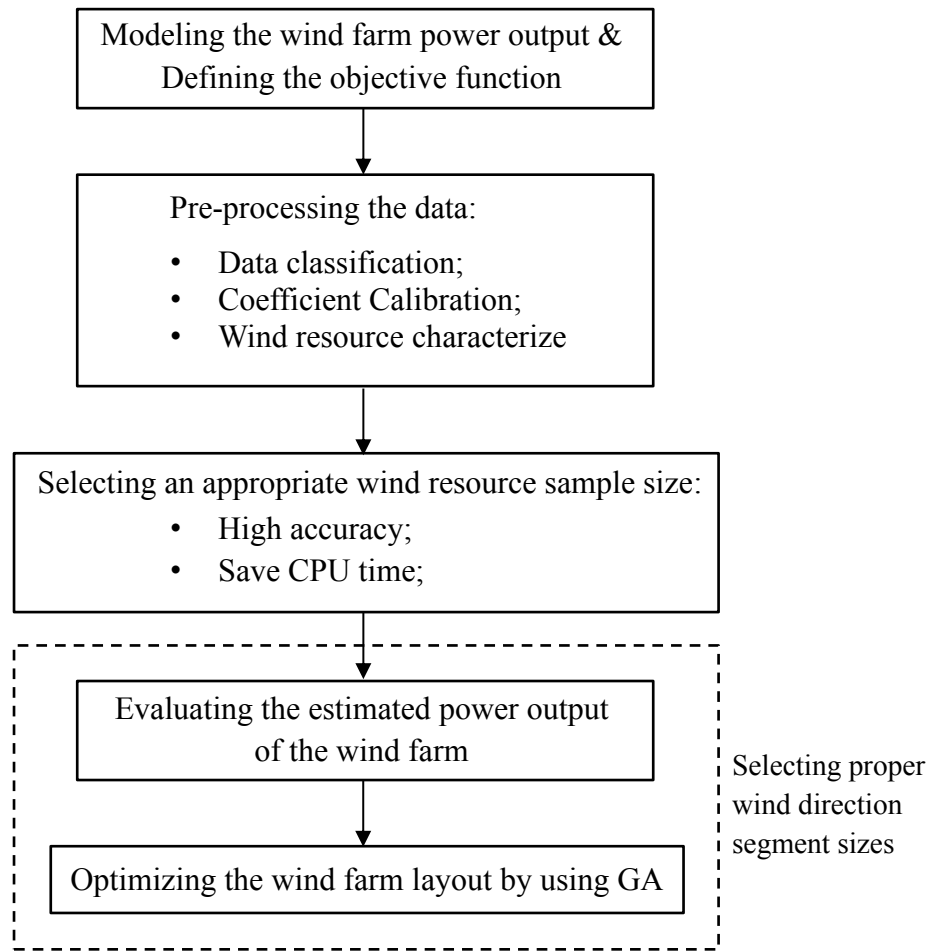


Figure 3.14 Flow chart of the proposed approach for wind direction segment size selection in wind farm layout optimization

Detailed explanations of the proposed approach in Figure 3.14 are as follows.

Step 1: Modeling the wind farm power output and defining the objective function. The wind farm power output model in this thesis is composed by commonly used wind resource model [24], position model [31], wake effect model [25] and wind turbine power curve [54], which are introduced in Section 3.1 to 3.4. The wind resource is characterized by sector-wise Weibull distribution, which is expressed by Equation (3.1). The position model indicates the relationship of the wind direction and positions of wind turbines, which is formulized by Equation (3.2). This thesis considers multiple wake effects as shown in Figure 3.8. The expression of multiple wake effects is Equation (3.33),

which is derived from Jensen' model with considering different wake conditions. Wind speeds at wind turbines in the wind farm are estimated following the process shown in Figure 3.9. The expression of wind farm power output model used in this thesis is Equation (3.39), which is the sum of individual wind turbines power output calculated by Equation (3.38). The objective functions of this thesis are maximizing the APO and minimizing the CoP of the wind farm, which are expressed by Equation (3.40) and Equation (3.42) respectively.

Step 2: Pre-processing the data of the target wind farm. The required data involves the wind resource data, operational data, geographic data and wind turbine properties. In order to improve the power output estimation accuracy, coefficients of wind turbine power curve will be calibrated. This thesis uses cubic power curve expressed by Equation (3.37) to estimate the wind turbine power output. The root mean square error (RMSE) will be used to evaluate the estimated and observed power output of a selected wind turbine. The power curve with calibrated coefficients that leads to the best RMSE will be used to calculate the power output of wind turbines in the target wind farm. As mentioned in Section 3.1, the wind resource data will be characterized by the wind resource model to obtain p_k , a_k and b_k . Wind directions will be generated based on p_k . For each wind direction segment, the probability of wind speed occurs at this wind direction is different. Monte Carlo simulation will be used to randomly generate wind speed at k -th wind direction segment following the correlated Weibull distribution with a_k and b_k as scale and shape parameters. This step will be illustrated in Section 4.1 to 4.3.

Step 3: Selecting an appropriate wind resource sample size for wind farm layout optimization. The wind resource sample is a set of wind speed and direction data simulated by the wind resource model. The sample size determines the amount of wind resource data that will be used in the optimization process. Normally the sample size of the observed wind resource data is too large to be applied to the optimization process. Reducing the wind resource sample size can save CPU time, but the estimation accuracy on wind farm power output calculation will also decrease. Therefore, selecting an appropriate wind resource sample size that has high estimation accuracy and can also save the CPU time for wind farm power output calculation is important. Due to the

simulated wind resource are randomly generated, the calculated wind farm power output also exists difference. Thus, generating wind resource multiple times is necessary for analyzing the consistency of the calculated wind farm power output. For each wind resource sample size, wind resource will be generated multiple times by Monte Carlo simulation and wind farm power output will be calculated by Equation (3.39) in each time. An appropriate wind resource sample size will be selected by trading off the estimation accuracy and the CPU time for wind farm power output calculation. In this thesis, the estimation accuracy will be evaluated by the relative error (RE) of the estimated and observed wind farm power output. The RE will tend to be stable when the wind resource sample size is greater than the selected one. This step will be proved in Section 4.4.1.

Step 4: Evaluating the estimated power output of the target wind farm with different wind direction segment sizes. Wind characteristics of the target wind farm is obtained by the wind resource model with different wind direction segment sizes. In this thesis, 10 different wind direction segment sizes: 1° , 3° , 5° , 6° , 10° , 12° , 15° , 18° , 24° and 30° will be investigated for wind farm power output calculation and layout optimization. For each wind direction segment size, wind characteristics obtained in Step 2 are different. Monte Carlo simulation will be used to randomly generate wind resource following the correlated wind characteristics. The sample size of the simulated wind resource is selected by Step 3. Equation (3.39) will be used to calculate the APO of the wind farm. Proper wind direction segment sizes that lead to low RE of wind farm power output will be selected for wind farm power output calculation. Based on the result, the most accurate way to estimate the wind farm power output will be recommended to wind farm operators. This step will be illustrated in Section 4.4.2.

Step 5: Optimizing the wind farm layout by using GA. The wind farm layout will be optimized with 10 different wind direction segment sizes. The optimized wind farm will be evaluated by the APO, wind farm efficiency and CPU time of the optimization process. In addition, the most accurate way for wind farm power output calculation, which is obtained in Step 4, will be used to re-evaluate the optimized layouts. Based on the result, we will present the wind direction segment size that leads to an optimized layout with the

highest APO. Besides, proper wind direction segment sizes will be selected by trading off the re-evaluated APO and CPU time. The consistency of optimized results with different wind direction segment sizes will also be considered. The optimized APO will be compared with the re-evaluated APO of the wind farm by the relative error. Based on the consistency analysis, the most reliable, acceptable and optimal wind direction segment sizes for wind farm layout optimization will be recommended. The most reliable wind direction segment size used in wind farm layout optimization leads to the lowest RE. The RE of the optimized wind farm power output with acceptable wind direction segment sizes should be no greater than the maximum RE of the estimated wind farm power output of the original wind farm. The optimal wind direction segment size is selected by trading off the RE of the optimized result and the CPU time of the optimization process. The optimal wind direction segment size satisfies the requirement of saving the CPU time and obtaining a reliable wind farm layout. In addition, wind direction segment sizes that has high relative error on wind farm power output calculation should be avoided in wind farm layout optimization. Step 5 will be illustrated in Chapter 5.

Different wind direction segment size selection strategies will be proposed based on the optimized results in Chapter 5. Wind farm developers and researchers can select recommended wind direction segment sizes based on their requirements. For example, if the wind farm developer needs to design a wind farm layout and also needs to estimate the power output of the designed wind farm accurately, the most reliable wind direction segment size is suitable to be used. If a wind farm layout optimization study focuses on investigating the optimization algorithm used in the problem, then it needs multiple times of optimization. They can select wind direction segment sizes that cost a lower CPU time with acceptable accuracy.

3.8 Summary

In this chapter, models and methodologies used in this thesis are introduced. The wind farm power output model will be used to estimate the APO of the wind farm. Two objective functions for wind farm layout optimization are defined and GA used in the optimization process is explained. In addition, this chapter proposes the approach for selecting proper wind direction segment sizes in wind farm layout optimization. The proposed approach will be illustrated by case studies in Chapter 4 and Chapter 5.

Chapter 4

Data Description and Wind Farm Power Output Assessment

As mentioned in Section 3.7, the proposed approach for selecting proper wind direction segment sizes in wind farm layout optimization involves 5 steps. The first step is modeling the wind farm power output and defining the objective function, which are introduced in Chapter 3. Equation (3.39) is the wind farm power output model used in this thesis. The objective functions are maximizing the APO and minimizing the CoP of the wind farm, which are Equation (3.40) and Equation (3.42) respectively. The constraints of two objective functions are the same, which are the boundary constraints and proximity constraint expressed in Equation (3.41).

In this chapter, step 2 to 4 of the proposed approach will be illustrated. An onshore wind farm with one-year observed data will be used to calculate the APO of the wind farm with different wind direction segment sizes and wind resource sample sizes. Step 2 of the proposed approach will be illustrated in Section 4.1 to 4.3. Wind resource in the target wind farm is characterized by sector-wise Weibull distribution with different wind direction segment sizes. The observed data will be pre-processed to improve the power output estimation accuracy. Step 3 and Step 4 of the proposed approach will be illustrated in Section 4.4. An appropriate wind resource sample size for wind farm layout optimization will be presented. Besides, wind farm power output calculated by using different wind direction segment sizes will be evaluated and the most accurate way to estimate the power output of the target wind farm will be presented.

Section 4.1 introduces the target wind farm and data categories. Section 4.2 calibrates the coefficients of wind turbines. Section 4.3 presents the wind characteristics result of the target wind farm. Section 4.4 assesses the estimated wind farm power output. The last section is the summary.

4.1 Data description

The target wind farm of this study is a hypothetical onshore wind farm. The wind farm has 100 1.9 MW wind turbines. The data of the target wind farm is divided into four categories: wind resource data, operational data, geographic data and wind turbine properties. The first two categories are full year data observed every 10 minutes. The description of four categories data are as follows:

- 1) Wind resource data. It involves one-year observed wind speed and wind direction data. The wind speed and direction of the target wind farm will be characterized by wind resource model in Section 4.2.
- 2) Operational data. It is the observed power output of wind turbines in the wind farm.
- 3) Geographic data. It is the longitude and latitude of each wind turbine. The terrain of the target wind farm is relatively flat, so the altitude of wind turbines will not be considered in this study. The geographic data of wind turbines is transferred to coordinates by the Universal Transverse Mercator (UTM) coordinate system. The origin of the UTM system is the intersection of equator and central meridian.
- 4) Turbine properties. The target wind farm has 100 hypothetical 1.9 MW wind turbines. The turbine properties will be used to model the wind turbine power curve.

The size of the target wind farm is assumed to be $12600 \text{ m} \times 12600 \text{ m}$. As mentioned in Section 3.5, the minimum safe distance between two wind turbines is $5D$, where D is the diameter measured in meters of the rotor of each turbine. This thesis will use the grid method to design the wind farm and each grid size is set to be $5D \times 5D$ to guarantee the wind turbines keep a safe distance between each other.

4.2 Coefficient calibration

The main purpose of this section is to improve the wind turbine power output estimation accuracy by calibrating coefficients of the power curve. The calibrated power curve will be used to estimate the power output of wind turbines in the target wind farm.

The original wind turbine power curve is modeled based on the wind turbine properties. Table 4.1 shows the properties of the 1.9 MW wind turbine. As mentioned in Section 3.4, in this thesis, the wind turbine power curve is indicated by the cubic power curve. The original power curve will be calibrated to improve the estimation accuracy of wind turbine power output. The estimated power output by the power curve will be compared with the observed power output of a wind turbine in the target wind farm.

Table 4.1 Wind turbine properties

Cut-in wind speed	3.5 m/s
Rated wind speed	12 m/s
Cut-out wind speed	25 m/s
Rated power output	1900 kW

The rated wind speed will be calibrated to improve the accuracy of the power curve. In order to determine the best rated wind speed for wind turbines in the target wind farm, the root mean square error (RMSE) of the estimated and observed power output will be used to evaluate the rated wind speed. The rated wind speed is tested from 10 m/s to 12 m/s. The step size of the tested rated wind speed is 0.1 m/s. The RMSE of each rated wind speed is:

$$RMSE = \sqrt{\frac{1}{S} \sum_{r=1}^S (f_{estimate(r)} - \varphi(r))^2} \quad (4.1)$$

where S is the amount of the observed power output data, $f_{estimate}$ is the estimated power output by the cubic power curve with a tested rated wind speed and φ is the observed power output.

Figure 4.1 is the RMSE of the estimated and observed power output with different rated wind speeds. The result shows the RMSE is 204.54 kW when the rated wind speed is 12 m/s. The minimum RMSE is 110.24 kW with the rated wind speed equals to 10.9 m/s, which is much better than 12 m/s. Therefore, the rated wind speed will be adjusted

from 12 m/s to 10.9 m/s to improve the power output estimation accuracy of wind turbines in the target wind farm. The original and calibrated power curves are shown in Figure 4.2.

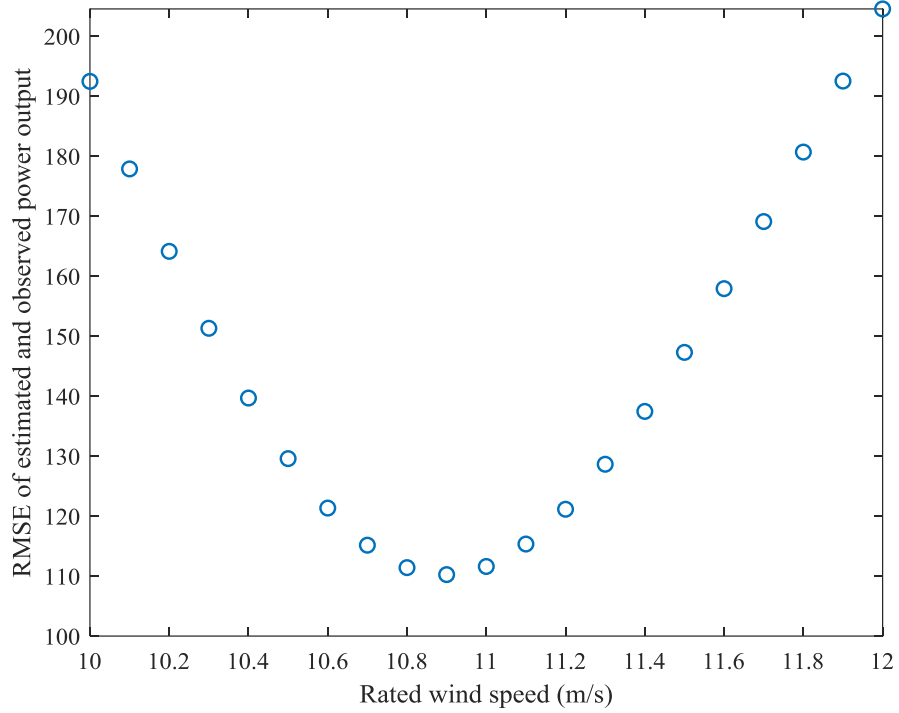


Figure 4.1 RMSE of the estimated and observed power output with different rated wind speeds

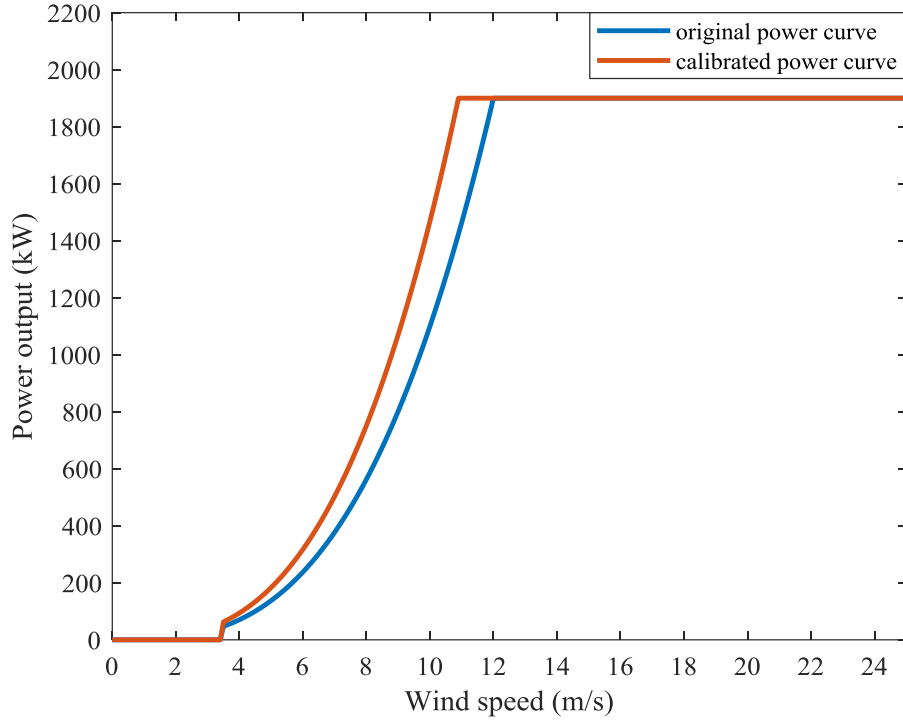


Figure 4.2 Original and calibrated power curves

The calibrated power curve will be used to estimate the power output of all wind turbines in the target wind farm. Equation (4.2) is the calibrated power curve function. The power output is measured by kilowatt and the wind speed is measured by meters per second.

$$P(v_i) = \begin{cases} 0, & 0 \leq v_i < 3.5 \\ 1.468v_i^3, & 3.5 \leq v_i < 10.9 \\ 1900, & 10.9 \leq v_i < 25 \\ 0, & v_i \geq 25 \end{cases} \quad (4.2)$$

Another important coefficient of the wind turbine is the thrust coefficient C_t . Figure 4.3 shows the thrust coefficient of the 1.9 MW wind turbine, which is from the cut-in wind speed to cut-out wind speed. The thrust coefficient is assumed to be 0 when the wind speed is lower than the cut-in wind speed. The numerical relationship of wind speed and the thrust coefficient will be used in the wake effect model.

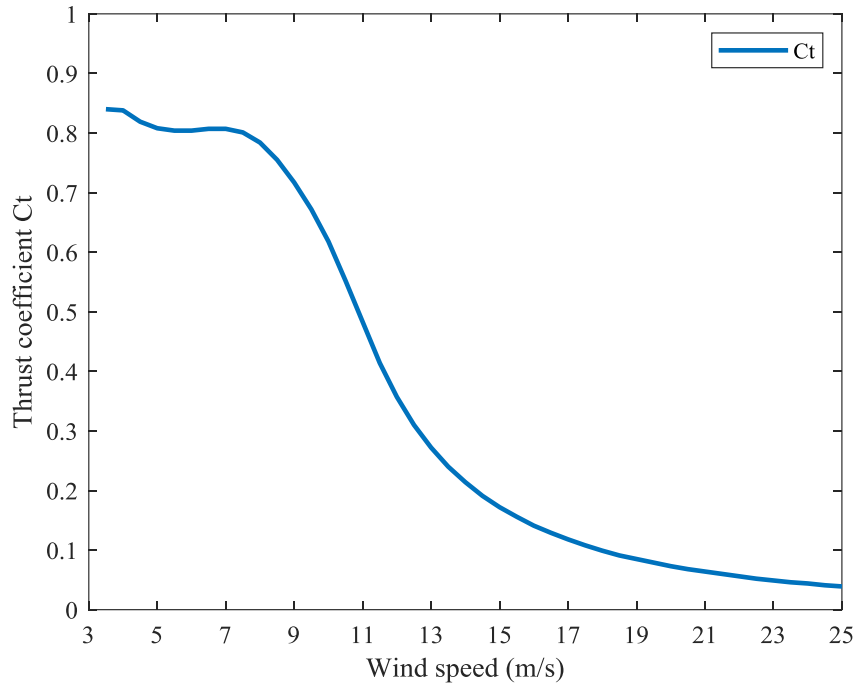


Figure 4.3 Thrust coefficient of the wind turbine

4.3 Wind characteristics result

The observed wind resource data of the target wind farm is by a baseline wind turbine. The baseline wind turbine is not in the wake regions of other wind turbines. As mentioned in Section 3.3.5, $20D$ is the maximum wake effect spreading distance in this thesis. In order to select the baseline wind turbine, the positions of wind turbines are set as centers. For each center, a circle with $20D$ as the radius is drawn to represent the wake region of the wind turbine. The baseline wind turbine is not covered in the circle areas. Figure 4.4 is an example of the baseline wind turbine (T_1). In the example, the baseline wind turbine is surrounded by T_2, T_3, T_4, T_5, T_6 and T_7 . The blue circles are the wake effect regions. The baseline wind turbine is not overlapped by wake effect generated by the surrounding wind turbines, so the wind resource data observed at T_1 is clean data.

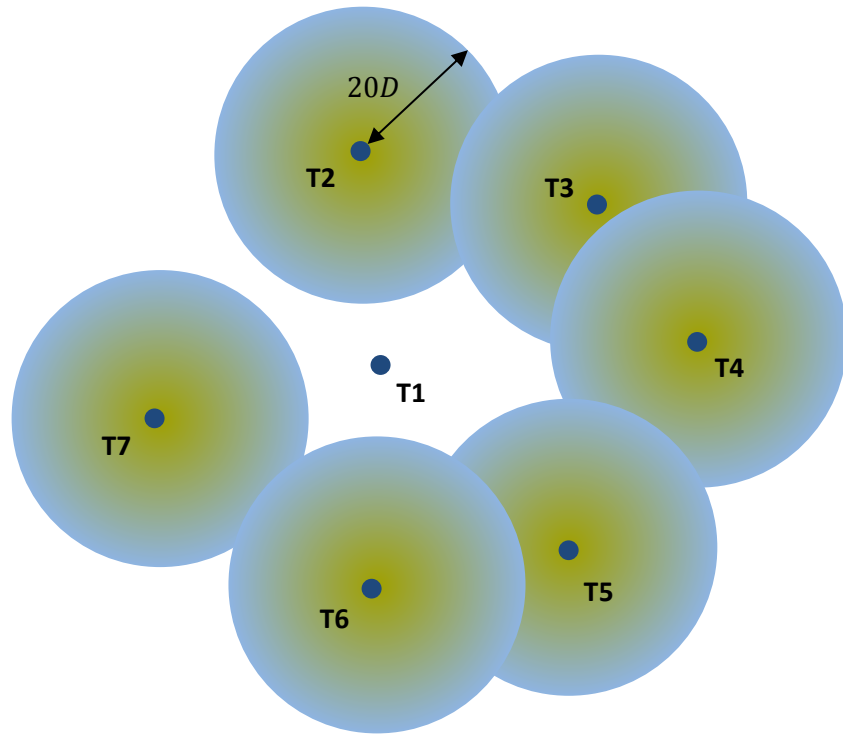


Figure 4.4 An example of the baseline wind turbine and surrounding wind turbines

The wind speed and direction are measured every 10 minutes for a whole year. Some of the wind speed and direction data are missed because the sensor was out of order or the wind turbine was overhauled. The missing data are excluded and the left data are valid. The valid wind resource data will be the observed wind resource data used to model the wind characteristics of the target wind farm. Figure 4.5 is the wind rose of the target wind farm, which gives a succinct view of wind conditions.

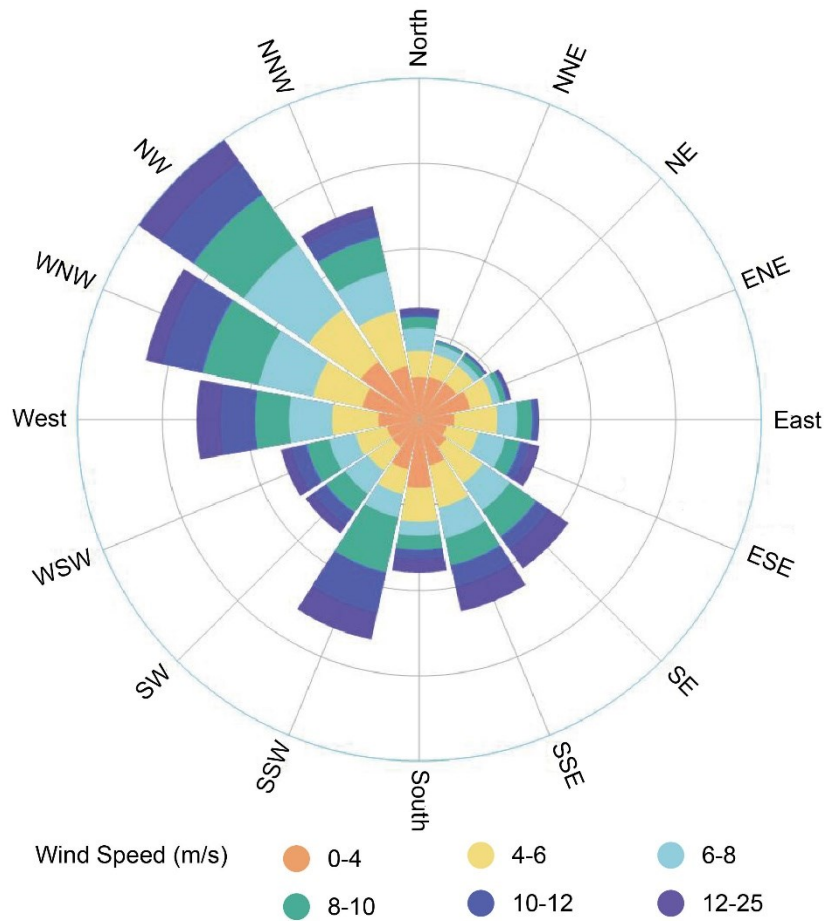


Figure 4.5 Wind rose of the target wind farm

The wind resource model is applied to characterize one-year wind speed and direction data observed in the target wind farm. The wind resource is fitted by sector-wise Weibull distribution. Wind direction is measured from 0° to 359° and wind speed is measured from 0 m/s to 22.5 m/s. The bin size of wind speed is set to be 0.5 m/s. In wind farm layout optimization studies, 15° [23] and 30° [22] are the most widely used wind direction segment sizes. Some wind farm layout optimization studies also use 1° [25], 5° [24] and 10° [20] as wind direction segment sizes. In order to select proper wind direction segment sizes used in wind farm layout optimization, in this thesis, 10 different wind direction segment sizes: 1° , 3° , 5° , 6° , 10° , 12° , 15° , 18° , 24° and 30° will be used to calculate the wind farm power output and the result will be evaluated.

We have used 15° as an example segment size to present the wind characteristics result. Other wind direction segment sizes in the wind resource model will be processed the same way as 15° . The wind direction is separated to 24 sectors with 15° as the wind direction segment size. Figure 4.6 shows the proportion of wind direction of the target wind farm. In each wind direction segment, Weibull distribution is used to represent the possibility of wind speed occurring at the correlated wind direction. Table 4.2 shows the wind characteristics of the target wind farm with 15° as the wind direction segment size, in which β_k is the wind direction, p_k is the proportion of wind direction, f_k is the Weibull distribution of wind speed occurring in k -th segment, a_k and b_k are scale parameter and shape parameter of Weibull distribution with $k = [1, 2, \dots, 24]$. In order to simplify the problem, wind direction is assumed to be the starting wind direction of each wind direction segment with $\beta_k = [0^\circ, 15^\circ, 30^\circ, \dots, 330^\circ, 345^\circ]$.

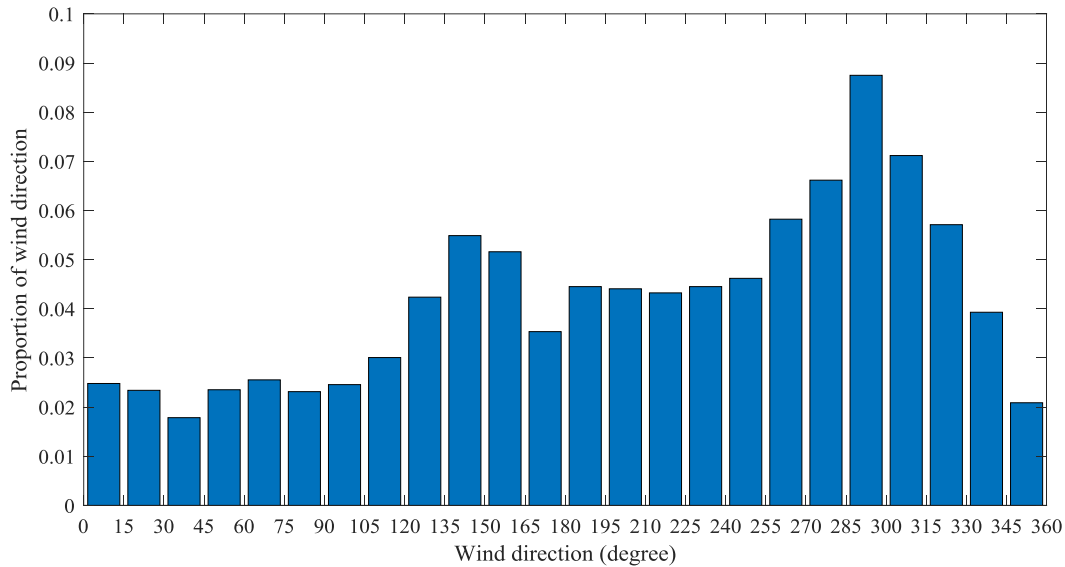


Figure 4.6 Proportion of wind direction with 15° as the wind direction segment size

Table 4.2 Wind characteristics of the target wind farm with 15° as the wind direction segment size

Wind direction (β_k)				Weibull distribution (f_k) of wind speed	
From	To	Data amount	Proportion (p_k)	Scale parameter (a_k)	Shape parameter (b_k)
0	14.9	1278	2.47%	6.23	2.25
15	29.9	1211	2.34%	6.27	2.40
30	44.9	919	1.77%	6.17	2.14
45	59.9	1220	2.36%	6.53	2.35
60	74.9	1322	2.55%	6.79	2.52
75	89.9	1201	2.32%	6.93	2.31
90	104.9	1271	2.46%	7.75	2.09
105	119.9	1551	3.00%	8.41	2.35
120	134.9	2183	4.22%	8.97	2.57
135	149.9	2847	5.50%	8.77	2.44
150	164.9	2676	5.17%	8.37	2.47
165	179.9	1833	3.54%	7.70	2.16
180	194.9	2304	4.45%	9.00	2.23
195	209.9	2274	4.39%	8.63	2.34
210	224.9	2236	4.32%	8.61	2.31
225	239.9	2304	4.45%	7.37	2.35
240	254.9	2397	4.63%	7.71	2.34
255	269.9	3010	5.81%	8.13	2.66
270	284.9	3424	6.61%	8.69	2.57
285	299.9	4517	8.73%	8.98	2.62
300	314.9	3678	7.11%	8.01	2.56
315	329.9	2974	5.75%	9.00	2.31
330	344.9	2036	3.93%	7.18	2.32
345	359.9	1097	2.12%	6.25	2.21

The wind direction will be generated based on p_k and Monte Carlo simulation will be used to randomly generate wind speed in each wind direction segment following f_k . The simulated wind speed and direction will be applied on wind farm power output calculation and wind farm layout optimization.

4.4 Wind farm power output assessment

The APO of the wind farm is calculated by the simulated wind resource, which is characterized by sector-wise Weibull distribution in Section 4.3. The simulated wind resource is different with the observed wind resource by time series. The relative error of the calculated wind farm power output by using the observed wind resource data is 0.5%. However, wind farm layout optimization needs a large amount of evaluations on layouts to select the best one, using the observed data with a large sample size will likely make the wind farm layout optimization computationally impossible. Therefore, a proper wind resource sample size and simulated wind resource should be considered in wind farm layout optimization.

4.4.1 Wind resource sample size selection

In this section, an appropriate wind resource sample size for onshore wind farm power output calculation and layout optimization will be analyzed. Theoretically, a large wind resource sample size leads to high power output estimation accuracy but also increases the CPU time. A small wind resource sample size can save more CPU time, but the estimation accuracy will also decrease. Therefore, a trade-off between the estimation accuracy and CPU time should be done before the optimization process.

The wind characteristics result with 10° , 15° and 30° as wind direction segment sizes are used to calculate the APO of the wind farm. For each wind direction segment size, the wind resource sample size will be tested from 1000 to 5000 with 500 as the step size. Considering the uncertainty of Monte Carlo simulation, for each wind resource sample size, Monte Carlo simulation will be used to randomly generate the wind resource data multiple times based on the wind characteristic results in Section 4.3. The wind farm power output will be calculated and recorded for each time. In this thesis, we will generate wind resource data ten times for each sample size. An appropriate wind resource

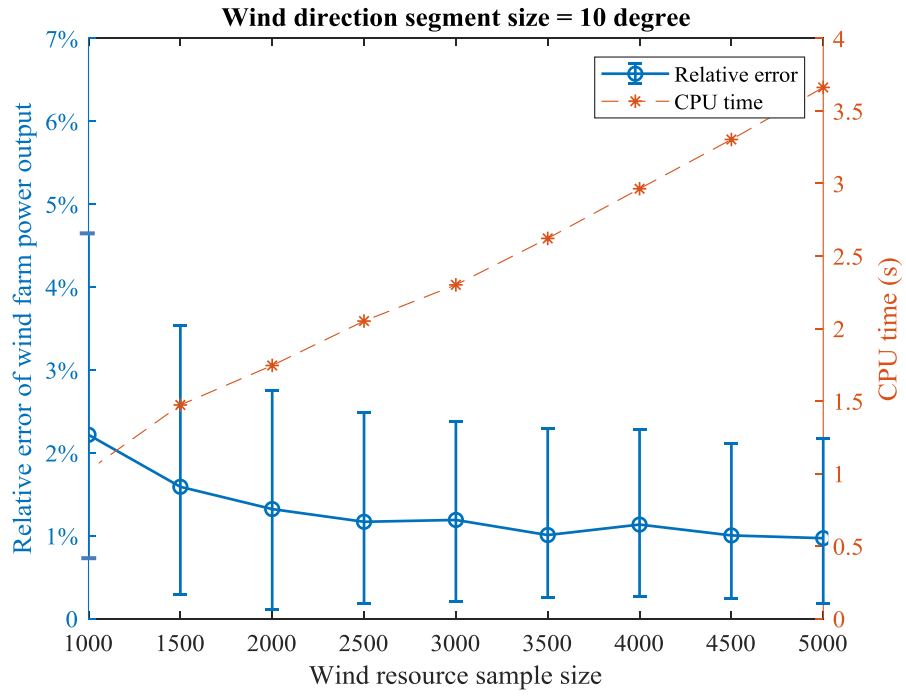
sample size will be selected based on the evaluated result. The selected wind resource sample size will be applied on wind farm power output calculation and layout optimization.

The estimated result will be evaluated by the mean value of the relative error (RE), range of the minimum and maximum RE, which is denoted by range of RE, and CPU time. The function of RE is shown below:

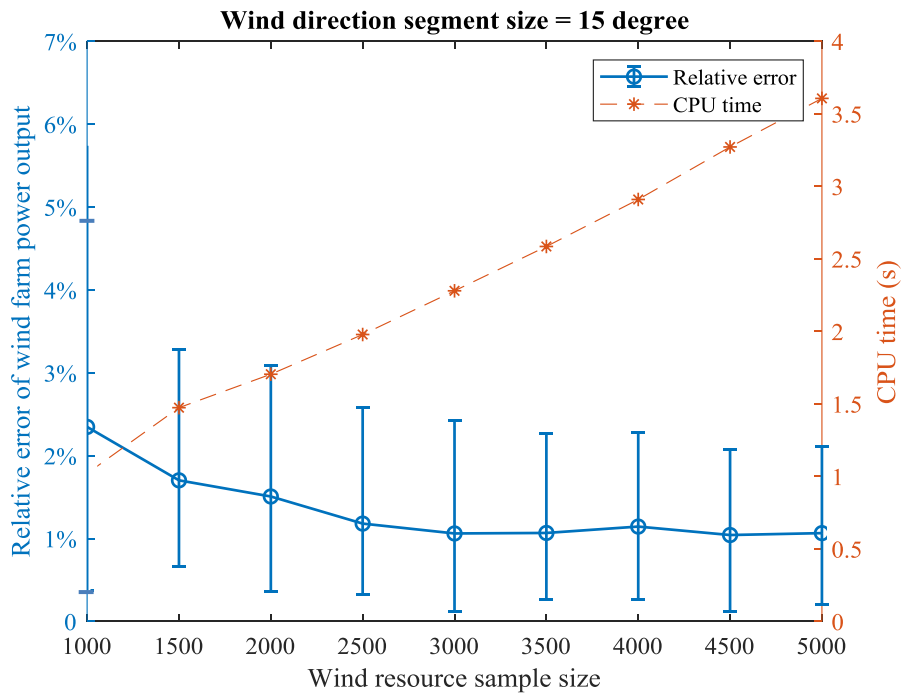
$$RE = \frac{|P_{estimate} - P_{farm}|}{P_{farm}} \times 100\% \quad (4.3)$$

where P_{farm} is the observed APO and $P_{estimate}$ is the estimated APO of the target wind farm.

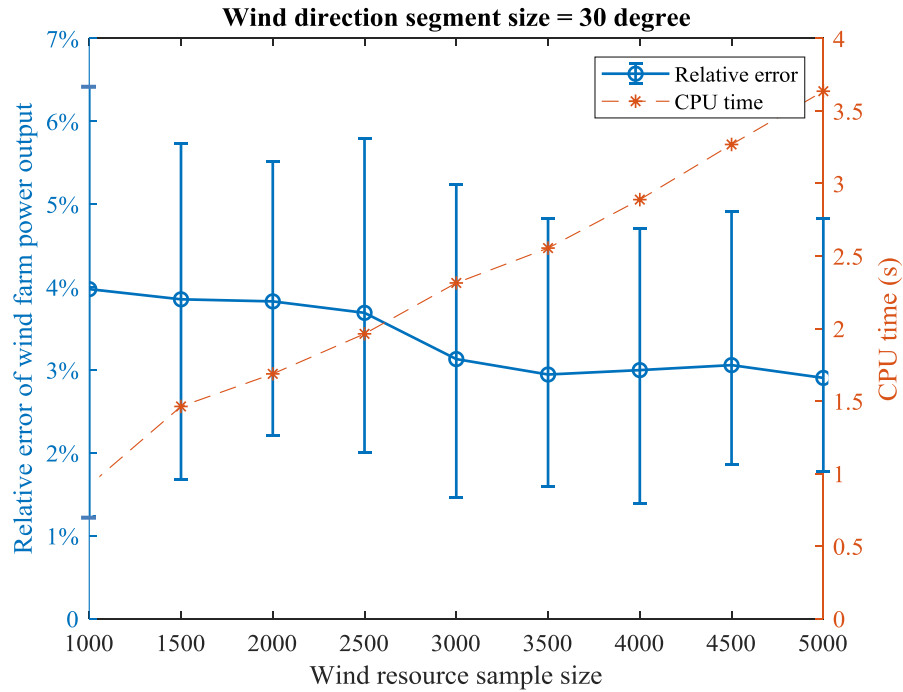
The result of RE and CPU time with 10°, 15° and 30° as wind direction segment sizes are shown in Figure 4.7 (a), (b) and (c) respectively. The mean RE is the average value of RE in ten times calculation, which is shown by blue dots in Figure 4.7. The maximum and minimum RE in ten times calculation is denoted by error bars in Figure 4.7, which shows the range of RE. The dashed line is the CPU time. In general, the RE of 10° and 15° is better than 30° for each wind resource sample size. When the wind resource sample size is 1000, the mean RE for 10°, 15° and 30° are 2.22%, 2.35% and 3.98% respectively. The range of RE at 1000 wind resource sample size for three wind direction segment sizes are 3.91%, 4.48% and 5.19% respectively. The mean RE and range of RE decreases with the increase of wind resource sample size. Meanwhile, the CPU time increases gradually. By trading off between the estimation accuracy and CPU time, 3500 is selected as the proper wind resource sample size. Although the RE calculated by 10°, 15° and 30° at each wind resource sample size are different, the mean RE and range of RE tends to stability when the wind resource sample size is greater than 3500. In addition, the CPU time at 3500 wind resource samples is not increased significantly. Therefore, 3500 will be the wind resource sample size used to estimate wind farm power output and optimize the wind farm layout.



(a)



(b)



(c)

Figure 4.7 Comparison of RE and CPU time with different wind resource sample sizes

4.4.2 Evaluation of wind direction segment sizes for wind farm power output calculation

In this section, 10 different wind direction segment sizes will be investigated for onshore wind farm power output calculation. The selected 10 wind direction segment sizes are: 1°, 3°, 5°, 6°, 10°, 12°, 15°, 18°, 24° and 30°, which are divisible by 360°. Similar as Section 4.4.1, due to the simulated wind resource exists uncertainty, 3500 wind resource data will be randomly generated ten times and the APO of the wind farm will be calculated in each time. The estimated APO will be evaluated with the observed APO of the target wind farm by RE and CPU time.

Figure 4.8 shows the result of RE and CPU time of the wind farm power output estimated with 10 different wind direction segment sizes. The blue dots are the mean RE in ten times calculation with different wind direction segment size. The error bar in Figure 4.8 shows the difference of the maximum and minimum RE in ten times calculation, which is the range of RE. The dashed line shows the average CPU time in ten

times calculation. In general, the mean RE increases with the growth of wind direction segment sizes. Except 30°, the mean RE by other wind direction segment sizes perform well, which are lower than 1.5%. The worst result of the mean RE is 3% by 30°. The range of RE at 30° is also the largest. The best RE is by 1°, which has the lowest range of RE and mean RE value. The CPU time is decreasing gradually with the increase of wind direction segment size. The change of CPU time from 1° to 30° is little when using 3500 wind resource data to calculate the APO.

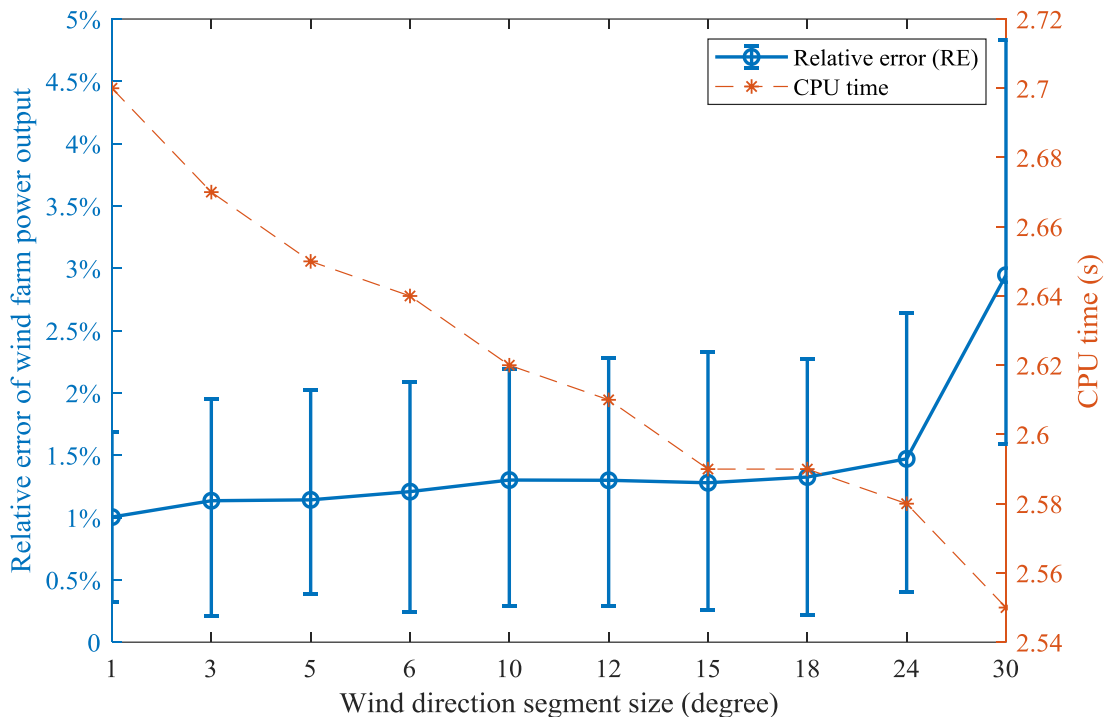


Figure 4.8 Comparison of RE and CPU time for different wind direction segment sizes calculated by 3500 wind resource data

The APO of the wind farm calculated by the simulated wind resource and observed wind resource exists difference. The RE of wind farm power output calculated by the observed wind resource data is 0.5%, which is better than using the simulated wind resource data to calculate the APO of the wind farm. Therefore, the most accurate way to calculate the wind farm power output is directly applying the observed wind resource data to the wind resource model. The CPU time of the APO calculated by the observed data is 210.15 seconds. Compared with the CPU time in Figure 4.8, using 3500 simulated

wind resource to calculate the APO of the wind farm is only 2.62 seconds in average, which is much lower than 210.15 seconds. The time cost will be more severe in the optimization process, which needs iterative evaluations on wind farm layouts. Therefore, for wind farm operators who aim to estimate the wind farm power output, directly using the wind farm power output model with the observed wind resource data can obtain the most accurate wind farm power output. While for wind farm developers, using the observed wind resource data in the optimization process is inappropriate due to the computation cost.

Some conclusions for layout optimization are made based on results in this section. For the wind resource sample size, using 3500 randomly generated wind resource data to calculate the wind farm power output is appropriate since the estimated result is close to the observed data and the CPU time is only about 2.62 seconds. The 3500 simulated wind resource data will be used in the optimization process. For the selection of wind direction segment size, wind resource modeled by sector-wise Weibull distribution with 1° to 24° as wind direction segment sizes have higher estimation accuracy on wind farm power output calculation than 30° . Due to the estimated wind farm power output exists uncertainty, the difference between the maximum and minimum RE are considered in evaluation. The smallest range of RE is at 1° , which means 1° is the most stable selection for wind farm power output calculation. The accuracy analysis in this section shows 1° may obtain the most reliable optimized result. The optimized result by large wind direction segment sizes may have a great error on wind farm power output estimation, which is less reliable.

4.5 Summary

In this chapter, the target wind farm for power output calculation and layout optimization is introduced. Step 2 to 4 of the proposed approach for wind direction segment size selection in wind farm layout optimization are illustrated. The wind turbine power curve is calibrated by processing the observed and estimated wind turbine power output. The wind resource is characterized by sector-wise Weibull distribution with different wind direction segment sizes. The wind farm power output is assessed with different wind resource sample sizes and wind direction segment sizes. We have selected

3500 as the appropriate wind resource sample size for power output calculation and layout optimization for the target wind farm. The APO of the target wind farm calculated with smaller wind direction segment sizes are closer to the observed APO of the target wind farm. The most accurate wind farm power output is calculated by directly applying the observed wind resource data to the wind farm power output model.

In the next chapter, the last step of the proposed approach for wind direction segment size selection in wind farm layout optimization will be illustrated. Thirty-five hundred simulated wind resources will be used to optimize the layout of the target wind farm. Ten different wind direction segment sizes will be used in the optimization process. The optimized result will be evaluated and the recommended wind direction segment sizes for onshore wind farm layout optimization will be presented.

Chapter 5 Wind Farm Layout Optimization

Results Discussion

In this chapter, four cases will be investigated. In order to select the proper wind direction segment sizes used in wind farm layout optimization, three different wind farms are considered. Case 1 is a 4×4 grids wind farm with 6 wind turbines. Case 2 is an 8×8 grids wind farm with 16 wind turbines. Case 3 aims to optimize a 28×28 grids wind farm with 83 wind turbines, which is the target wind farm introduced in Chapter 4. Case 4 also aims to optimize the target wind farm layout while the number of wind turbines is varying. The grid size is $5D \times 5D$, where D is the diameter of the rotor of a turbine measured in meters. The last step of the proposed approach for wind direction segment size selection will be illustrated by optimizing the wind farm layouts in Case 1, Case 2 and Case 3, which are from simple to complex. Only one wind direction segment size will be used to optimize the wind farm layout as an example in Case 4. The objective function and constraints for Case 1, Case 2 and Case 3 are mentioned in Section 3.5.1. The objective function and constraints for Case 4 is mentioned in Section 3.5.2. Descriptions of four cases are shown in Table 5.1.

Table 5.1 Description of 4 case studies

	Case 1	Case 2	Case 3	Case 4
Size	4×4 grids	8×8 grids	28×28 grids	28×28 grids
Number of variables	12	32	166	0 to 400
Number of turbines	6	16	83	0 to 200

Section 5.1 introduces the evaluation framework of this chapter. Section 5.2 solves wind farm layout optimization problem with a fixed number of wind turbines, which involves Case 1, Case 2 and Case 3 and the summary. Section 5.3 is wind farm layout optimization with various number of wind turbines, which includes Case 4 and the summary.

5.1 Evaluation framework

GA in MATLAB focuses on solving the minimization problem, which will be used to solve the wind farm layout optimization problem in this thesis. Parameters setting for GA is mentioned in Section 3.6. The best fitness value by GA is represented by f_{best} and the optimized APO of the wind farm is represented by $P_{optimize}$. $P_{optimize}$ equals to $-f_{best}$.

As mentioned in Section 4.4, the most accurate APO of the wind farm is calculated by applying the observed wind resource data to Equation (3.39). Therefore, wind farms optimized by 10 wind direction segment sizes will be re-evaluated by using the most accurate way to calculate the wind farm power output, which is denoted by P_{re} . We have used P_{ri} to denote the APO improvement, which is expressed by Equation (5.1).

$$P_{ri} = \frac{P_{re} - P_{un}}{P_{un}} \times 100\% \quad (5.1)$$

where P_{un} is the APO of an unoptimized wind farm.

The relative error of P_{re} and $P_{optimize}$ is denoted by RE_r , which is used to evaluate the estimation accuracy of the APO of optimized wind farms with different wind direction segment sizes. The expression of RE_r is:

$$RE_r = \frac{|P_{re} - P_{optimize}|}{P_{re}} \times 100\% \quad (5.2)$$

Wind farm efficiency μ is another measurement used to evaluate the optimized wind farm, which is given as [25]:

$$\mu = \frac{P_{tot}}{P_{ideal}} \quad (5.3)$$

where P_{tot} is the APO of the wind farm considering the wake effect, P_{ideal} is the APO of the wind farm without the wake effect, and μ equals to 1 if all wind turbines in the wind farm are wake-free.

We have used $\mu_{improve}$ to denote the wind farm efficiency improvement by the optimized layout, which is expressed in Equation (5.4) and μ_{un} and $\mu_{optimize}$ to denote

the wind farm efficiency of a wind farm with an unoptimized layout and optimized layout, respectively.

$$\mu_{improve} = \mu_{optimize} - \mu_{un} \quad (5.4)$$

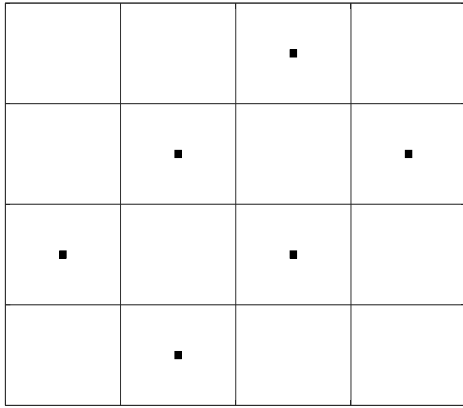
Wind farm power output and its estimation accuracy, together with computing time will be considered in the optimization process.

5.2 Wind farm layout optimization with a fixed number of wind turbines

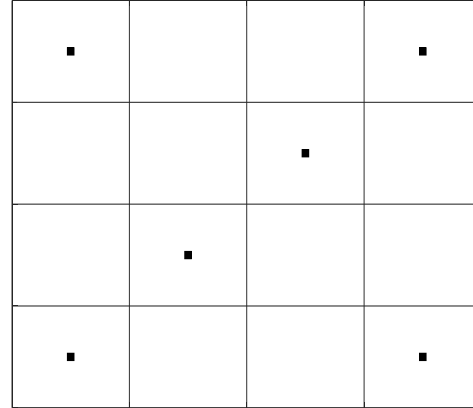
The first objective for wind farm layout optimization in this thesis is maximizing the APO of the wind farm. GA will be used to optimize the wind farm layout. Thirty-five hundred randomly generated wind resource data will be applied to the optimization process and the wind farm layout will be optimized with 10 different wind direction segment sizes. By evaluating the optimized results, the proper wind direction segment sizes for three cases will be proposed at the end of this section.

5.2.1 Case 1

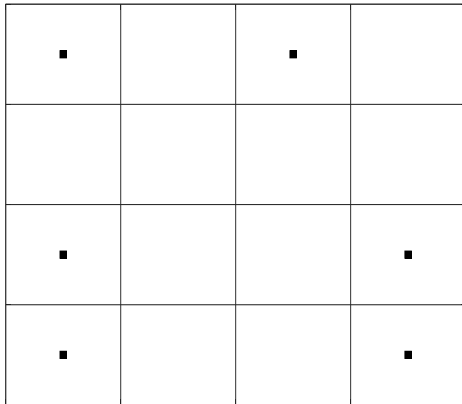
In Case 1, the layout of a 4×4 grids wind farm with 6 wind turbines is optimized to obtain the maximal wind farm power output. The optimized wind farm layouts with 10 different wind direction segment sizes are shown in Figure 5.1, where (a) is the layout optimized by using 30° as the wind direction segment size, (b) is the layout optimized by using 24° as the wind direction segment size, (c) is the layout optimized by using 18° as the wind direction segment sizes, (d) is the layout optimized by using 15° , 12° , 10° and 6° as the wind direction segment sizes, and (e) is the layout optimized by using 5° , 3° and 1° as the wind direction segment sizes. Figure 5.1 shows for some wind direction segment sizes, the optimized wind farm layouts are the same.



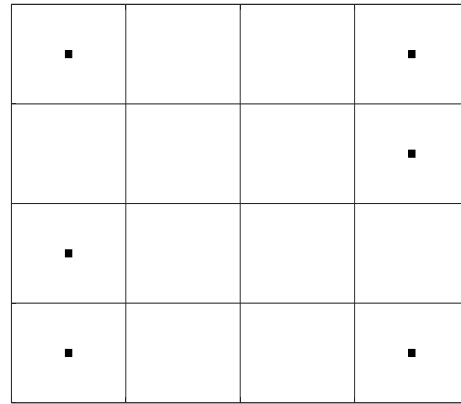
(a) Wind direction segment size = 30°



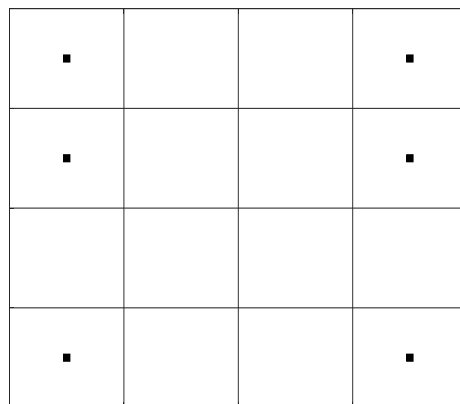
(b) Wind direction segment size = 24°



(c) Wind direction segment size = 18°



(d) Wind direction segment size = 15° ,
 12° , 10° and 6°



(e) Wind direction segment size = 5° , 3° and 1°

Figure 5.1 Optimized wind farm layouts with different wind direction segment sizes for Case 1

Figure 5.1 is P_{re} of five optimized wind farms, which is calculated by applying the observed wind resource data to the wind farm power output model. The result of P_{re} is shown in Figure 5.2. It shows the optimized layout in Figure 5.1 from the best to the worst are Layout (e), Layout (d), Layout (c), Layout (b) and Layout (a). In general, wind farms optimized by smaller wind direction segment sizes generate higher P_{re} than larger wind direction segment sizes. In addition, for wind direction segment sizes in a certain range, the optimized wind farm layouts are the same, such as 6° to 15° , and 1° to 5° .

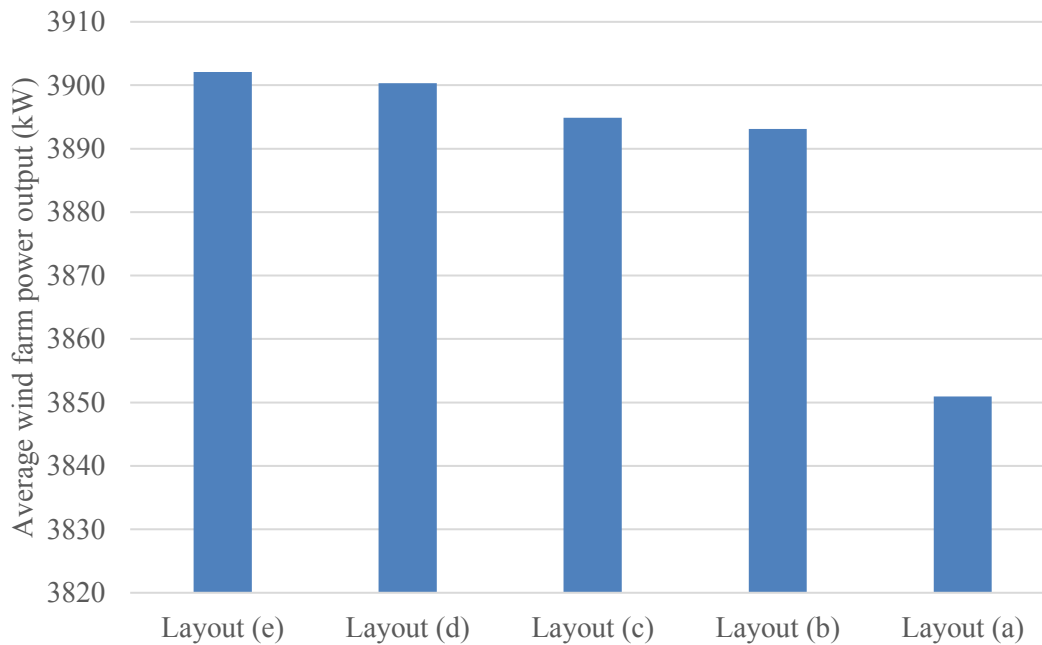


Figure 5.2 P_{re} of optimized wind farms in Case 1

GA is found converged in 90 generations for 10 different wind direction segments. In order to fairly compare the CPU time of the optimization process, the maximum generation of GA is reset to be 90 and the optimization process is reproduced. The CPU time of the optimization process with different wind direction segment sizes is shown in Figure 5.3. The result shows although 30° costs the lowest CPU time, P_{re} of Layout (a) in Figure 5.2 is significantly lower than other optimized wind farms. The highest P_{re} is by Layout (e) in Figure 5.1, which is optimized by using $1^\circ, 3^\circ$ and 5° as the wind direction segment sizes. As shown in Figure 5.3, the CPU time increases with the decrease of wind direction segment size. Therefore, 5° is the best wind direction segment size for Case 1,

which optimizes the wind farm layout with the highest power output and saves more CPU time.

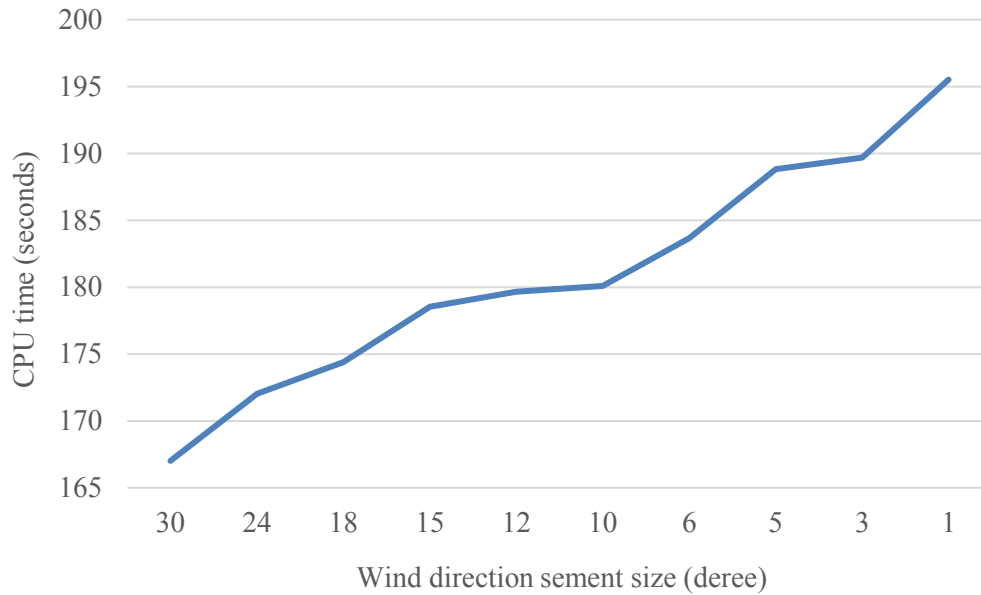
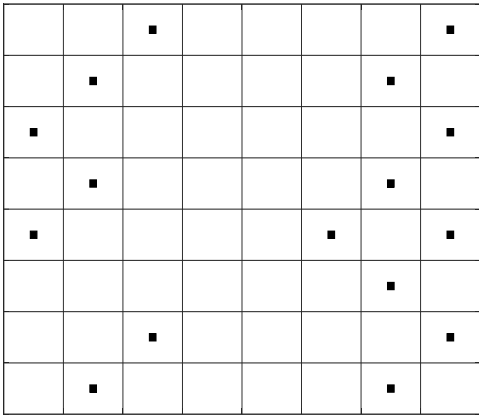


Figure 5.3 CPU time of wind farm layout optimization with different wind direction segment sizes in Case 1

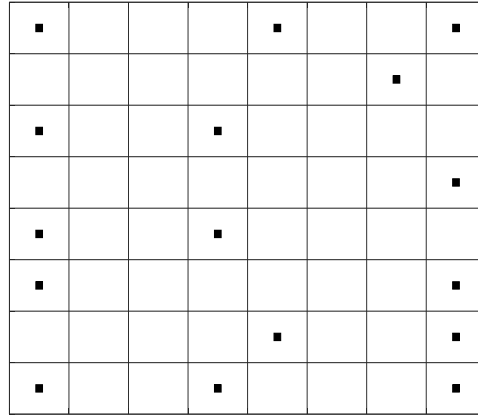
In summary, for small wind farm with low grid density and few wind turbines, wind direction segment sizes in certain ranges will obtain the same optimized layouts. Besides, in this case, no need to select a very small wind direction segment size, such as 1° in layout optimization. 3° and 5° can obtain the best layout and cost lower CPU time.

5.2.2 Case 2

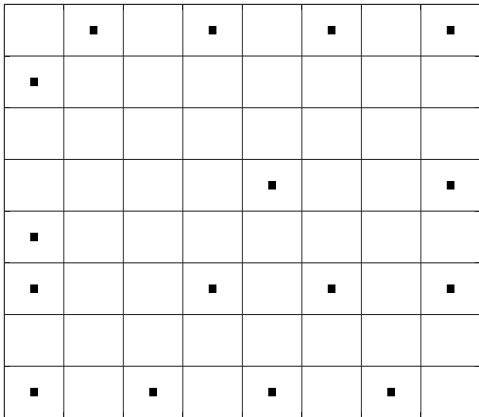
In Case 2, the layout of an 8×8 grids wind farm with 16 wind turbines is optimized to obtain the maximal wind farm power output. The optimized wind farm layouts with 10 different wind direction segment sizes are shown in Figure 5.4. The result shows for 10 wind direction segment sizes, the optimized wind farm layouts are different. Besides, for large wind direction segment size, for example 30° , the optimized layout is quite different with other optimized layouts.



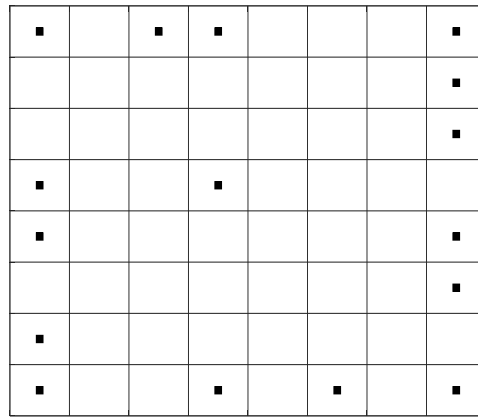
(a) Wind direction segment size = 30°



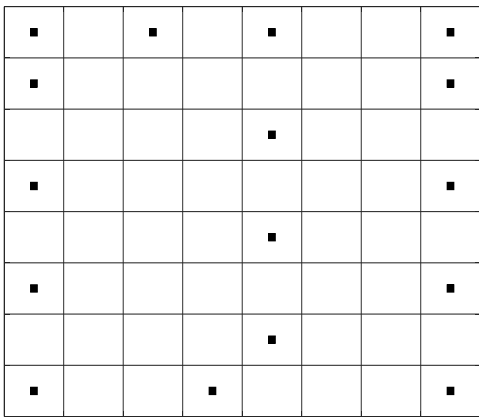
(b) Wind direction segment size = 24°



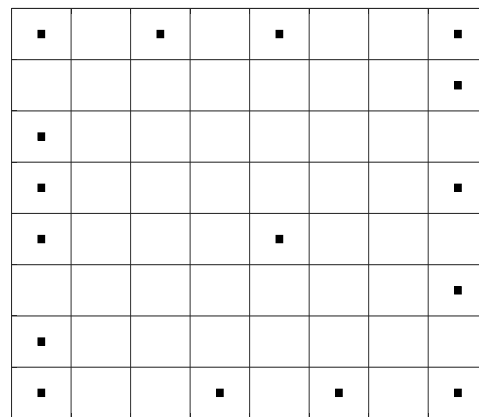
(c) Wind direction segment size = 18°



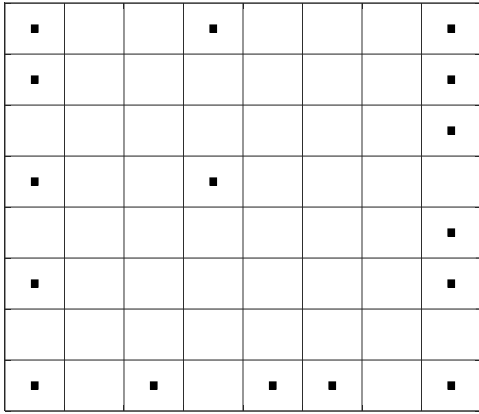
(d) Wind direction segment size = 15°



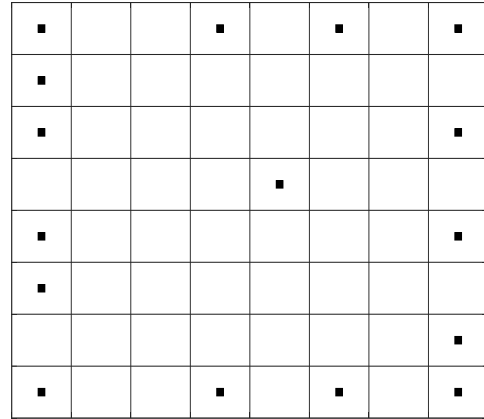
(e) Wind direction segment size = 12°



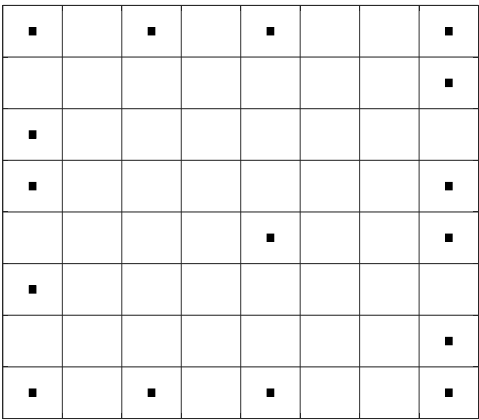
(f) Wind direction segment size = 10°



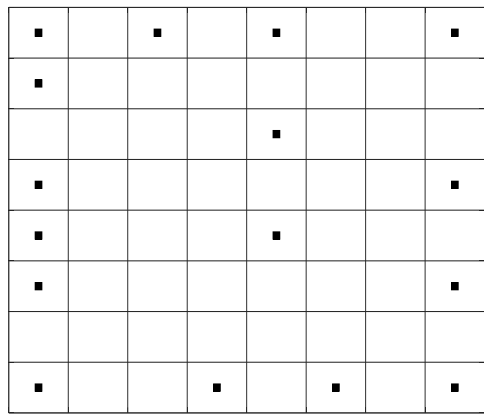
(g) Wind direction segment size = 6°



(h) Wind direction segment size = 5°



(i) Wind direction segment size = 3°



(j) Wind direction segment size = 1°

Figure 5.4 Optimized wind farm layouts with different wind direction segment sizes for Case 2

Figure 5.5 shows P_{re} of optimized layouts. The result in Figure 5.5 shows wind farms optimized by using smaller wind direction segment sizes will obtain a better layout, which leads to higher P_{re} . The wind farm optimized by using 1° as the wind direction segment size has the highest P_{re} among 10 optimized wind farms in Figure 5.4. Besides, wind farm optimized by using 30° as the wind direction segment size is much worse than other wind direction segment sizes.

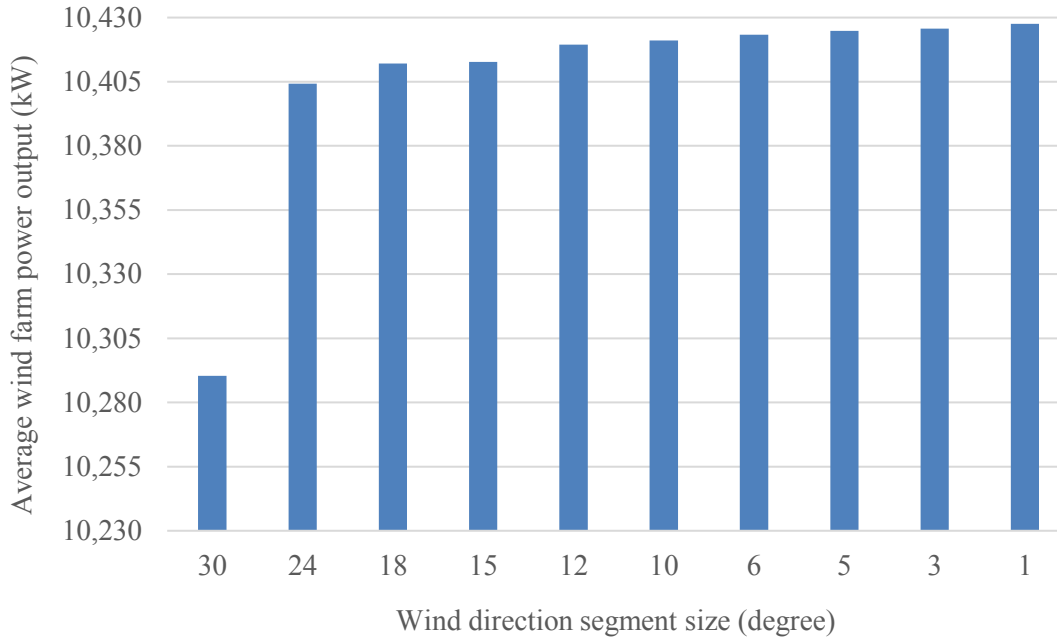


Figure 5.5 P_{re} of optimized wind farms with different wind direction segment sizes in Case 2

Figure 5.6 is the CPU time for the optimization process. GA is found converged in 550 generations for 10 different wind direction segments. The maximum generation of GA is reset to be 550 and the optimization process is reproduced to compare the CPU time. The result in Figure 5.6 shows with the decrease of wind direction segment size, the CPU time for the optimization process increases. Although P_{re} by 1° is the best, the CPU time for 1° is the highest. P_{re} of wind farm optimized by using 1° as the wind direction segment size does not show a significant improvement though it takes more CPU time. Take an example, Figure 5.5 shows P_{re} by 1° is just higher than P_{re} by 12° about 7 kW, while Figure 5.6 shows the CPU time by 1° is much higher than 12° .

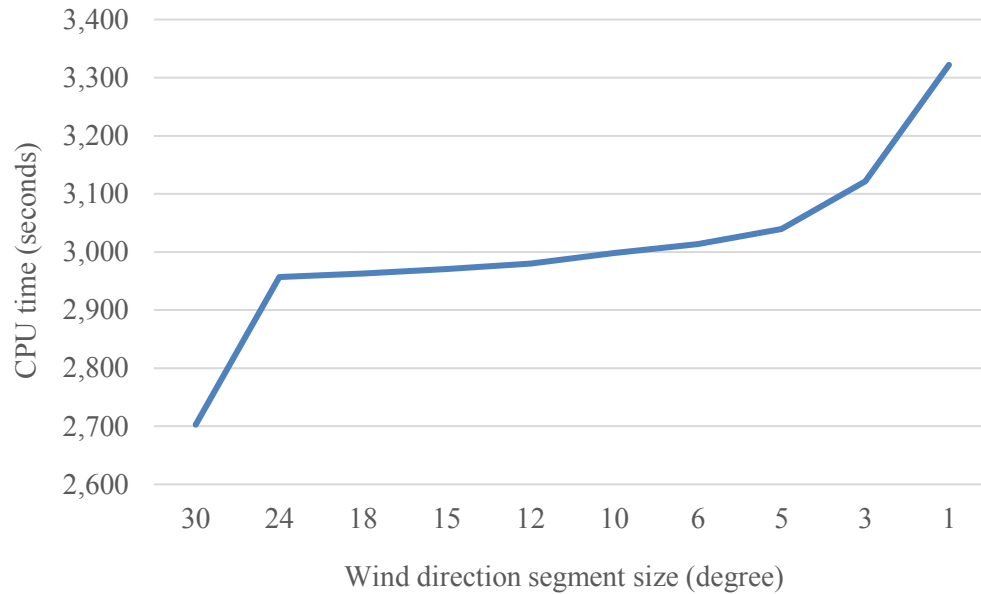


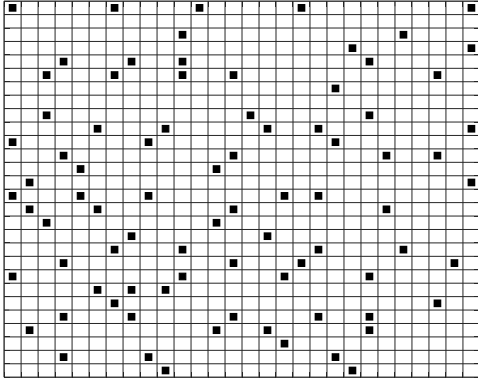
Figure 5.6 CPU time of wind farm layout optimization with different wind direction segment sizes in Case 2

Compared with Case 1, Case 2 is more complex. The wind farm size and number of wind turbines in Case 2 is larger than Case 1. Meanwhile, the amount of feasible solutions for Case 2 is more than Case 1. The optimized results in Case 1 and Case 2 show wind direction segment size is less sensitive to wind farm layout optimization with simple conditions. For wind farm with more complex conditions, smaller wind direction segment sizes can obtain better optimized wind farm layouts and wind farm optimized by using 1° as the wind direction segment size leads to the highest P_{re} . The time-consuming problem is more severe in Case 2 compared with Case 1. The CPU time of wind farm layout optimization with 1° as the wind direction segment size is much higher than using large wind direction segment sizes in Case 2. Except 1° , 3° and 5° are also proper selections for the wind direction segment size, since they save more CPU time and the optimized APO by 3° and 5° are very close to 1° .

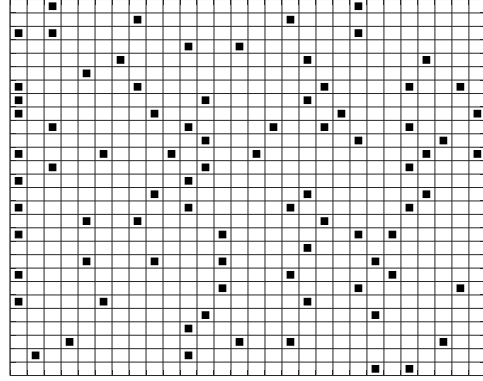
5.2.3 Case 3

In this case, the layout of the wind farm with 83 wind turbines introduced in Chapter 4 is optimized. The optimized wind farm layouts with 10 different wind direction segment sizes are shown in Figure 5.7. 10 Ten optimized layouts in Figure 5.7 are different and

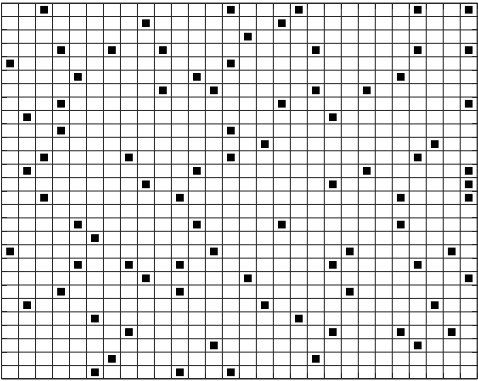
show low similarity. The optimized result of $P_{optimize}$, μ and the CPU time with different wind direction segment sizes are shown in Table 5.2.



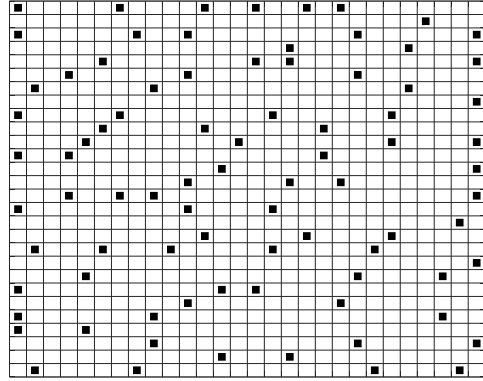
(a) Wind direction segment size = 30°



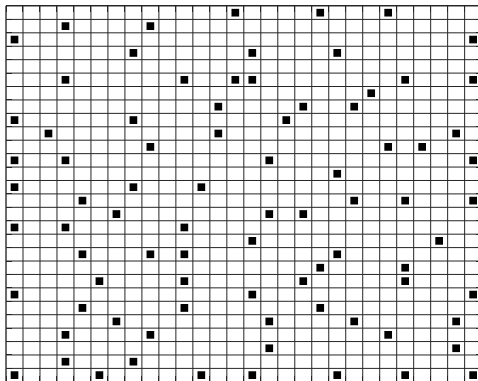
(b) Wind direction segment size = 24°



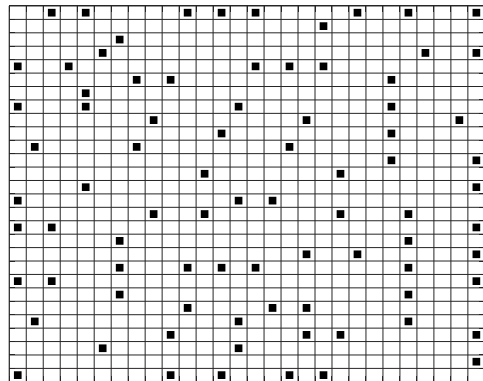
(c) Wind direction segment size = 18°



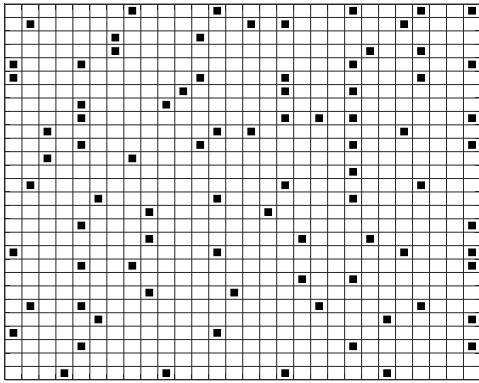
(d) Wind direction segment size = 15°



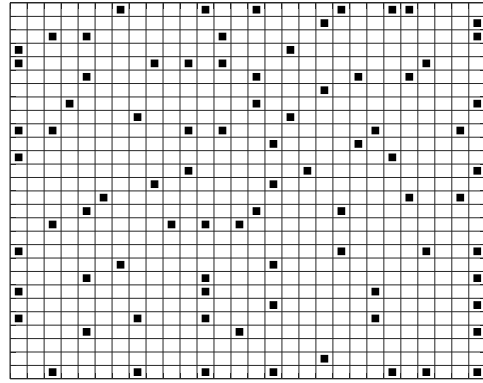
(e) Wind direction segment size = 12°



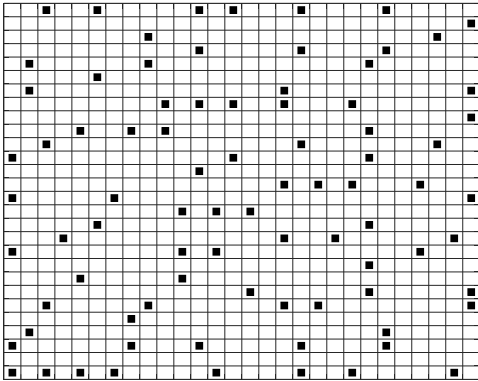
(f) Wind direction segment size = 10°



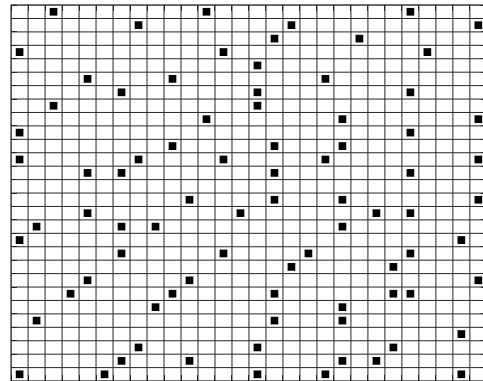
(g) Wind direction segment size = 6°



(h) Wind direction segment size = 5°



(i) Wind direction segment size = 3°



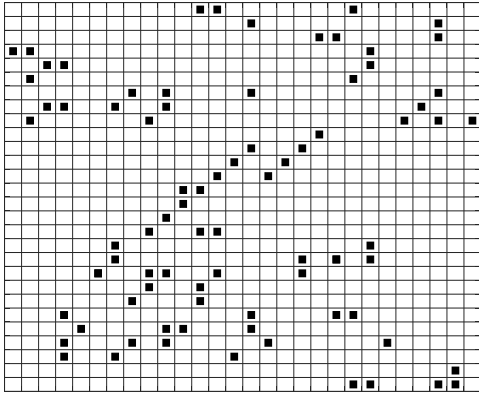
(j) Wind direction segment size = 1°

Figure 5.7 Optimized wind farm layout with different wind direction segment sizes for Case 3

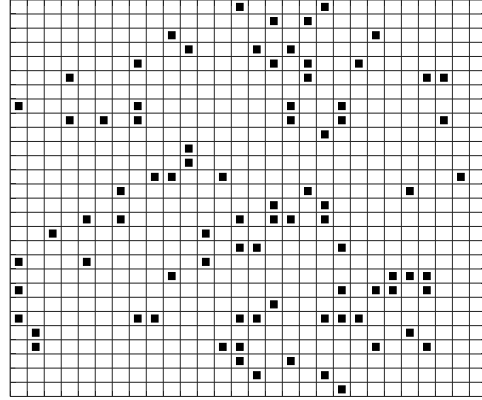
Table 5.2 Optimized result with different wind direction segment sizes for Case 3

Wind direction segment size	Optimized APO of the wind farm $P_{optimize}$	Optimized wind farm efficiency μ	CPU time for one generation (seconds)
30°	55349.98 kW	99.13%	42.87
24°	55429.19 kW	98.97%	45.50
18°	55496.36 kW	99.16%	46.01
15°	55254.38 kW	99.03%	46.69
12°	55186.16 kW	99.05%	49.93
10°	55517.82 kW	99.24%	50.03
6°	55291.35 kW	98.99%	50.27
5°	55206.45 kW	99.08%	50.63
3°	54600.97 kW	99.04%	52.71
1°	54449.29 kW	99.04%	64.05

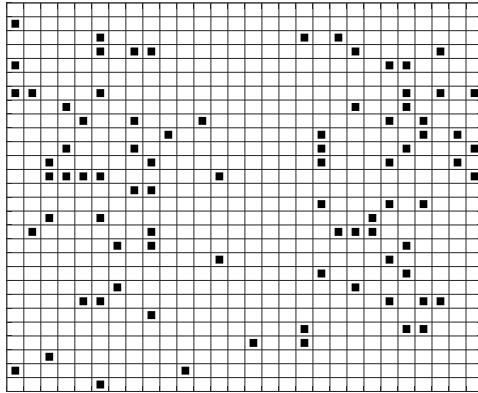
The result in Table 5.2 shows $P_{optimize}$ of 10 optimized layouts are around 55 thousands kilowatt and wind farm efficiency is around 99%. In general, the CPU time for one generation increases with the decrease of wind direction segment size. To protect the confidentiality of the target wind farm, the optimized results will not be compared with the real layout of the target wind farm. Layout-1, Layout-2 and Layout-3 are designed randomly following the constraints mentioned in Section 3.5 to compare with the optimized layouts. Figure 5.8 shows three designed layouts.



Layout-1



Layout-2



Layout-3

Figure 5.8 Randomly designed wind farms

We have used P_{ri} to denote the APO improvement of optimized layouts. As mentioned in Section 4.4, the most accurate way to calculate the APO is directly applying the observed wind resource data to the wind farm power output model. Therefore, P_{ri} calculated by the observed data will be used to evaluate the power output improvement of optimized wind farms compared with Layout-1, Layout-2 and Layout-3. The result of P_{ri} is shown in Table 5.3. The APO improvement shows the optimized wind farms with 10 direction segment sizes improve the APO of the wind farm compared with Layout-1, Layout-2 and Layout-3 in different extent. The lowest P_{ri} is by the wind farm optimized with 30° as the wind direction segment size. The layout optimized by using 10° as the wind direction segment size leads to the highest P_{ri} compared with 3 designed layouts,

which means Layout (f) in Figure 5.7 is the best one among 10 optimized layout. Figure 5.9 shows the APO of optimized wind farms calculated by using the observed wind resource data, which is denoted by P_{re} .

Table 5.3 Comparison of APO improvement of different optimized wind farms

Wind farm optimized with different wind direction segment sizes	APO improvement P_{ri} compared with		
	Layout-1	Layout-2	Layout-3
30°	9.13%	0.91%	0.91%
24°	9.15%	0.93%	0.93%
18°	9.35%	1.11%	1.11%
15°	9.60%	1.35%	1.34%
12°	9.59%	1.33%	1.33%
10°	9.89%	1.61%	1.61%
6°	9.42%	1.18%	1.17%
5°	9.58%	1.33%	1.32%
3°	9.56%	1.31%	1.31%
1°	9.33%	1.10%	1.10%

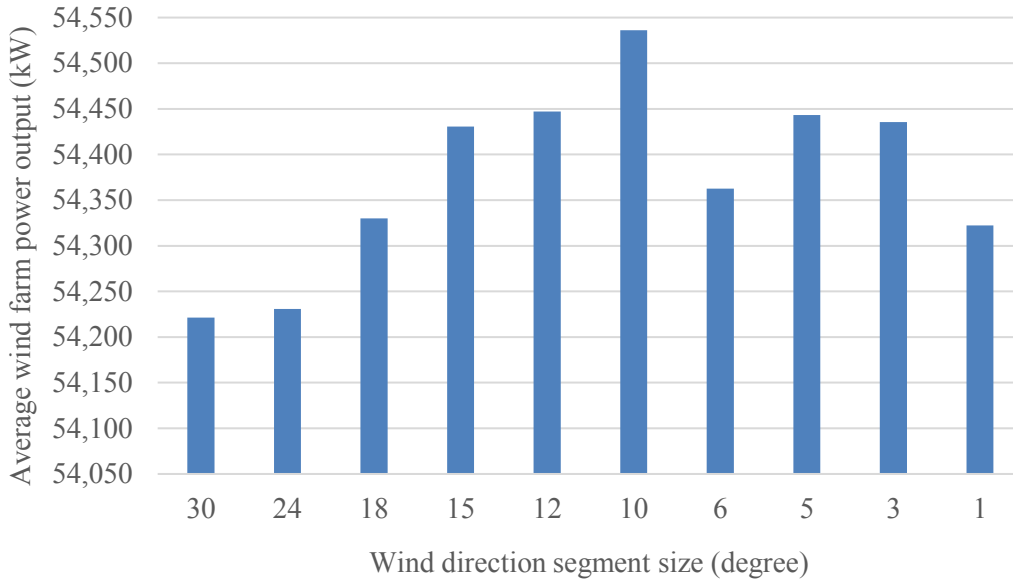


Figure 5.9 Comparison of APO of different optimized wind farms in Case 3

The result in Figure 5.9 shows P_{re} increases when the wind direction segment size reduces from 30° to 10° . P_{re} fluctuates when the wind direction segment size reduces from 10° to 1° . In Case 1, P_{re} shows an increase trend with the decrease of ranges of wind direction segment sizes. In Case 2, P_{re} increases monotonically with the decrease of wind direction segment sizes. However, in this Case 3, P_{re} is not increasing when the wind direction segment size is from 10° to 1° . The size of wind farm in Case 3 is 28×28 grids and the number of wind turbines is 83, which is much more complex than Case 1 and Case 2. Figure 5.10 shows the fitness curve of GA by using 1° as the wind direction segment size. The y-axis is the best fitness value in each generation. As mentioned in Section 3.6, two stopping criteria are set for GA: when it reaches 5000 generations, or the best fitness value in the last 50 generations keeps the same. According to Figure 5.10, GA stops due to it satisfies the second stopping criterion. Compared with Case 1 and Case 2, Case 3 has more feasible solutions and GA requires more generations to converge to the global optimum considering the complexity of the problem. Therefore, coefficients of GA should be further adjusted to optimize wind farms with high grid density and large amount of wind turbines. Meanwhile, the CPU time will dramatically increase and we may need a more powerful computer for operation.

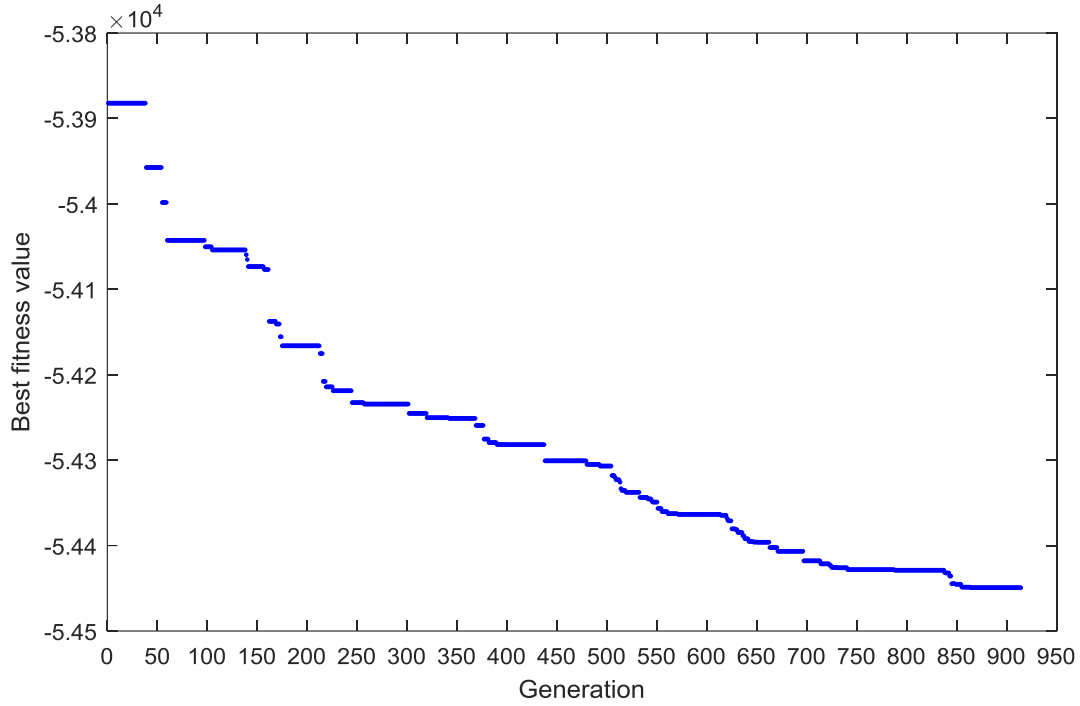


Figure 5.10 Fitness curve of the optimized wind farm layout with 1° as the wind direction segment size

The consistency of the optimized APO with different wind direction segment sizes is considered to select proper wind direction segment sizes in Case 3. The estimation accuracy of the optimized APO is denoted by RE_r , which is defined in Equation (5.2). The result of RE_r is shown in Figure 5.11. The x-axis is the wind direction segment size used in wind farm layout optimization and the correlated optimized wind farms are shown in Figure 5.7. We find RE_r shows a general trend of decrease and fluctuates at some wind direction segment sizes. Based on the result, the most accurate, acceptable and optimal wind direction segment sizes for layout optimization of the target wind farm will be proposed.

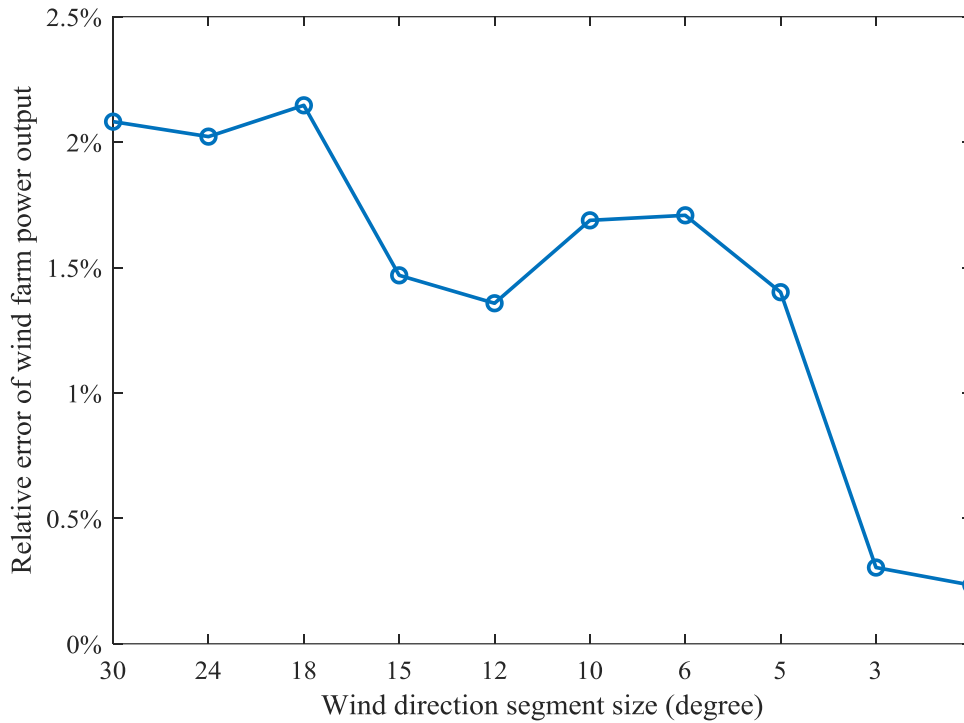


Figure 5.11 Relative error of wind farm power output of different optimized wind farms calculated by the simulated and observed wind resource

The most accurate wind direction segment size for wind farm layout optimization is 1° . Figure 5.11 shows the lowest RE_r is the wind farm optimized by using 1° as the wind direction segment size, which is only 0.23%. In general, the optimized wind farm using a smaller wind direction segment size in the optimization process is more reliable.

The acceptable wind direction segment size for wind farm layout optimization are from 1° to 15° . As mentioned in Section 4.4.2, the maximum RE of the APO of the original wind farm by different wind direction segment sizes is about 2.5%, except 30° , which is 4.7%. The RE of the APO of the original wind farm calculated by the observed wind resource data is 0.5%. The difference between the maximum RE by the simulated data and the RE by the observed data is 2%. Figure 5.11 shows the RE_r by using wind direction segment sizes between 1° to 15° are lower than 2%. Therefore, wind direction segment sizes no greater than 15° are acceptable wind direction segment sizes for wind

farm layout optimization. The optimized wind farms by using 18° , 24° and 30° as the wind direction segment size are less reliable.

The optimal wind direction segment size for Case 3 is 3° . Figure 5.11 shows RE_r by 3° performs well, which is 0.3%. It is only 0.07% higher than using 1° as the wind direction segment size. Figure 5.9 shows the power output improvement of the wind farm optimized by using 3° as the wind direction segment size is higher than using 1° as the wind direction segment size. In addition, the CPU time of wind farm layout optimization increases with the decrease of wind direction segment size. Table 5.2 shows with using 3° as the wind direction segment size to optimize the wind farm layout, the CPU time for GA to run one generation is 22% lower than using 1° as the wind direction segment size. Therefore, using 3° as the wind direction segment size is the optimal selection for layout optimization in Case 3, which satisfies the requirement of high estimation accuracy and saving the CPU time.

5.2.4 Summary

In this section, three case studies are investigated to select proper wind direction segment sizes in wind farm layout optimization. The size of the wind farm enlarges and the number of wind turbines increases from Case 1 to Case 3.

The wind direction segment size selection strategies are different based on the complexity of the wind farm. The result shows for simple wind farms, such as Case 1, using wind direction segment sizes in a certain range for wind farm layout optimization will lead to the same optimized layout. For wind farm with more complex conditions, such as Case 2, applying different wind direction segment sizes in layout optimization will obtain different optimized layouts. The APO of the optimized wind farm layout by using a small wind direction segment size is higher than using a large wind direction segment size. Besides, the CPU time for the optimization process increases with the decrease of wind direction segment size. For wind farms with simple conditions, we can select 5° in the optimization process to obtain the best result and save the CPU time. For larger wind farms with more wind turbines, 1° is the best wind direction segment size used for wind farm layout optimization. While 3° and 5° are proper wind direction

segment sizes to be used, since they save more CPU time and the optimized APO by 1° shows little improvement compared with using 3° and 5° as wind direction segment sizes.

For the target wind farm in Case 3, wind farm layouts optimized with all wind direction segment sizes used in this thesis improve the APO compared with three randomly designed wind farms. The result in Case 3 also shows for wind farms with complex conditions, GA requires more generations to search for the best optimized layout if applying small wind direction segment sizes in the optimization process. Meanwhile, the CPU time will dramatically increase. The consistency analysis in Case 3 evaluates the estimation accuracy of the optimized APO. The result shows 1° is the most reliable wind direction segment size for wind farm layout optimization. Wind farms optimized by using wind direction segment sizes between 1° to 15° are acceptable. In addition, 3° is the optimal wind direction segment size for wind farm layout optimization, which leads to high estimation accuracy on power output calculation of the optimized wind farm and also saves the CPU time. Wind farm developers and researchers can select proper wind direction segment sizes used in wind farm layout optimization based on their requirement.

5.3 Wind farm layout optimization with various number of wind turbines

The second objective for wind farm layout optimization in this thesis is minimizing the CoP of the target wind farm. In this case, the number of wind turbines is varying. GA is used to optimize the wind farm layout. Thirty-five hundred randomly generated wind resource data will be applied in the optimization process. In this section, 15° is selected as the wind direction segment size to optimize the wind farm layout as an example. The optimized result will be evaluated based on the CoP and APO of the optimized wind farm.

5.3.1 Case 4

The optimized wind farm with the minimal CoP is shown in Figure 5.12, which has 60 wind turbines. Figure 5.13 is the fitness curve.

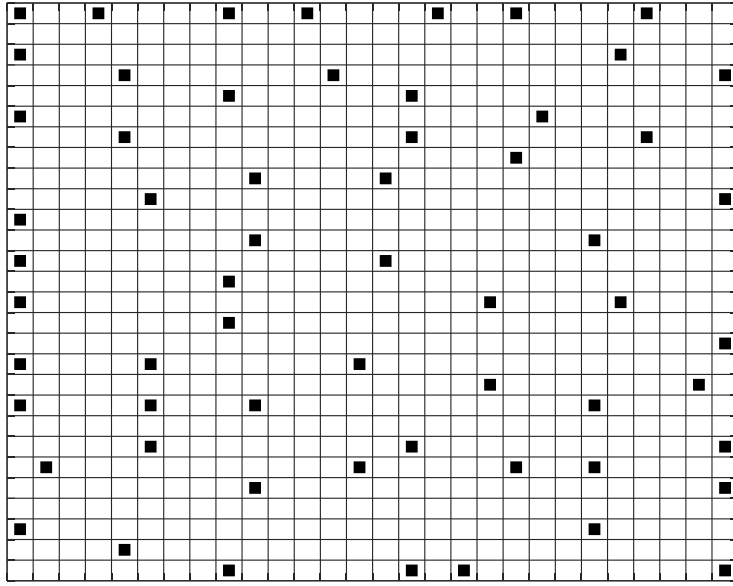


Figure 5.12 Optimized wind farm with the minimal CoP

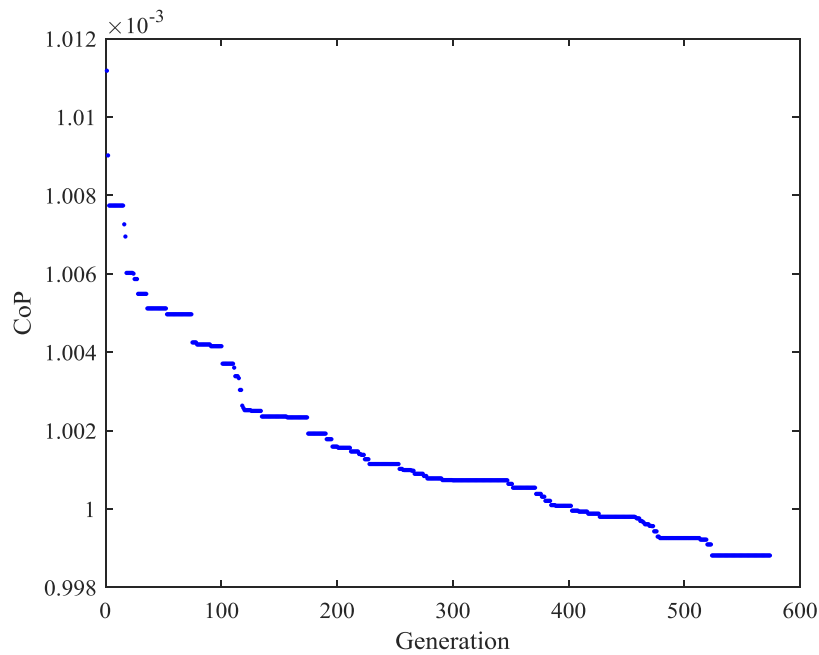


Figure 5.13 Fitness curve of the optimized wind farm with the minimal CoP

The comparison results of Layout-1, Layout-2 and Layout-3 and the optimized wind farm are shown in Table 5.4. The number of wind turbines of the optimized wind farm is 60, while the three designed wind farms have 83 wind turbines. The CoP of the optimized wind farm with 60 wind turbines is 9.9881×10^{-4} . The optimized wind farm decreases

9.16%, 2% and 2.1% of CoP compared with Layout-1, Layout-2 and Layout-3, respectively. Furthermore, the optimized wind farm improves the wind farm efficiency to 99.55%, which is 9.14%, 2.11% and 2.11% higher than the wind farm efficiency by Layout-1, Layout-2 and Layout-3, respectively.

Table 5.4 Comparison of Layout-1, Layout-2, Layout-3 and optimized wind farm

	Layout-1	Layout-2	Layout-3	Optimized layout
Cost of power output (CoP)	1.0987×10^{-3}	1.0185×10^{-3}	1.0195×10^{-3}	9.9881×10^{-4}
Wind farm efficiency	90.41%	97.44%	97.44%	99.55%

The wind farm layout is also optimized with specific numbers of wind turbines, which are from 58 to 83. The optimized result is evaluated by the CoP, APO and efficiency of the optimized wind farm. The CoP and APO of the optimized wind farm with various number of wind turbines is shown in Figure 5.14. Equation 4.3 shows both the numerator and denominator of CoP are nonlinear, which is difficult to directly find the trend. Based on the result shown in Figure 5.14, CoP of the wind farm decreases from 58 wind turbines to 60 wind turbines and then increases in wave. Although the APO of the optimized wind farm seems increasing linearly, the APO improvement with various numbers of wind turbine are different. The average gradient of the APO is 656.84 kW and the standard deviation of the gradient is 14.33 kW. The APO of Layout-1, Layout-2 and Layout-3 calculated with 15° as the wind direction segment size are 50361 kW, 54329 kW and 54277 kW, respectively. The result shows the APO of the optimized wind farm with 76 wind turbines reaches the energy generation capacity of Layout-1, which reduces 7 wind turbines compared with Layout-1. The optimized wind farm with 82 wind turbines meets the energy generation capacity of Layout-2 and Layout-3, which reduces 1 wind turbine. In addition, the CoP of optimized wind farms with 76 and 81 wind turbines is lower than the CoP of Layout-1, Layout-2 and Layout-3.

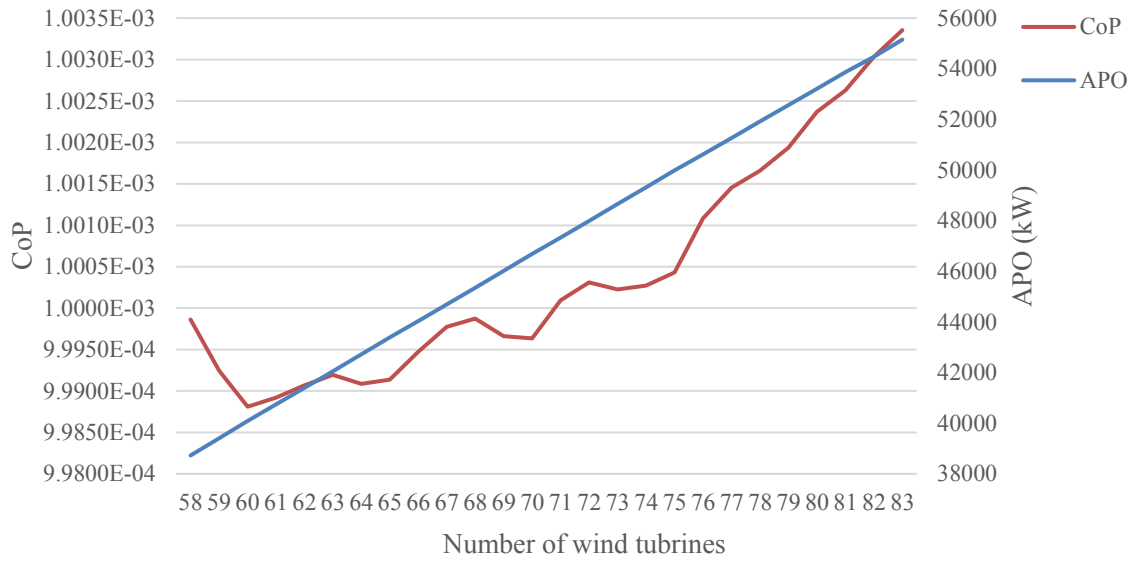


Figure 5.14 CoP and APO of the optimized wind farms with various number of turbines

Figure 5.15 is the wind farm efficiency of optimized wind farms with various number of turbines. The maximum wind farm efficiency is 99.55%, which is by the optimized wind farm with 60 wind turbines. The wind farm efficiency curve shows a reverse trend compared with the CoP curve in Figure 5.14. The wind farm efficiency gradually decreases when the number of wind turbines increases from 60 to 83 wind turbines, which means the wake effect in the wind farm is increasingly severe.

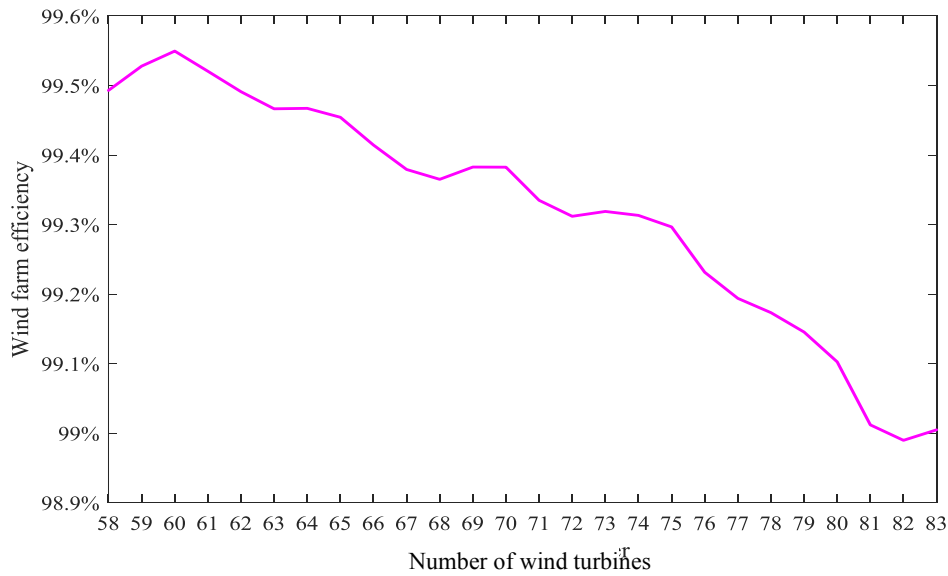


Figure 5.15 Wind farm efficiency of optimized wind farms with various number of turbines

5.3.2 Summary

In this section, the CoP of the target wind farm is minimized by optimizing the number and positions of wind turbines in the wind farm. 15° is selected as the wind direction segment size for wind farm layout optimization. The result shows 60 wind turbines with an optimized wind farm layout has the minimum CoP. The optimized wind farm reduces the CoP and improves the wind farm efficiency compared with Layout-1, Layout-2 and Layout-3. Besides, the optimized wind farm layouts with fewer wind turbines can meet the energy generation capacity of Layout-1, Layout-2 and Layout-3. It reduces wind turbines and decreases the CoP of the wind farm. Other wind direction segment sizes for this case will be investigated in the future.

Chapter 6

Summary and Future Work

6.1 Summary

Wind farm layout optimization is an important problem when designing a wind farm. A good wind farm layout can mitigate the wake effect, which leads to high APO and low CoP of the wind farm. The main contributions of this thesis are on two aspects: 1) proposing a comprehensive approach for selecting proper wind direction segment sizes in wind farm layout optimization studies. 2) demonstrating the proposed approach by case studies and presenting different wind direction segment size selection strategies based on the optimization results. The work on two contributions are summarized as follows.

The proposed procedure involves five steps: modeling the wind farm power output and defining the objective function, pre-processing the data of the target wind farm, selecting an appropriate wind resource sample size for wind farm layout optimization, evaluating the estimated power output of the target wind farm, and optimizing the wind farm layout by using GA. The proposed approach can be applied on any wind farm power output model to select the proper wind direction segment size for this model. In this thesis, 10 different wind direction segment sizes used in wind farm layout optimization are investigated.

The first step of the proposed approach is illustrated in Chapter 3. The wind farm power output model in this thesis is composed by commonly used wind resource model [24], position model [31], wake effect model [25] and wind turbine power curve [54]. Wind resource is modeled by sector-wise Weibull distribution. Multiple wake effect model derived from Jensen's model considering wake conditions is used to simulate wind speeds at wind turbines in the wind farm. Wind turbine power output is estimated by cubic power curve. Two objective functions are defined: maximizing the APO and minimizing the CoP of the wind farm by optimizing the wind farm layout. The first and second objective function consider a fixed and various number of wind turbines

respectively. The grid method is used to design the wind farm and GA is employed as the optimization algorithm.

The second to the fourth steps of the proposed approach are illustrated by calculating and evaluating the power output of an onshore wind farm in Chapter 4. The wind resource data, operational data, geographic data and wind turbine properties are pre-processed. The coefficients of wind turbine power curve are calibrated based on the observed wind turbine power output. The calibrated wind turbine power curve improves the wind turbine power output estimation accuracy. The wind resource data is characterized by sector-wise Weibull distribution with different wind direction segment sizes. Wind resource is randomly generated by Monte Carlo simulation following the correlated Weibull distribution. Thirty-five hundred is selected as the appropriate wind resource sample size for wind farm layout optimization by trading off the power output estimation accuracy and CPU time. Wind farm power output calculated with different wind direction segment sizes are evaluated by the mean RE, range of RE and CPU time. The result shows 1° is the best wind direction segment size for wind farm power output calculation. Besides, the most accurate way to calculate the wind farm power output is directly applying the observed wind resource data to the wind farm power output model.

The last step of the proposed approach is illustrated by optimizing layouts of wind farms in Chapter 5. Four case studies are considered: Case 1, Case 2 and Case 3 aim to maximize the APO of the wind farm, and Case 4 aims to minimize the CoP of the wind farm by optimizing the wind farm layout. The selection of wind direction segment sizes in wind farm layout optimization is investigated in the first three cases. Wind farm power output and its estimation accuracy, together with computing time, are considered in the optimization process. The observed wind resource is used to re-evaluate the APO of the optimized layout. The conclusions of four case studies are as follows.

- Wind direction segment size has a clear impact on wind farm layout optimization. Smaller wind direction segment sizes generally result in better layouts with higher wind farm power output. The computing time for the optimization process increases with the decrease of wind direction segment size.

- For wind farms of different sizes and number of wind turbines, suitable wind direction segment sizes used in wind farm layout optimization are recommended. For wind farms with simple conditions, 5° is the best selection of wind directions segment size. For wind farms with complex conditions, wind farm optimized by using 1° as the wind direction segment size leads to the highest APO while it costs higher CPU time. We also select 3° and 5° as proper wind direction segment sizes since they cost lower CPU time and the optimized APO is close to the result by 1° .
- For the target wind farm, all the optimized wind farms with 10 wind direction segment sizes improve the APO compared with three randomly designed wind farms. The consistency analysis shows 1° is the most reliable wind direction segment size for wind farm layout optimization. The acceptable wind direction segment sizes are from 1° to 15° . In addition, we select 3° as the optimal wind direction segment size, which has high estimation accuracy on power output calculation and also saves the CPU time.
- The CoP of the target wind farm is minimized by using 15° as the wind direction segment size. The result shows 60 wind turbines with an optimized wind farm layout leads to the minimum CoP, which reduces the CoP and improves the wind farm efficiency compared with three randomly designed wind farms. Besides, the optimized wind farm layouts with fewer wind turbines meet the energy generation capacity of designed wind farms, which reduce wind turbines and decrease the CoP.

6.2 Future work

Wind farm layout optimization is a comprehensive research topic. In this study, we found two main challenges to be solved in the future.

The first challenge is finding the global optimum of wind farm layout optimization problems with complex conditions. In Case 3, the wind farm size is 28×28 grids and the number of wind turbines is 83. The wind farm condition in Case 3 is much more complex than Case 1 and Case 2. The result in Case 3 shows when selecting small wind direction segment size in wind farm layout optimization, such as 1° , it is more difficult for GA to

find the global optimum compared with using large wind direction segment size. Besides, the CPU time will dramatically increase by using small wind direction segment size to find the global optimum. The result in Case 2 shows the APO of the wind farm optimized by using 1° as the wind direction segment size does not show a significant improvement though it takes more CPU time. The time-consuming problem will be more severe when the wind farm has high grid density and large amount of wind turbines. Therefore, we should consider whether 1° is worth to be selected as the wind direction segment size when optimizing a wind farm layout with complex conditions, or to use a more efficient algorithm to find the global optimum.

The second challenge is the improvement of wind farm power output model. As mentioned in Section 3.4, wind farm power output is the sum of wind turbine power output. An appropriate power curve has high accuracy on wind turbine power output estimation. This thesis selects the most widely used power curve in wind farm layout optimization: the cubic power curve, which is very simple and easy to fit. In our previous study [72], we proposed a probabilistic power curve, which is proved has higher accuracy on wind turbine power output calculation than the cubic power curve. The proposed probabilistic power curve is more complex than the cubic power curve and needs more CPU time on simulation. Future work will consider the proposed probabilistic power curve in wind farm layout optimization and compare the optimized result with this thesis.

Bibliography

- [1] S. R. Reddy, “Wind Farm Layout Optimization (WindFLO): An advanced framework for fast wind farm analysis and optimization,” *Applied Energy*, vol. 269, p. 115090, Jul. 2020, doi: 10.1016/j.apenergy.2020.115090.
- [2] W. E. Council, “World energy resources 2016,” *World Energy Council, London, UK*, 2016.
- [3] “Global Wind Report 2019,” *Global Wind Energy Council*, Mar. 19, 2020. <https://gwec.net/global-wind-report-2019/> (accessed Sep. 24, 2020).
- [4] J. F. Cao, W. J. Zhu, W. Z. Shen, J. N. Sørensen, and Z. Y. Sun, “Optimizing wind energy conversion efficiency with respect to noise: A study on multi-criteria wind farm layout design,” *Renewable Energy*, vol. 159, pp. 468–485, Oct. 2020, doi: 10.1016/j.renene.2020.05.084.
- [5] R. H. Wiser and M. Bolinger, “2018 Wind Technologies Market Report,” 2019.
- [6] C. Jung, D. Schindler, and L. Grau, “Achieving Germany’s wind energy expansion target with an improved wind turbine siting approach,” *Energy Conversion and Management*, vol. 173, pp. 383–398, Oct. 2018, doi: 10.1016/j.enconman.2018.07.090.
- [7] “Why Wind Works,” *Canadian Wind Energy Association*. <https://canwea.ca/wind-facts/why-wind-works/> (accessed Jul. 17, 2020).
- [8] P. Gipe, *Wind Energy Comes of Age*. John Wiley & Sons, 1995.
- [9] P. Enevoldsen and S. V. Valentine, “Do onshore and offshore wind farm development patterns differ?,” *Energy for Sustainable Development*, vol. 35, pp. 41–51, Dec. 2016, doi: 10.1016/j.esd.2016.10.002.
- [10] P. Enevoldsen, “Onshore wind energy in Northern European forests: Reviewing the risks,” *Renewable and Sustainable Energy Reviews*, vol. 60, pp. 1251–1262, Jul. 2016, doi: 10.1016/j.rser.2016.02.027.
- [11] M. Bilgili, A. Yasar, and E. Simsek, “Offshore wind power development in Europe and its comparison with onshore counterpart,” *Renewable and Sustainable Energy Reviews*, vol. 15, no. 2, pp. 905–915, Feb. 2011, doi: 10.1016/j.rser.2010.11.006.
- [12] W. Zhixin, J. Chuanwen, A. Qian, and W. Chengmin, “The key technology of offshore wind farm and its new development in China,” *Renewable and Sustainable Energy Reviews*, vol. 13, no. 1, pp. 216–222, Jan. 2009, doi: 10.1016/j.rser.2007.07.004.
- [13] T. Göçmen, P. van der Laan, P.-E. Réthoré, A. P. Diaz, G. Chr. Larsen, and S. Ott, “Wind turbine wake models developed at the technical university of Denmark: A review,” *Renewable and Sustainable Energy Reviews*, vol. 60, pp. 752–769, Jul. 2016, doi: 10.1016/j.rser.2016.01.113.
- [14] R. Shakoar, M. Y. Hassan, A. Raheem, and Y.-K. Wu, “Wake effect modeling: A review of wind farm layout optimization using Jensen’s model,” *Renewable and Sustainable Energy Reviews*, vol. 58, pp. 1048–1059, May 2016, doi: 10.1016/j.rser.2015.12.229.
- [15] B. Sandeise, “Aerodynamics of wind turbine wakes - literature review,” 2009.
- [16] N. Sedaghatizadeh, M. Arjomandi, R. Kelso, B. Cazzolato, and M. H. Ghayesh, “Modelling of wind turbine wake using large eddy simulation,” *Renewable Energy*, vol. 115, pp. 1166–1176, Jan. 2018, doi: 10.1016/j.renene.2017.09.017.
- [17] M. F. Howland, S. K. Lele, and J. O. Dabiri, “Wind farm power optimization through wake steering,” *PNAS*, vol. 116, no. 29, pp. 14495–14500, Jul. 2019, doi: 10.1073/pnas.1903680116.
- [18] S. Chowdhury, J. Zhang, A. Messac, and L. Castillo, “Optimizing the arrangement and the selection of turbines for wind farms subject to varying wind conditions,” *Renewable Energy*, vol. 52, pp. 273–282, Apr. 2013, doi: 10.1016/j.renene.2012.10.017.

- [19]F. Porté-Agel, Y.-T. Wu, and C.-H. Chen, “A Numerical Study of the Effects of Wind Direction on Turbine Wakes and Power Losses in a Large Wind Farm,” *Energies*, vol. 6, no. 10, Art. no. 10, Oct. 2013, doi: 10.3390/en6105297.
- [20]H. Yang, K. Xie, H. Tai, and Y. Chai, “Wind Farm Layout Optimization and Its Application to Power System Reliability Analysis,” *IEEE Transactions on Power Systems*, vol. 31, no. 3, pp. 2135–2143, May 2016, doi: 10.1109/TPWRS.2015.2452920.
- [21]J. Feng and W. Shen, “Modelling Wind for Wind Farm Layout Optimization Using Joint Distribution of Wind Speed and Wind Direction,” *Energies*, vol. 8, no. 4, pp. 3075–3092, Apr. 2015, doi: 10.3390/en8043075.
- [22]R. A. Rivas, J. Clausen, K. S. Hansen, and L. E. Jensen, “Solving the Turbine Positioning Problem for Large Offshore Wind Farms by Simulated Annealing,” *Wind Engineering*, vol. 33, no. 3, pp. 287–297, May 2009, doi: 10.1260/0309-524X.33.3.287.
- [23]L. Wang, “Comparative Study of Wind Turbine Placement Methods for Flat Wind Farm Layout Optimization with Irregular Boundary,” *Applied Sciences*, vol. 9, no. 4, p. 639, Feb. 2019, doi: 10.3390/app9040639.
- [24]N. Kirchner-Bossi and F. Porté-Agel, “Realistic Wind Farm Layout Optimization through Genetic Algorithms Using a Gaussian Wake Model,” *Energies*, vol. 11, no. 12, Art. no. 12, Dec. 2018, doi: 10.3390/en11123268.
- [25]J. Feng and W. Z. Shen, “Solving the wind farm layout optimization problem using random search algorithm,” *Renewable Energy*, vol. 78, pp. 182–192, Jun. 2015, doi: 10.1016/j.renene.2015.01.005.
- [26]G. Mosetti, C. Poloni, and B. Diviacco, “Optimization of wind turbine positioning in large windfarms by means of a genetic algorithm,” *Journal of Wind Engineering and Industrial Aerodynamics*, vol. 51, no. 1, pp. 105–116, Jan. 1994, doi: 10.1016/0167-6105(94)90080-9.
- [27]S. A. Grady, M. Y. Hussaini, and M. M. Abdullah, “Placement of wind turbines using genetic algorithms,” *Renewable Energy*, vol. 30, no. 2, pp. 259–270, Feb. 2005, doi: 10.1016/j.renene.2004.05.007.
- [28]L. Chen, C. Harding, A. Sharma, and E. MacDonald, “Modeling noise and lease soft costs improves wind farm design and cost-of-energy predictions,” *Renewable Energy*, vol. 97, pp. 849–859, Nov. 2016, doi: 10.1016/j.renene.2016.05.045.
- [29]L. Chen and E. MacDonald, “A system-level cost-of-energy wind farm layout optimization with landowner modeling,” *Energy Conversion and Management*, vol. 77, pp. 484–494, Jan. 2014, doi: 10.1016/j.enconman.2013.10.003.
- [30]L. Wang, M. J. Zuo, J. Xu, Y. Zhou, and A. C. Tan, “Optimizing wind farm layout by addressing energy-variance trade-off: A single-objective optimization approach,” *Energy*, vol. 189, p. 116149, Dec. 2019, doi: 10.1016/j.energy.2019.116149.
- [31]S. Chowdhury, J. Zhang, A. Messac, and L. Castillo, “Unrestricted wind farm layout optimization (UWFLO): Investigating key factors influencing the maximum power generation,” *Renewable Energy*, vol. 38, no. 1, pp. 16–30, Feb. 2012, doi: 10.1016/j.renene.2011.06.033.
- [32]J. Yan, H. Zhang, Y. Liu, S. Han, and L. Li, “Uncertainty estimation for wind energy conversion by probabilistic wind turbine power curve modelling,” *Applied Energy*, vol. 239, pp. 1356–1370, Apr. 2019, doi: 10.1016/j.apenergy.2019.01.180.
- [33]J. F. Manwell, J. G. McGowan, and A. L. Rogers, *Wind Energy Explained: Theory, Design and Application*. John Wiley & Sons, 2010.
- [34]C. G. Justus, “Winds and wind system performance,” *Research supported by the National Science Foundation and Energy Research and Development Administration. Philadelphia, Pa., Franklin Institute Press, 1978. 120 p.*, 1978, Accessed: Sep. 30, 2020. [Online]. Available: <http://adsabs.harvard.edu/abs/1978erda.book.....J>.

- [35] C. G. Justus, W. R. Hargraves, and A. Yalcin, "Nationwide Assessment of Potential Output from Wind-Powered Generators," *J. Appl. Meteor.*, vol. 15, no. 7, pp. 673–678, Jul. 1976, doi: 10.1175/1520-0450(1976)015<0673:NAOPOF>2.0.CO;2.
- [36] R. B. Corotis, A. B. Sigl, and J. Klein, "Probability models of wind velocity magnitude and persistence," *Solar Energy*, vol. 20, no. 6, pp. 483–493, Jan. 1978, doi: 10.1016/0038-092X(78)90065-8.
- [37] C. G. Justus, W. R. Hargraves, A. Mikhail, and D. Graber, "Methods for Estimating Wind Speed Frequency Distributions," *J. Appl. Meteor.*, vol. 17, no. 3, pp. 350–353, Mar. 1978, doi: 10.1175/1520-0450(1978)017<0350:MFEWSF>2.0.CO;2.
- [38] A. Garcia, J. L. Torres, E. Prieto, and A. de Francisco, "Fitting wind speed distributions: a case study," *Solar Energy*, vol. 62, no. 2, pp. 139–144, Feb. 1998, doi: 10.1016/S0038-092X(97)00116-3.
- [39] J. A. Carta, P. Ramírez, and S. Velázquez, "A review of wind speed probability distributions used in wind energy analysis: Case studies in the Canary Islands," *Renewable and Sustainable Energy Reviews*, vol. 13, no. 5, pp. 933–955, Jun. 2009, doi: 10.1016/j.rser.2008.05.005.
- [40] L. Wang, A. C. C. Tan, and Y. Gu, "Comparative study on optimizing the wind farm layout using different design methods and cost models," *Journal of Wind Engineering and Industrial Aerodynamics*, vol. 146, pp. 1–10, Nov. 2015, doi: 10.1016/j.jweia.2015.07.009.
- [41] L. Parada, C. Herrera, P. Flores, and V. Parada, "Wind farm layout optimization using a Gaussian-based wake model," *Renewable Energy*, vol. 107, pp. 531–541, Jul. 2017, doi: 10.1016/j.renene.2017.02.017.
- [42] J. A. Carta, P. Ramírez, and C. Bueno, "A joint probability density function of wind speed and direction for wind energy analysis," *Energy Conversion and Management*, vol. 49, no. 6, pp. 1309–1320, Jun. 2008, doi: 10.1016/j.enconman.2008.01.010.
- [43] L. J. Vermeer, J. N. Sørensen, and A. Crespo, "Wind turbine wake aerodynamics," *Progress in Aerospace Sciences*, vol. 39, no. 6, pp. 467–510, Aug. 2003, doi: 10.1016/S0376-0421(03)00078-2.
- [44] M. Bastankhah and F. Porté-Agel, "A new analytical model for wind-turbine wakes," *Renewable Energy*, vol. 70, pp. 116–123, Oct. 2014, doi: 10.1016/j.renene.2014.01.002.
- [45] N. O. Jensen, *A note on wind generator interaction*. Risø National Laboratory, 1983.
- [46] G. C. Larsen, *A Simple Wake Calculation Procedure*. Risø National Laboratory, 1988.
- [47] S. Frandsen *et al.*, "Analytical modelling of wind speed deficit in large offshore wind farms," *Wind Energy*, vol. 9, no. 1–2, pp. 39–53, 2006, doi: 10.1002/we.189.
- [48] S. Brusca *et al.*, "On the Wind Turbine Wake Mathematical Modelling," *Energy Procedia*, vol. 148, pp. 202–209, Aug. 2018, doi: 10.1016/j.egypro.2018.08.069.
- [49] I. Katic, J. Højstrup, and N. O. Jensen, "A SIMPLE MODEL FOR CLUSTER EFFICIENCY," p. 5.
- [50] H. Sun and H. Yang, "Study on an innovative three-dimensional wind turbine wake model," *Applied Energy*, vol. 226, pp. 483–493, Sep. 2018, doi: 10.1016/j.apenergy.2018.06.027.
- [51] H. Sun, X. Gao, and H. Yang, "Validations of three-dimensional wake models with the wind field measurements in complex terrain," *Energy*, vol. 189, p. 116213, Dec. 2019, doi: 10.1016/j.energy.2019.116213.
- [52] R. Brogna, J. Feng, J. N. Sørensen, W. Z. Shen, and F. Porté-Agel, "A new wake model and comparison of eight algorithms for layout optimization of wind farms in complex terrain," *Applied Energy*, vol. 259, p. 114189, Feb. 2020, doi: 10.1016/j.apenergy.2019.114189.
- [53] E. Taslimi-Renani, M. Modiri-Delshad, M. F. M. Elias, and N. Abd. Rahim, "Development of an enhanced parametric model for wind turbine power curve," *Applied Energy*, vol. 177, pp. 544–552, Sep. 2016, doi: 10.1016/j.apenergy.2016.05.124.

- [54]C. Carrillo, A. F. Obando Montaña, J. Cidrás, and E. Díaz-Dorado, “Review of power curve modelling for wind turbines,” *Renewable and Sustainable Energy Reviews*, vol. 21, pp. 572–581, May 2013, doi: 10.1016/j.rser.2013.01.012.
- [55]M. Lydia, S. S. Kumar, A. I. Selvakumar, and G. E. Prem Kumar, “A comprehensive review on wind turbine power curve modeling techniques,” *Renewable and Sustainable Energy Reviews*, vol. 30, pp. 452–460, Feb. 2014, doi: 10.1016/j.rser.2013.10.030.
- [56]B. Manobel, F. Sehnke, J. A. Lazzús, I. Salfate, M. Felder, and S. Montecinos, “Wind turbine power curve modeling based on Gaussian Processes and Artificial Neural Networks,” *Renewable Energy*, vol. 125, pp. 1015–1020, Sep. 2018, doi: 10.1016/j.renene.2018.02.081.
- [57]Tongdan Jin and Zhigang Tian, “Uncertainty analysis for wind energy production with dynamic power curves,” in *2010 IEEE 11th International Conference on Probabilistic Methods Applied to Power Systems*, Singapore, Singapore, Jun. 2010, pp. 745–750, doi: 10.1109/PMAPS.2010.5528405.
- [58]M. De-Prada-Gil, C. G. Alías, O. Gomis-Bellmunt, and A. Sumper, “Maximum wind power plant generation by reducing the wake effect,” *Energy Conversion and Management*, vol. 101, pp. 73–84, Sep. 2015, doi: 10.1016/j.enconman.2015.05.035.
- [59]Y. Chen, “Commercial wind farm layout design and optimization,” M.S., Texas A&M University - Kingsville, United States -- Texas, 2013.
- [60]J. Izquierdo-Pérez, B. M. Brentan, J. Izquierdo, N.-E. Clausen, A. Pegalajar-Jurado, and N. Ebsen, “Layout Optimization Process to Minimize the Cost of Energy of an Offshore Floating Hybrid Wind-Wave Farm,” *Processes*, vol. 8, no. 2, p. 139, Jan. 2020, doi: 10.3390/pr8020139.
- [61]J. Aldersey-Williams and T. Rubert, “Levelised cost of energy – A theoretical justification and critical assessment,” *Energy Policy*, vol. 124, pp. 169–179, Jan. 2019, doi: 10.1016/j.enpol.2018.10.004.
- [62]P. Mittal, K. Mitra, and K. Kulkarni, “Optimizing the number and locations of turbines in a wind farm addressing energy-noise trade-off: A hybrid approach,” *Energy Conversion and Management*, vol. 132, pp. 147–160, Jan. 2017, doi: 10.1016/j.enconman.2016.11.014.
- [63]J. S. González, A. G. Gonzalez Rodriguez, J. C. Mora, J. R. Santos, and M. B. Payan, “Optimization of wind farm turbines layout using an evolutive algorithm,” *Renewable Energy*, vol. 35, no. 8, pp. 1671–1681, Aug. 2010, doi: 10.1016/j.renene.2010.01.010.
- [64]P. Sood, V. Winstead, and P. Steevens, “Optimal placement of wind turbines: A Monte Carlo approach with large historical data set,” in *2010 IEEE International Conference on Electro/Information Technology*, May 2010, pp. 1–5, doi: 10.1109/EIT.2010.5612130.
- [65]M. Bilbao and E. Alba, “Simulated Annealing for Optimization of Wind Farm Annual Profit,” in *2009 2nd International Symposium on Logistics and Industrial Informatics*, Sep. 2009, pp. 1–5, doi: 10.1109/LINDI.2009.5258656.
- [66]C. Wan, J. Wang, G. Yang, H. Gu, and X. Zhang, “Wind farm micro-siting by Gaussian particle swarm optimization with local search strategy,” *Renewable Energy*, vol. 48, pp. 276–286, Dec. 2012, doi: 10.1016/j.renene.2012.04.052.
- [67]K. Veeramachaneni, M. Wagner, U.-M. O’Reilly, and F. Neumann, “Optimizing energy output and layout costs for large wind farms using particle swarm optimization,” in *2012 IEEE Congress on Evolutionary Computation*, Jun. 2012, pp. 1–7, doi: 10.1109/CEC.2012.6253002.
- [68]F. González-Longatt, P. Wall, and V. Terzija, “Wake effect in wind farm performance: Steady-state and dynamic behavior,” *Renewable Energy*, vol. 39, no. 1, pp. 329–338, Mar. 2012, doi: 10.1016/j.renene.2011.08.053.
- [69]J. Kollwitz, *Defining the Wake Decay Constant as a Function of Turbulence Intensity to Model Wake Losses in Onshore Wind Farms*. 2016.

- [70]V. L. Okulov, I. V. Naumov, R. F. Mikkelsen, and J. N. Sørensen, “Wake effect on a uniform flow behind wind-turbine model,” *J. Phys.: Conf. Ser.*, vol. 625, p. 012011, Jun. 2015, doi: 10.1088/1742-6596/625/1/012011.
- [71]E. K. P. Chong and S. H. Zak, *An Introduction to Optimization*. John Wiley & Sons, 2013.
- [72]S. Ge, M. J. Zuo, and Z. Tian, “Wind Turbine Power Output Estimation with Probabilistic Power Curves,” in *2020 Asia-Pacific International Symposium on Advanced Reliability and Maintenance Modeling (APARM)*, Aug. 2020, pp. 1–6, doi: 10.1109/APARM49247.2020.9209346.